UNIVERSIDAD
NACIONAL
DE COLOMBIA

Forearc Basin Evolution in Response to a Changing Subduction System: Neogene to Recent Geological Record of the Northwestern Colombian Andes

Santiago León Vasco

Universidad Nacional de Colombia

Facultad de Minas, Departamento de Materiales y Minerales

Medellín, Colombia

2022

Evolución de una Cuenca de Antearco en Respuesta a un Régimen de Subducción Cambiante: Registro Geológico Neógeno al Reciente del Noroccidente de los Andes Colombianos

Santiago León Vasco

Tesis presentada como requisito parcial para optar al título de:

Doctor en Ingeniería

Director:

PhD. Gaspar Monsalve Mejía

Línea de Investigación:

Geología

Universidad Nacional de Colombia

Facultad de Minas, Departamento de Materiales y Minerales

Medellín, Colombia

2022

This thesis is partially based on the following publications:

León, S., Avellaneda-Jiménez, D.S., Monsalve, G., Bustamante, C., Valencia, V. Evidence for magmatic activity of the Central American arc at ~100-84 Ma supports its spontaneous origin by plume-lithosphere interaction. Revision submitted to GSA Bulletin.

León, S., Monsalve, G., Jaramillo, C., Posada, G., Miranda, T.S., Echeverri, S., Valencia, V., 2021. Increased megathrust shear force drives topographic uplift in the Colombian coastal forearc. Tectonophysics 820, 229132. https://doi.org/10.1016/j.tecto.2021.229132

León, S., Monsalve, G., Bustamante, C., 2021. How much did the Colombian Andes rise by the collision of the Caribbean oceanic plateau? Geophysical Research Letters. 48, e2021GL093362. https://doi.org/10.1029/2021GL093362.

León, S., Marulanda, U.M., Monsalve, G., Parra, M., Avellaneda-Jiménez, D.S., Jaramillo, C., Echeverri, S., Vallejo-Hincapié, D.F., Trejos-Tamayo, R.A., Pardo-Trujillo, A., Valencia, V. A. Forearc basin evolution during the transition from collision to subduction: Neogene tectonostratigraphy and sedimentary provenance of the northwesternmost Andes. In preparation.

Contents

List of Figures and Tables

Acknowledgements

This doctoral research project was funded by the Smithsonian Tropical Research Institute, the Fundación para la Promoción de la Investigación y la Tecnología (project 4.304), the Corrigan Fund (ACGGP-Ares), and through academic collaborations with the Washington State University (USA), the University of Sao Paulo (Brazil), and the Instituto de Investigaciones en Estratigrafía (Universidad de Caldas, Colombia). All those people who are part of the above-mentioned institutions and were somehow involved in the development of this research are deeply acknowledged for providing academic and financial support. I am also thankful to the Michel Polanyi research group for providing additional funding.

Special thanks to Gaspar Monsalve and Carlos Jaramillo for their guidance and for encouraging me to continue with my doctoral research. I also appreciate the thorough reviews and suggestions on each chapter of this thesis made by Mauricio Parra, Camilo Bustamante, Tiago Siqueira and César Vinasco, as well as by the coauthors of the associated papers, which certainly helped me to improve the quality of this work.

Abstract

The growth of accretionary orogens, such as the northern Andes, involves both subduction-related tectonics and the collision of exotic terranes, including oceanic plateaus and island arcs. These contrasting tectonic regimes control the spatiotemporal evolution of deformational patterns and topography, whose signal is preserved in the tectonostratigraphic record of marginal basins, which is particularly true for forearc systems. This work presents a detailed geochronological and compositional characterization of Cretaceous magmatic rocks and Neogene strata of the northern Colombian forearc basin (Atrato Basin), which record the long-term evolution of the northwesternmost Andean region, since the early interactions with the Caribbean plate to the most recent shallow subduction of the Nazca plate.

New petrochronological data from the Cupica and Tribugá gulfs allowed the recognition of a previously undocumented Upper-Cretaceous arc-related magmatic unit, which likely represents the earliest activity of the intra-oceanic Central American arc and the coeval island arc nowadays exposed along the north-Andean Western Cordillera. The collision of the latter and its plateau-like basement caused a major topographic uplift of the Colombian Central Cordillera during the Late Cretaceous-Paleocene, as suggested by new paleoelevation estimations presented in this work. Such collisional episode marked the early constitution of the northwestern Colombian forearc, whose evolution was subsequently controlled by the Neogene transition from the collision of the Central American arc and the subduction of the Nazca plate.

A comprehensive tectonostratigraphic analysis of the Neogene infill of the Atrato Basin allowed identifying three main tectonic phases, which drove changes in the configuration of source areas and the depositional settings. First, the collision of the Central American arc against northwestern South America was recorded by the accumulation in a tectonically active back-arc basin of Oligocene-middle Miocene deep-marine strata sourced by both colliding domains. The advance of the collision triggered basin inversion and shallowing of accumulation depths during the middle Miocene, as well as accelerated erosional exhumation

of the continental paleomargin and increased siliciclastic input to suture-related and the colliding back-arc basin.

Second, the transition from collision to the subduction of the Nazca plate during the middle-late Miocene caused the formation of a post-collisional arc in northwestern Colombia, as well as the initial topographic uplift of the newly established forearc basin (former allochthonous back-arc) nearby the suture zone. This was accompanied by a major shallowing of accumulation depths and a dramatic change in the detrital signal of forearc deposits, which were isolated from continental source areas (i.e. Western Cordillera) by newly uplifted ranges.

Finally, the late Miocene flattening of the subducting Nazca slab beneath northern Colombia caused widespread deformation that drove the uplift of the outer forearc high, represented by the coastal Baudó Range, and the establishment of the modern physiographic configuration. This episode led to the fragmentation of the forearc basin into an outer (coastal) and inner (inland) segments and strong reworking of older strata, as suggested by the provenance of late Miocene to Pliocene rocks accumulated in high-energy fluvial environments. The pulsated nature of Miocene mountain building along the northwesternmost Andean forearc, as a consequence of interspersed collisional and subduction-related tectonics, seemingly played a major role in the biogeographic evolution of the region and the constitution of the modern extremely humid tropical rainforest that hosts a biodiversity hotspot.

This work allowed proving how valuable the tectonostratigraphic record of forearc basins and the surrounding mountain ranges is to disentangle the effects of a changing subduction system on the upper-plate landscape evolution, which, as demonstrated in this work, could be successfully studied through a combination of petrochronological, stratigraphic and structural analyses.

Keywords: Forearc basins, Northern Andes, Arc-continent collision, Atrato Basin, Sedimentary provenance, Tectonostratigraphy.

Resumen

El crecimiento de orógenos acrecionarios como los Andes del norte, involucra procesos tectónicos relacionados con subducción, así como la colisión de terrenos exóticos, incluyendo plateaux oceánicos y arcos de islas. Estos regímenes tectónicos contrastantes controlan la evolución espaciotemporal de los patrones de deformación y la topografía, cuya señal es preservada en el registro tectonoestratigráfico de las cuencas marginales, lo cual es particularmente cierto para sistemas de antearco. Este trabajo presenta una caracterización geocronológica y composicional detallada de las rocas magmáticas Cretácicas y sedimentos Neógenos del antearco norte de Colombia (Cuenca Atrato), las cuales registran la evolución de largo plazo de la región más noroccidental de los Andes, desde las interacciones tempranas con la placa Caribe hasta la más reciente subducción plana de la placa de Nazca.

Nuevos datos petrocronológicos de sedimentos modernos de los golfos de Cupica y Tribugá permitieron reconocer una unidad magmática del Cretácico Tardío afín con un arco de islas que no había sido previamente documentada, la cual podría representar la actividad más temprana del arco Centro Americano y el arco de islas ahora expuesto a lo largo de la Cordillera Occidental de los Andes del norte. La colisión de este último, en conjunto con su basamento de tipo plateau, durante el Cretácico Tardío-Paleoceno, causó un importante levantamiento topográfico de la Cordillera Central Colombiana, como lo sugieren nuevas estimaciones de paleoelevación presentadas en este trabajo. Este episodio colisional marcó la conformación temprana del antearco noroccidental Colombiano, cuya evolución fue subsecuentemente controlada por la transición Neógena de colisión del arco Centro Americano y la subducción de la placa de Nazca.

Un análisis tectonoestratigráfico integral del relleno Neógeno de la Cuenca Atrato permitió identificar tres fases tectónicas principales, las cuales detonaron cambios en la configuración de las áreas fuente y de los ambientes deposicionales. Primero, la colisión del arco Centro Americano con el noroccidente de Suramérica fue registrado por la acumulación, en una cuenca tras-arco tectónicamente activa, de rocas marinas profundas del Oligoceno-Mioceno medio con procedencia de ambos dominios en colisión. El avance del evento colisional detonó la inversión de la cuenca y la somerización de las profundidades de

acumulación durante el Mioceno Medio, así como la exhumación por erosión acelerada de la paleomargen continental y el incremento del flujo siliciclástico hacia la cuenca de sutura y la cuenca de tras-arco en colisión.

Segundo, la transición de colisión a subducción de la placa de Nazca durante el Mioceno medio-tardío causó la formación de un arco poscolisional en el noroccidente de Colombia, y también el levantamiento topográfico inicial de la recientemente establecida cuenca de antearco (antes tras-arco alóctono) en cercanías a la zona de sutura. Esto fue acompañado por una somerización importante de los ambientes de acumulación y un cambio dramático en la señal detrítica de los depósitos de antearco, los cuales fueron aislados de fuentes continentales (i.e. Cordillera Occidental) por montañas recientemente levantadas.

Finalmente, el aplanamiento de la losa subducente de la placa de Nazca por debajo del norte de Colombia causó deformación ampliamente distribuida y condujo al levantamiento del alto externo del antearco, representado por la Serranía de Baudó, y al establecimiento de las condiciones fisiográficas modernas. Este episodio llevó a la fragmentación de la cuenca de antearco en un segmento externo (costero) y uno interno (continental), así como al fuerte retrabajamiento de rocas más antiguas, como lo sugiere la procedencia de rocas del Mioceno tardío al Plioceno acumuladas en ambientes fluviales de alta energía. La naturaleza episódica de la construcción de montañas durante el Mioceno a lo largo del antearco más noroccidental de los Andes, como consecuencia de tectónica colisional y de subducción, jugó, aparentemente, un papel importante en la evolución biogeográfica de la región y en la constitución del bosque tropical extremadamente húmedo de la actualidad, el cual hospeda un punto caliente de biodiversidad.

Este trabajo permitió probar lo valioso que es el registro tectonoestratigráfico de las cuencas de antearco y las cadenas de montaña adyacentes para revelar los efectos de un sistema de subducción cambiante en la evolución del paisaje de la placa superior. Esto, como pudo demostrarse en este trabajo, puede ser exitosamente estudiado a través de la integración de análisis petrocronológicos, estratigráficos y estructurales.

Palabras clave: Cuencas antearco, Andes del Norte, Colisión arco-continente, Cuenca Atrato, Procedencia sedimentaria, Tectonoestratigrafía

CHAPTER 1

1. Introduction

1.1. Forearc basins as key elements to study subduction zones

The growth of continental crust at convergent margins results from the addition of intermediate-acidic volcanic and plutonic rocks by arc-related magmatism due to subduction of oceanic lithosphere, and by the collision/accretion of intra-oceanic arcs (Cawood et al., 2009; Stern, 2002). Interspersed collisional and subduction-related tectonics are also responsible for the rise of some of the highest mountain ranges on Earth, which in turn have played a major role on the long-term evolution of the global climate and biogeography (e.g. Blisniuk et al., 2006; Champagnac et al., 2012; Rahbek et al., 2019). The locus and timing of topographic growth at convergent margins largely depends on the nature of the tectonic processes involved, and identifying them requires a thorough study of the coupled evolution of sedimentary basins and adjacent mountain ranges (e.g. Bayona et al., 2008; Encinas et al., 2021; Wang et al., 2020).

Forearc basins are elongated and narrow depressions formed between the volcanic arc and the trench (Dickinson, 1973), and their proximity to plate boundaries renders their tectonostratigraphic record highly sensitive to the effects of changes in the subduction zone configuration (e.g. Aizprua et al., 2019; Hernández et al., 2020; Martinod et al., 2016; Noda, 2016; Ridgway et al., 2011). For instance, parameters such as dip angle, convergence rate and obliquity, megathrust shear force and plate coupling, and basal underplating, in addition to mantle dynamics and the effects of collisional episodes, are interpreted as first-order controls of the subsidence/uplift patterns of forearc basins and the configuration of source areas (e.g. Delph et al., 2021; Dickinson, 1995; Finzel et al., 2016; León et al., 2021b; Xie and Heller, 2009).

However, given the complexity of subduction zones, particularly those involving the collision of exotic terranes (i.e. accretionary orogens; Cawood et al., 2009), the drivers of

vertical deformation of forearcs are very diverse and less predictable than those of foreland or strike-slip basins, for which the causes and rates of subsidence are better understood (Xie and Heller, 2009). Hence, comprehensive analyses of the stratigraphy, provenance, structural geology, magmatism, seismicity and gravity are required in order to provide robust frameworks to disentangle the mid- to long-term evolution of forearc basins and the underlying tectonic controls (Encinas et al., 2021; Finzel and Enkelmann, 2017; Hernández et al., 2020; Mora et al., 2018; Tassara, 2010).

1.2. Objectives and Research Questions

The northern Andes (north of ~3°S), unlike the central and southern segments of the mountain belt, is an accretionary orogen, and its Mesozoic-Cenozoic evolution has been shaped by interspersed subduction tectonics and the collision of Caribbean-derived terranes, including oceanic plateaus and island arcs nowadays exposed along the Colombian Andes (León et al., 2018; Montes et al., 2019; and references therein). Such diverse tectonic styles have left an imprint on the magmatic, erosional and deformational record that has been mostly studied along the hinterland and foreland regions (e.g. Bayona et al., 2008, 2020; Horton, 2018a; León et al., 2021a; Parra et al., 2010, 2012; Villagómez and Spikings, 2013; Zapata et al., 2019). This, even though it has been shown that the tectonostratigraphy of foreland basins might be strongly influenced by far-field (e.g. continental-scale) tectonic forcing that could mask the signal of subduction- or collision-related mechanisms as observed in the Peruvian and Patagonian Andes (e.g. Gianni et al., 2020; Hurtado et al., 2018).

The tectonostratigraphy of Colombian forearc basins has been barely addressed in the context of the Neogene transition from the collision of the Central American arc (CAA) to the subduction of the Nazca oceanic plate, and the imprints of the tectonic drivers of orogenic growth and mountain building are still barely known (Borrero et al., 2012; Echeverri et al., 2015b; León et al., 2021b, 2018; Pardo-Trujillo et al., 2020b). In fact, the northwesternmost Andean forearc (~5°-7°N), represented by the Atrato Basin (AB; Fig. 4.1), is perhaps the least known of the entire orogenic belt in spite of comprising a thick (up to 10 km) Cenozoic sedimentary infill (Duque-Caro, 1990a), coupled with a high-relief fragmented topography

(i.e. presence of a coastal range or forearc high), whose evolution likely preserves the effects of the complex Neogene transition from collision to subduction (León et al., 2018). This makes the northwesternmost Colombian Andes a key area to assess how forearc basins respond to a changing subduction system and the collision of oceanic terranes by means of its mid- to long-term topographic growth and modification of source-to-sink systems.

The main goal of this doctoral thesis is contributing to our understanding of how changes in the subduction zone configuration and the collision of intra-oceanic terranes (e.g. plateaus and island arcs) control the upper-plate topographic and landscape evolution in accretionary orogens. For this, the thick (up to 10 km) Neogene infill of the Atrato Basin and its Upper Cretaceous to Eocene-Oligocene volcano-plutonic and volcaniclastic basement (northwesternmost forearc basin of the Andes) were studied through a combination of new and previous field and stratigraphic constraints with structural, geochronological, geochemical and isotopic data. During the development of this research, the following questions were addressed:

- ✓ How did the igneous basement of the northern Colombian forearc formed?
- ✓ What were the effects of the early collision of oceanic terranes on the initial topographic growth of the Colombian Andes?
- ✓ How did the Neogene switch from collision to subduction modified the forearc source-to-sink systems in northwesternmost Colombia?
- ✓ Is the along-strike morphological segmentation of the Colombian Pacific margin a consequence of contrasting subduction zone configurations?

The obtained results and their corresponding implications on the tectonic and topographic evolution of the northwesternmost Andes are presented and discussed in four different chapters, which are intended as individual research articles. Chapter 2 addresses the origin of the Upper Cretaceous magmatic rocks that represent the basement of the northernmost Pacific coast of Colombia, which is discussed in the context of subduction initiation at the southwestern proto-Caribbean region and their linkages with the geodynamic setting of northwestern South America. Chapter 3 presents new quantitative estimations for the early topographic growth of the Colombian Andes during the initial tectonic amalgamation of the Caribbean oceanic plateau and associated island arcs, whose origin were discussed in Chapter

2. A detailed reconstruction of the tectonostratigraphy of the northern Colombian forearc basin (Atrato Basin), whose infill unconformably overlies Upper-Cretaceous plateau- and arc-related rocks formed during the evolution of the Caribbean plate (see Chapter 2), is provided in Chapter 4. There, stratigraphic, petrological and structural methods are combined to study the spatiotemporal patterns of forearc subsidence/uplift in response to a shift from collisional to subduction tectonics during the Neogene. Chapter 5 presents a discussion of the plausible tectonic drivers of recent uplift along the northern Pacific coast and the observed along-strike morphological segmentation. Finally, Chapter 6 provides a synthesis and some concluding remarks.

CHAPTER 2

2. Origin of the northwestern Colombian forearc basement: Late Cretaceous plume-induced subduction initiation in the southwestern proto-Caribbean

2.1. Introduction

Subduction zones represent a primary geodynamic setting for the long-term evolution of continental crust and the growth of some of the highest mountain ranges on Earth (e.g. the Andes; Oncken et al., 2006); yet, how subduction initiates is still a matter of debate (Crameri et al., 2020; Stern and Gerya, 2018). Several geodynamic mechanisms involved in the initiation of subduction zones are included into two contrasting modes. Induced subduction initiation (SI) that requires ongoing plate convergence for a new subduction zone to nucleate, and spontaneous SI, which does not require active plate convergence but the existence of lithospheric weaknesses or discontinuities (e.g. transform faults, large density/buoyancy contrasts, or thermal weakening by plume-lithosphere interactions; see a review in Stern and Gerya, 2018). Discerning between the several mechanisms involved in SI requires a robust chronological framework for the growth of magmatic arcs and a priori knowledge on the surrounding regional tectonics (Crameri et al., 2020; Stern and Gerya, 2018).

The Cretaceous tectonic evolution of the Caribbean region involved the formation of several island arcs emplaced onto the plume-derived Caribbean Oceanic Plateau (COP), which were subsequently accreted to the American continental margins during the late Mesozoic and Cenozoic (Kerr et al., 2003; Montes et al., 2019; Pindell and Kennan, 2009). Of particular interest, is the SI along the southwestern proto-Caribbean region (former Farallon plate) that led to the birth of the Caribbean plate (Boschman et al., 2019), and the formation of both the Central American (CAA) and the Ecuadorian-Colombian-Leeward

Antilles (ECLA) arcs (Whattam and Stern, 2015; Wright and Wyld, 2011). The timing and nature of the mechanisms involved in SI and the growth of the CAA and the ECLA are still debated though, and both induced and spontaneous mechanisms have been proposed (Buchs et al., 2010; Weber et al., 2015; Whattam and Stern, 2015; Wright and Wyld, 2011).

The lack of consensus on the SI process is probably due to the difficulty to construct a robust petrological framework for the oldest arc-related rocks of the CAA and the ECLA, and the uncertainty regarding its linkage with Cretaceous tectonics of northwestern South America, which hinders placing the onset of subduction in a regional geodynamic context. In this work, we present new petrochronological data from detrital zircons recovered from Neogene and modern sediments of the Colombian Pacific coast, where Upper Cretaceous magmatic rocks are exposed. We aimed to characterize previously unexplored basement rocks of the coastal Baudó Range that is supposed to be composed of either plateau- and/or arc-related units (Kerr et al., 1997; Whattam and Stern, 2015), and to contribute to the construction of a chronological framework for the early evolution of the CAA. This, in order to gain insights into the SI process and its implications on the tectonic evolution of the southwestern Caribbean and the northwestern Andes.

2.2. Geological Setting

Fragments of accreted plateau-like crust, interpreted as part of the COP, are exposed in the margins of the Caribbean and the Pacific regions of Central and South America (Fig. 2.1; Kerr et al., 2003). The bulk of these mafic and ultramafic rocks, which formed most of the Caribbean plate prior to its interaction with the margins of the Americas, are tholeiitic and isotopically juvenile (Kerr et al., 2003). They are thought to have formed by decompression melting of a heterogeneous mantle plume probably associated with the Galápagos hotspot with a main magmatic pulse at ~95-83 Ma (Dürkefälden et al., 2019; Hastie and Kerr, 2010). Fault-bounded fragments of the COP compose the basement of the northern forearc (Atrato Basin) and the Western Cordillera of Colombia (Fig. 2.1; (Kerr et al., 1997). These rocks are intruded by Cretaceous to Eocene island arc units that are thought to have formed along the southwestern margin of the Caribbean plate (Whattam and Stern, 2015; Wright and Wyld, 2011). Turonian-Santonian (~94-80 Ma) units of the ECLA intra-oceanic arc that intrude the

COP are mainly exposed along the north-Andean Western Cordillera and the Leeward Antilles (Vallejo et al., 2006; Villagómez et al., 2011; Weber et al., 2015; Wright and Wyld, 2011). This island arc collided with the South-American paleomargin at ~75-65 Ma (León et al., 2021a; Vallejo et al., 2006) and is sutured to the east to Cretaceous arc-related and Jurassic to Permian metamorphic rocks of the Colombian Central Cordillera along the Romeral Fault System (RFS; Fig. 2.1; e.g. (Villagómez et al., 2011). The ECLA is also sutured to the west by the Uramita Fault Zone (UFZ; Fig. 2.1; (Duque-Caro, 1990a; León et al., 2018) to volcaniclastic and plutonic rocks of the CAA, which originated either at ~100-90 Ma together with the ECLA and coeval with the main magmatic pulse of the COP (i.e. spontaneous plume-driven SI; Whattam and Stern, 2015), or as a separated arc at ~75-73 Ma during the collision of the leading edge of the Caribbean plate with northwestern South America (i.e. collision-related induced SI; Buchs et al., 2010). The CAA is mostly exposed along the northwestern flank of the Western Cordillera of Colombia and central-eastern Panama (Fig. 2.1), and is mainly represented by ~70-40 Ma or probably older mafic-intermediate plutonic rocks emplaced onto the COP (Barbosa-Espitia et al., 2019; Cardona et al., 2018), prior to its collision against the already accreted ECLA during the early-middle Miocene (~20-15 Ma; León et al., 2018).

In northwestern Colombia, the CAA and its plateau-like basement are overlain by Oligocene to Pliocene strata of the forearc Atrato Basin (Fig. 2.1), for which biostratigraphic constraints suggest a tectonically-driven switch from deep- to shallow marine conditions during the middle Miocene, and to terrestrial accumulation settings during the late Miocene-Pliocene (Duque-Caro, 1990b). These rocks seem to preserve the erosional record of the ~20-15 Ma collision of the CAA and its COP basement with the ECLA that was already docked to the continent (León et al., 2018). Subsequent deformation attributed to the subduction of the Nazca plate, resulted in the post-middle Miocene uplift of the ~1000 meters-high coastal Baudó Range that fragmented the Atrato basin into an inner (landward) and an outer (oceanward) segment (León et al., 2021b).

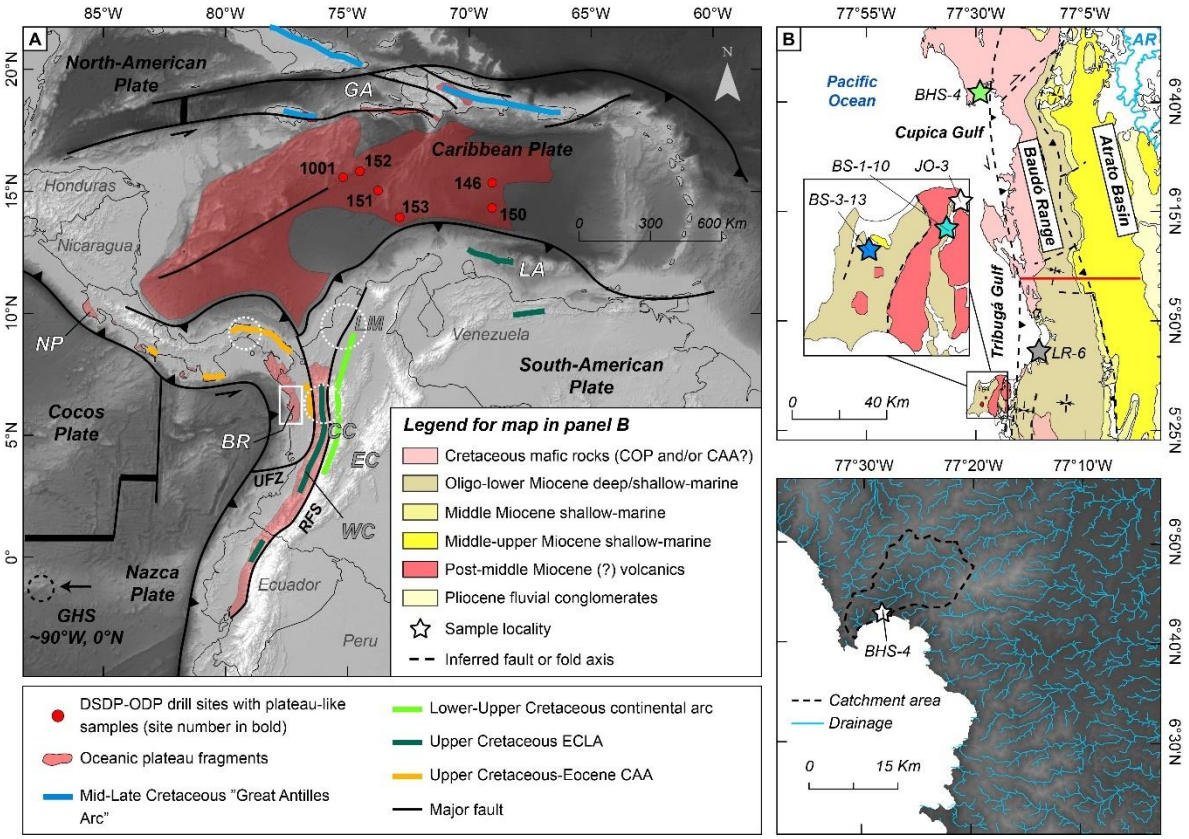

Figure 2.1. Regional tectonic configuration and geology of the Caribbean and north Andean regions, modified from Serrano et al. (2011), Whattam and Stern (2015), and references therein. A) Map showing the reported occurrences of Cretaceous COP and arc-related rocks, and location (coordinates) of the Galápagos hotspot (GHS). Black dashed line delimitates the occurrence of COP rocks in the Caribbean Sea. CC, EC and WC stand for Central, Eastern, and Western Cordilleras; BR=Baudó Range, CP=Caribbean Plate, GA=Greater Antilles, LA=Leeward Antilles, LM=Lower Magdalena Valley, NP=Nicoya Peninsula, RFS=Romeral Fault System, UFZ=Uramita Fault Zone. Black rectangle delineates the area mapped in (B), and white dashed circles depict the areas where Cretaceous to Pliocene samples used for comparison were collected (see text for references). B) Local geology of the NW Colombian forearc and sample locations, modified from León et al. (2021b). C) Catchment area (black dashed line) and drainage configuration in the northernmost Cupica Gulf, where sample BHS-4 was collected.

Available petrological constraints suggest that the Baudó Range is mostly composed of Upper Cretaceous tholeiitic massive and pillowed basalts, and minor gabbros and dolerites, formed by partial melting of an heterogeneous mantle plume as part of the COP, which accreted together with the CAA to northwestern South America (Kerr et al., 1997; León et al., 2021b). However, a recent review of available geochemical data from Cretaceous magmatic rocks of the circum-Caribbean region suggests that some of those mafic rocks of the Baudó Range have subduction-related signatures (e.g. Nb and Ti depletion and low-Fe calc-alkaline affinity) and could be interpreted as part of the CAA (Whattam and Stern, 2015).

2.3. Sampling and Methods

We aimed to study the nature of Upper Cretaceous magmatic rocks of the Baudó Range in the northern Pacific coast of Colombia (Fig. 2.1). However, most of this region is inaccessible due to social and political unrest, and the extremely dense vegetation of one of the wettest and most biodiverse tropical rainforests on Earth (mean annual precipitation >7,000 mm/yr; Poveda and Mesa, 2000). To overcome these limitations, we conducted detrital zircon petrochronological analyses on modern sediments collected from three rivers draining the Baudó range towards the Pacific Ocean (Fig. 2.1). We also sampled texturally immature deep- to shallow-marine Oligocene-middle Miocene and middle-upper Miocene strata of the outermost Atrato Basin (Duque-Caro, 1990b), which likely accumulated prior to basin fragmentation driven by the post-middle Miocene uplift of the Baudó Range (León et al., 2021b). These rocks were analyzed to establish a provenance baseline and to evaluate the potential occurrence of reworking in modern sediments that could hinder investigating petrological features of igneous source areas exposed in previously unexplored regions of the Baudó Range.

Modern sediment samples of fine- to coarse-grained sands were collected above the area of tidal influence from three rivers that originate in the Baudó Range and flow into the Pacific Ocean. These samples were collected to study the rock units outcropping in mid- to high elevations of the mountain range, which are inaccessible due to the extremely dense vegetation of the tropical rainforest. Sample BHS-3-13 was collected from Oligocene-middle

Miocene strata, which are represented by interlayered fossiliferous limestones and calcareous litharenites. The latter are fine- to medium-grained and composed of quartz, feldspar, bioclasts, and sedimentary (mudstones) and volcanic lithic fragments, and are interpreted as accumulated in bathyal depths (Duque-Caro, 1990b; León et al., 2021b). Overlying middle-upper Miocene rocks mostly include interlayered calcareous mudstones and litharenites from which sample BS-1-10 was collected. Litharenites are fine- to coarse-grained and composed of quartz, feldspar, volcanic and lithic fragments, bioclasts, and remnants of organic matter (León et al., 2021b), and are thought to be accumulated in shallow-marine conditions (Duque-Caro, 1990b).

Detrital zircon U-Pb ages were measured by LA-ICP-MS at the Radiogenic Isotope Geochronology Lab (RIGL) at the Washington State University, following the procedures of (Chang et al., 2006). After U-Pb analyses, Lu-Hf isotopes and trace element compositions were measured on dated zircons. For comparison, we compiled 2442 detrital U-Pb ages from Cretaceous to Pliocene strata of northwestern Colombia exposed in the inner Atrato Basin, Western Cordillera, Cauca Valley and Lower Magdalena Valley, and central Panama (Fig. 2.1). These units are interpreted to preserve the erosional record and the source areas configuration of the suture zone and surrounding regions prior to and after the collision of the CAA and its COP basement (Lara et al., 2018; León et al., 2018; Montes et al., 2015, 2012; Ramírez et al., 2016). We aimed to provide a broad picture of the regional provenance signal of Cenozoic strata that could represent potential source areas for modern sediments along the study area, and to evaluate their dissimilarity in terms of their detrital U-Pb ages distribution with our newly analyzed samples.

2.4. Results

2.4.1. Detrital zircon dating and Hf isotopes

Studied zircons are mostly subhedral to euhedral, 80-250 µm-long, show oscillatory zoning, and yielded Th/U ratios between 0.2 and 8.7, indicating a magmatic origin (Hoskin and Schaltegger, 2003). Oligocene-middle Miocene strata (sample BS-1-10) show two prominent age peaks at ~18 and ~52 Ma, with >100 Ma ages representing up to ~25% of the analyzed zircons, whereas sample BS-3-13 from middle-upper Miocene strata yielded a

single peak at ~52 Ma (Fig. 2.2). Individual ages of modern sediments collected to the south of the study area (Tribugá Gulf; samples LR-6 and JO-3), span the late Miocene to the Proterozoic with a common Eocene peak (~50 Ma) that represents up to 52% of the analyzed grains. Distinctly, sample BHS-4, collected in the northern study area (Cupica Gulf), virtually lacks Eocene ages (only one grain dated at 56.2 ± 4.0 Ma) and yielded a single peak at ~92 Ma, with individual ages ranging between ~100 and ~84 Ma. This makes sample BHS-4 very dissimilar to the modern sediments of the Tribugá Gulf and the Neogene strata in terms of the distribution of detrital zircon U-Pb ages (Fig. 2.2).

Paleozoic to Precambrian zircons found in Oligocene-Miocene strata and modern sediments of the Tribugá Gulf show evolved isotopic signatures with εHf_i varying from -24.5 to +4.5, whereas Cretaceous, Paleogene and Neogene zircons are more juvenile with εHf_i shifting from +1.6 to +14.7. Zircons from sample BHS-4 show a nearly invariant Hf isotopic composition with εHf_i between +11.0 and +12.9 (Fig. 2.3).

2.4.2. Zircon trace element composition

Only Cretaceous and younger zircons were analyzed by trace element composition as we were interested in their petrogenetic significance regarding the early magmatic history of the CAA. Zircons younger than 100 Ma, from both modern sediments and Neogene samples, are Ti-poor (4.8-6.2 ppm) and have low to medium Rare Earth Element (REE) abundances (~292-3987 ppm), with variable Nb and Hf concentrations shifting from 0.8 to 13.8 ppm and 5730 to 11270 ppm, respectively. Analyzed zircons show positive Ce anomalies (Ce/Ce* ~4-90; after Loader et al., 2017), slightly negative to positive Eu anomalies (Eu/Eu* ~0.4-2.2), and U/Yb and Nb/Yb ratios ranging from <0.1 to 1.3, and 0.001 to 0.013, respectively (Figs. 2.3 and 2.4). In summary, Cretaceous to Eocene zircons, analyzed from Oligocene-Miocene and modern sediments samples, are similar in terms of their trace element composition, characterized by relative depletion in HSFE (i.e. Nb and Ti) and enrichment in incompatible elements such as U and Ce (Figs. 2.3 and 2.4).

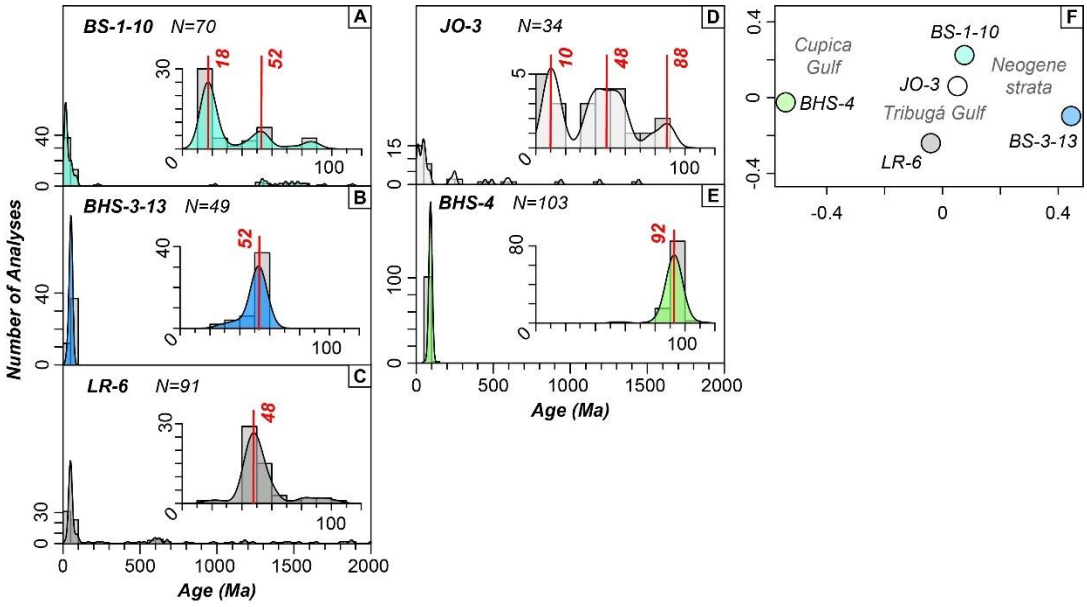

Figure 2.2. Normalized Kernel Density Estimate (KDE; bandwidth=15 Ma) curves for detrital zircon U-Pb data of Oligocene-middle Miocene strata (A-B), and modern sediments (C-E). F) Non-metric multi-dimensional scaling (MDS) plot showing the dissimilarity (large distance) of sample BHS-4 compared to the rest of the data; see Fig. 1 for sample location. N indicates the number of grains. Figures were drawn using the IsoplotR package (Vermeesch, 2018).

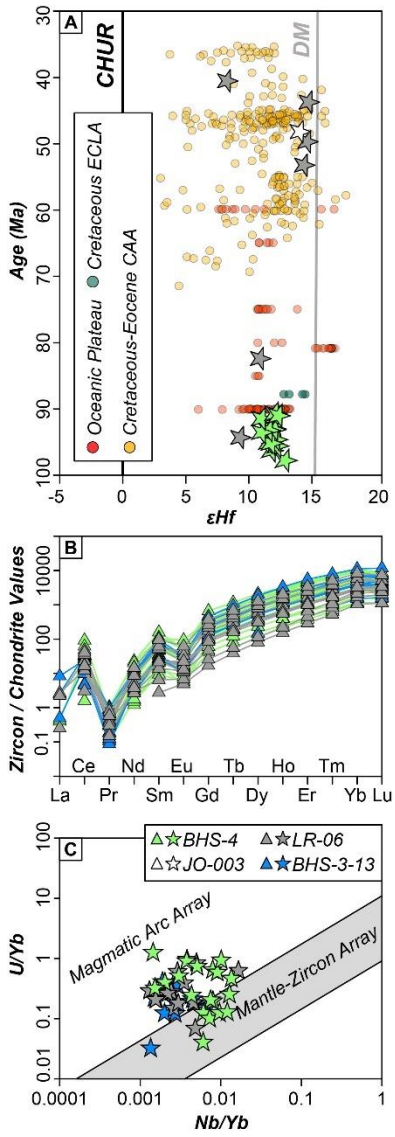

Figure 2.3. Isotopic and geochemical composition of detrital zircons (<100 Ma) from modern sediments and Neogene sedimentary rocks. A) εHfi vs. age diagram with whole-rock data from COP and ECLA rocks (Geldmacher et al., 2003; Kerr et al., 2009; Thompson et al., 2004), and zircon data from the CAA (Barbosa-Espitia et al., 2019; Ramírez et al., 2016), plotted for comparison. B) REE composition of zircons normalized to the chondrite composition of McDonough and Sun (1995). C) Nb/Yb vs. U/Yb discrimination diagram after Grimes et al. (2015).

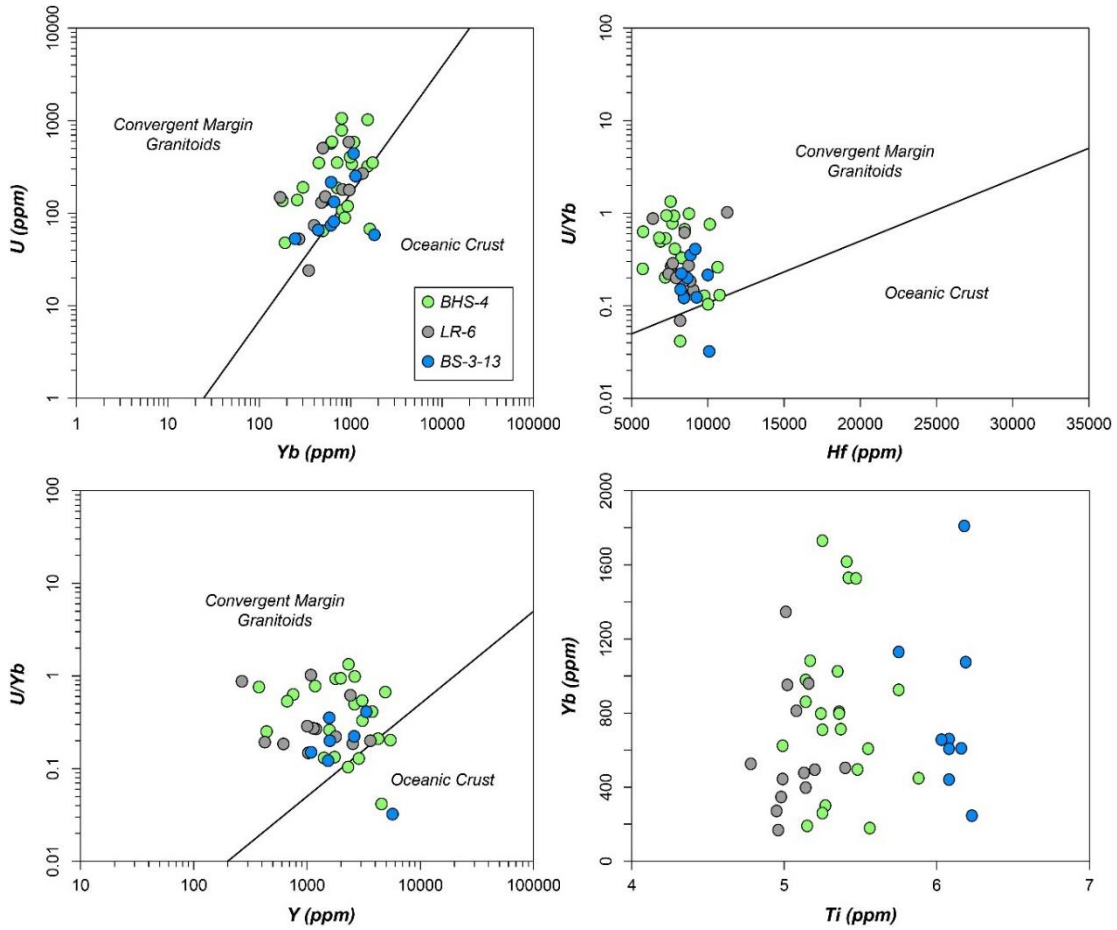

Figure 2.4. Geochemical discrimination diagrams for zircons (<100 Ma) analyzed in this work after Grimes et al. (2007), showing their affinity to arc-related magmatic rocks, and the partial overlapping with oceanic crust-derived zircons.

2.5. Discussion

2.5.1. Provenance interpretation for Neogene strata

Oligocene-middle Miocene strata of the outer forearc of northern Colombia (Atrato Basin) were accumulated in deep- to shallow-marine conditions during and after the collision of the CAA against northwestern South America (Duque-Caro, 1990b; León et al., 2018). This is supported by our finding in these rocks of Triassic and older isotopically evolved zircons akin to pre-Cretaceous continental basement of the northern Andes (see a review in George et al., 2021), and isotopically juvenile Cretaceous and Paleocene zircons resembling the age and composition of the CAA and its COP basement (Fig. 2.3; e.g. León et al., 2018; Montes et al., 2015). Eocene (~53-40 Ma) zircons from Neogene samples are depleted in HFSE, and have moderately high U/Yb ratios (Figs. 2.3 and 2.4), which suggest a subduction origin (Grimes et al., 2007), as expected from their potential derivation from CAA-related rocks. This is also supported by the presence of positive Ce and Eu anomalies, which arguably indicates that zircons could have crystallized under oxidized subduction-related magmatic conditions that enhanced both the substitution of $(Zr, Hf)^{4+}$ by Ce^{4+} into the zircon lattice, and the prevalence of high Eu^{3+}/Eu^{2+} ratios (Grimes et al., 2015, 2007; Trail et al., 2012).

Zircons with continental affinity were hardly sourced from primary crystalline rocks of inland domains of the Colombian Andes, but likely derived from recycled Late Cretaceous-Paleogene siliciclastic units of the Western Cordillera (Pardo-Trujillo et al., 2020a), as the latter seems to have been emerged since the Oligocene (Lara et al., 2018; Zapata et al., 2020), and therefore represents a barrier for sediments derived from easterly sources (e.g. Central Cordillera). Therefore, the Oligocene-Miocene strata of the Atrato Basin, exposed along the northern Colombian Pacific coast (Duque-Caro, 1990b), were likely accumulated oceanward (westward in present coordinates) of the CAA and Western Cordillera (both probably emerged at least since the Eocene-Oligocene; Montes et al., 2012; Zapata et al., 2020), prior to the uplift of the Baudó Range that has been taking place since the late Miocene (León et al., 2021b). Otherwise, the topography of the Baudó Range would have prevented the arrival of sediments derived from the Western Cordillera or farther inland domains to the outermost Atrato Basin, as observed in the present-day physiography.

2.5.2. Potential sources of modern sediments of the Cupica Gulf

Detrital petrochronology of modern sediments, collected in the Tribugá Gulf (samples LR-6 and JO-3), suggests recycling of Neogene strata as supported by the strong similarities of their detrital zircon U-Pb age spectra and trace element composition (Figs. 2.2, 2.3 and 2.4), which was expected by the spatial proximity of sampling localities and exposures of Neogene rocks (Fig. 2.1). Modern sediments of the Tribugá Gulf also show the appearance of younger (~10 Ma) zircons, for which a feasible source area, presumably related to the middle-upper Miocene continental arc (Jaramillo et al., 2019), has yet to be documented. Conversely, sample BHS-4, collected in the Cupica Gulf, where Neogene sedimentary rocks are apparently not exposed (Fig. 2.1), shows a very different detrital signature characterized by the presence of ~100-80 Ma zircons only (Fig. 2.2). These zircons overlap the age spectra and the juvenile Hf isotopic composition of both plateau and arc rocks of the Caribbean realm (Fig. 2.3) and are likely derived from magmatic rocks exposed somewhere upstream in the Baudó Range.

The trace element composition of zircons from sample BHS-4 (~98-87 Ma) shows a subduction-related signature, as suggested by their depletion in HSFE such as Nb and Ti, enrichment in U and Ce (Figs. 2.3 and 2.4), and the presence of positive Ce and Eu anomalies indicating oxidized magmatic conditions (Grimes et al., 2007; Trail et al., 2012). This is also supported by the low Nb/Yb and moderately high U/Yb ratios, which allow analyzed zircons to follow the magmatic arc trend in the discrimination diagram of Grimes et al. (2015), slightly overlapping the field of mantle-derived zircons (Fig. 2.3). Furthermore, the oscillatory zoning and high Th/U ratios, together with the low to moderate abundance of REE, Ti and Hf, suggest that ~98-87 Ma subduction-related zircons are probably derived from mafic-intermediate magmatic rocks (Belousova et al., 2002), which must be exposed upstream in the catchment where sample BHS-4 was collected in the northern Baudó Range. These rocks are likely correlatable with small mafic-intermediate units outcropping along the northern Pacific coast of Colombia, which despite their geochemical dissimilarities with surrounding COP lavas (e.g. depletion in HFSE such as Zr, Nb, and Ti), had been considered as part of the oceanic plateau (Kerr et al., 1997).

Our results provide evidence for the occurrence of ~100-80 Ma arc-related rocks in the Baudó Range (northwesternmost Colombia), whose presence had been tentatively proposed from an extensive review of petrological constraints, which show the existence of magmatic rocks with subduction-related geochemical signatures (e.g. depletion in HFSE and low-Fe calc-alkaline affinity; Whattam and Stern, 2015). According to recent tectonic and paleogeographic reconstructions (Boschman et al., 2019; Whattam et al., 2020; Whattam and Stern, 2015), we interpret these rocks as probably representing the southeasternmost extension and some of the most primitive products of the CAA. Further petrological work on already documented mafic-intermediate intrusives and previously unexplored areas of the Baudó Range will allow testing our interpretations.

2.5.3. Could the ~100-84 Ma zircons of the Cupica Gulf be reworked from older strata?

The lack of Eocene, Triassic and older zircons in sample BHS-4 makes it very dissimilar to the rest of the analyzed samples from both modern sediments and Neogene strata in terms of their detrital age spectra (Fig. 2.2). The dissimilarity with other modern sediments collected father to the south (Tribugá Gulf) could be explained by the confined catchment area where sample BHS-4 was collected, which implies a very localized provenance represented by Upper Cretaceous arc-related rocks of the Baudó Range (Fig. 2.1). Yet, it is still possible that previously unmapped Cenozoic sedimentary rocks, like those exposed elsewhere in northwestern Colombia and central-eastern Panama, could outcrop somewhere upstream in the northern Baudó Range, representing a potential source for modern sediments of the Cupica Gulf. In this scenario, the provenance signal of sample BHS-4 is expected to be similar to any of the Cenozoic units from which the sediments would be derived, since local dispersion or dilution of detrital material is not considered to be relevant in such a short sedimentary system (Fig. 2.1; e.g. Malkowski et al., 2019).

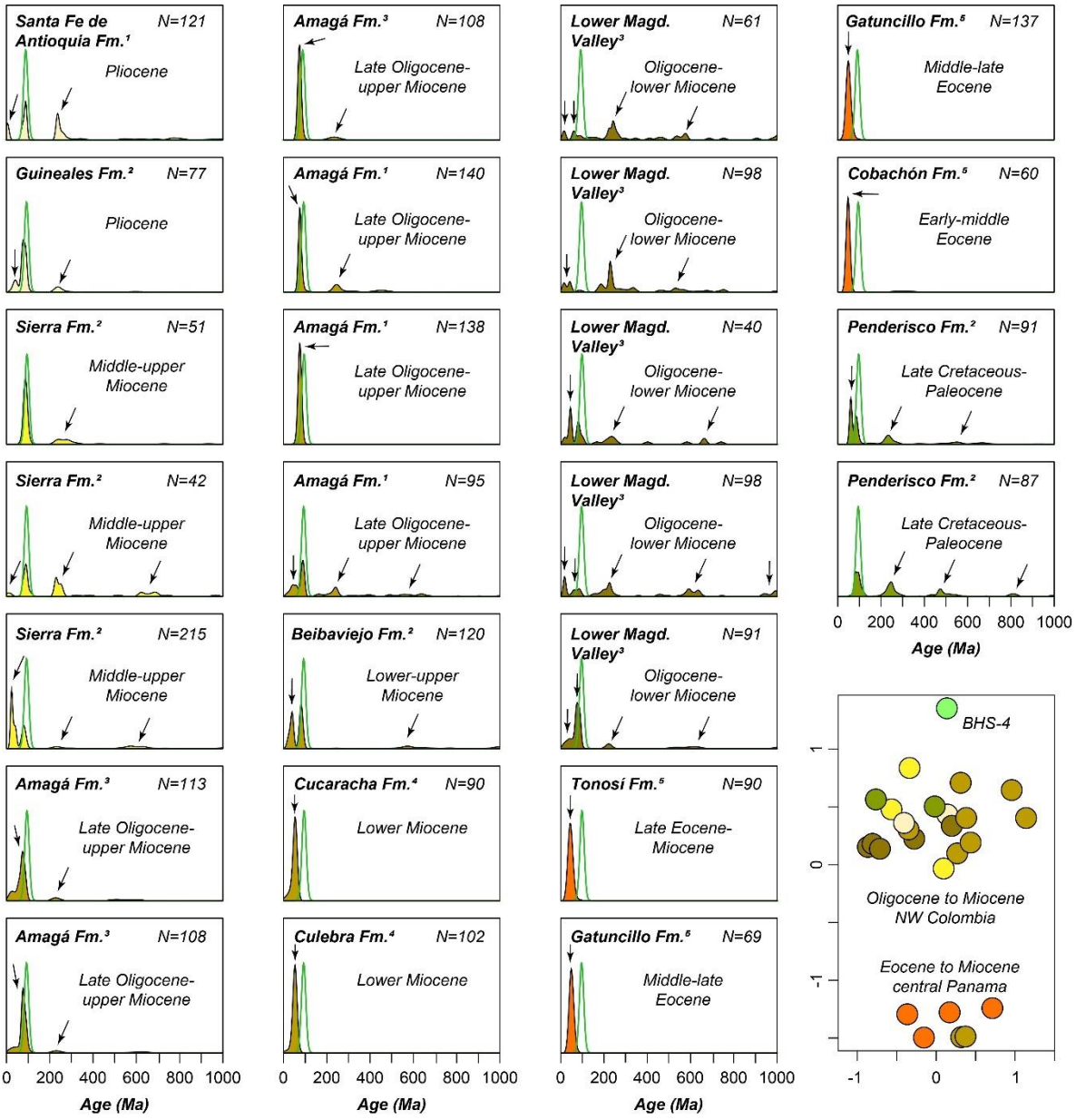

Figure 2.5. Kernel Density Estimate (KDE; bandwidth = 15 Ma) for Upper Cretaceous to Pliocene strata (see proposed accumulation age within each box) of central Panama and northwestern Colombia compiled from Lara et al. (2018)[1], León et al. (2018)[2], Montes et al. (2015)[3], Montes et al. (2012)[4] and Ramírez et al. (2016)[5], including data from sample BHS-4 for comparison (non-shaded black curve); black arrows indicate age peaks absent in sample BHS-4. (Bottom-right) Non-metric multi-dimensional scaling (MDS) showing the dissimilarity (large distance) of sample BHS-4 with respect to Cretaceous to Pliocene samples.

From our compilation of detrital zircon U-Pb data, we aimed to characterize the detrital signature of Cretaceous to Pliocene strata of northwestern Colombia and central-eastern Panama, which may represent previously unmapped sources for the newly analyzed modern sediments of the Cupica Gulf, given its spatial proximity (Fig. 2.1). The compiled geochronological data show that the age spectra of the Cretaceous-Pliocene units are represented by Cretaceous (~90-70 Ma), Eocene (~50 Ma), and/or Triassic and older (>220 Ma) age peaks (Fig. 2.5). These provenance constraints have been used to propose that Eocene to Miocene sediments of central-eastern Panama were derived from the progressive unroofing (erosion) of the CAA (Montes et al., 2012; Ramírez et al., 2016), whereas Cretaceous to Pliocene strata of northwestern Colombia record the input of accreted oceanic domains (e.g. COP, ECLA and CAA) and/or the pre-Cretaceous continental basement of inland domains of the Colombian Andes (Lara et al., 2018; León et al., 2018; Montes et al., 2015; Pardo-Trujillo et al., 2020a). It is worth noting that, regardless of the provenance of the sediments forming the Cretaceous-Pliocene strata, which is beyond the scope of this work, their detrital ages distribution strongly differs from that of sample BHS-4 (Fig. 2.5). This arguably indicates that none of the units included for comparison represents a potential source for the modern sediments of the Cupica Gulf.

Moreover, it has been suggested that variable zircon fertility of source areas and differential erosion rates, as well as secondary processes such as hydrodynamic sorting and temporal storage of sediments along major river systems, could modify the provenance signature of detrital rocks, masking the signal of primary sources (Malkowski et al., 2019; von Eynatten and Dunkl, 2012). However, these processes are mostly effective in large-scale drainage systems, as shown for the Sacramento-San Joaquin rivers in western North America (Malkowski et al., 2019) and the Amazon river in South America (Mason et al., 2019). We consider that the effects of these processes are negligible in our case study because neither the Neogene strata nor the modern sediments appear to have been associated with large drainage systems, as suggested by the textural and compositional immaturity of Oligocene-Miocene rocks and the small catchment area where modern sediments were collected (Fig. 2.1).

An alternative explanation for the distinctive detrital signature of sample BHS-4 could be the reworking of a previously unrecognized sedimentary source, whose primary provenance

would be represented only by ~100-84 Ma arc-related units, like ~80-70 Ma forearc deposits of northwestern Costa Rica, which seem to have been sourced solely by ~90-80 Ma CAA and COP rocks (Calvo, 2003). If this were the case, the ~100-84 Ma zircons found in sample BHS-4, even though recycled from older strata, would have been primarily derived from arc and/or plateau rocks of the Caribbean, which would still allow them to be used to make considerations on SI and the early growth of the CAA.

2.5.4. Timing and mechanisms of subduction initiation in the southwestern Caribbean

Although our database is limited, and our interpretations still need to be tested with further mapping of unexplored areas and in-situ petrological work in the Baudó Range, we claim that our new detrital petrochronological constraints provide valuable insights into the oldest activity of the CAA, whose implications are relevant for the regional tectonic context. When integrated with previous tectono-magmatic models built upon large geological and geophysical data sets (Kerr et al., 2003; Pindell and Kennan, 2009; Whattam and Stern, 2015; Wright and Wyld, 2011), our new data support the existence of subduction-related magmatism at ~100-84 Ma in the southwestern margin of the proto-Caribbean. If correct, the development of this intra-oceanic convergent margin could have led to the formation of the CAA and the ECLA, and the birth of the Caribbean plate (Fig. 2.6). This plate would have been kinematically detached from Farallon lithosphere once it was surrounded by active subduction zones (Boschman et al., 2019), including that newly formed at ca. 100 Ma (Whattam and Stern, 2015), and the southwest-dipping subduction in the northeastern proto-Caribbean beneath the Greater Antilles Arc (GAA) that seems to have been active between ~135 and 70 Ma (Fig. 2.6; Pindell et al., 2012).

Subduction initiation in the southwestern proto-Caribbean at ~100 Ma and early magmatic activity of the ECLA and the CAA at ~100-80 Ma overlap with the main pulse of plume-related magmatism and COP formation (~95-83 Ma; Dürkefälden et al., 2019; Whattam and Stern, 2015), which argues for the proposed plume-related spontaneous SI hypothesis associated with the interaction between the Farallon plate and the Galápagos hotspot (Fig. 2.6; Baes et al., 2021; Boschman et al., 2019; Stern and Gerya, 2018; Whattam and Stern, 2015). The subduction-related signature of our analyzed ~98-87 Ma zircons also show some overlap with mantle-like geochemistry (Fig. 2.3 and 2.4), which has been widely documented

from whole-rock geochemical data and used to track the earliest magmatic activity in the CAA and the ECLA (Buchs et al., 2010; Whattam et al., 2020; Whattam and Stern, 2015), further supporting our interpretation above.

The ECLA has been alternatively interpreted as formed by westward subduction beneath the COP that nucleated on a former transform boundary between the Farallon plate (later becoming the Caribbean plate) and northwestern South America (Weber et al., 2015; Wright and Wyld, 2011). This transform-to-subduction scenario is unlikely, as recent work on the petrology and tectonostratigraphy of Cretaceous magmatic, metamorphic and sedimentary rocks of western Colombia, provide robust evidence for ongoing eastward subduction (not a transform plate boundary) of the Farallon plate beneath northwestern South America (e.g. Zapata et al., 2019). Furthermore, our new and previous petrological constraints suggest an overlap between plateau- and arc-like magmatic activity at ~100-80 Ma, which seemingly took place in an intra-oceanic setting farther to the southwest in the Pacific according to available paleomagnetic data (Hincapié-Gómez et al., 2018), supporting the spontaneous plume-driven SI.

A growing body of evidence gathered from numerical modeling and observations of natural Meso-Cenozoic examples suggests that the formation of a single-slab subduction zone by plume-lithosphere interactions, as seemingly occurred in the southwestern proto-Caribbean at ~100 Ma, requires either a thin oceanic crust in the overriding plate or a thick crust under tectonic extension (Baes et al., 2021, 2020). The prevalence of thin oceanic crust in the proto-Caribbean plate is unlikely as available geophysical constraints suggest that it is mostly represented by thick crust (8-20 km; (Kerr et al., 2003). Thus, the regional stress regime in the nascent Caribbean plate should have been dominantly extensional in order to facilitate spontaneous plume-related SI and the formation of the ECLA and CAA (Baes et al., 2020). The prevalence of an extensional regime is a reasonable assumption because the area of plume-lithosphere interaction that led to SI along the southwestern proto-Caribbean was located in the back-arc region of the older southwest-dipping subduction beneath the GAA (Fig. 2.6; Pindell et al., 2012; Pindell and Kennan, 2009). In this region, extensional tectonics could have been prompted by the subduction of the proto-Caribbean spreading center (PCSC; Fig. 2.6), which was active from at least ~135 Ma to ~70 Ma (Pindell and Kennan, 2009), and could have resulted in the formation of a slab window (Serrano et al.,

2011) that was likely to be accompanied by extension in the upper-plate (Groome and Thorkelson, 2009).

The extensional tectonic regime seemingly prevailed during and shortly after SI as suggested by: i) our new trace element data showing high Th/U ratios of ~98-87 Ma zircons (Th/U > 1 in over 63% of analyzed grains), which arguably indicate high-temperature magma crystallization under tectonic extension (McKay et al., 2018), and ii) the emplacement of 80-70 Ma ophiolitic rocks associated with a slow-spreading zone in a forearc or back-arc setting related to the later stages of growth of the ECLA (Weber et al., 2009; Whattam and Stern, 2015).

2.5.5. Coeval opposite-dipping subduction of the Farallon plate

Recent work on the Cretaceous evolution of the Colombian Andes proposes the existence of a ~120-80 Ma continental arc system built upon Jurassic and older metamorphic rocks (Fig. 2.6; e.g. Zapata et al., 2019). This active continental convergent margin, which seemingly extended farther south to Ecuador and Peru (e.g. George et al., 2021; Mukasa, 1986), was contemporaneous with subduction along the southwestern proto-Caribbean, as supported by our new and previous data indicating ongoing arc-related magmatism in the ECLA and the CAA by ca. 100-80 Ma (Whattam and Stern, 2015). This scenario requires a divergent double subduction of the Farallon plate (Fig. 2.6; e.g. Soesoo et al., 1997), where a fragment of this oceanic lithosphere was being consumed to the north-northwest beneath the nascent Caribbean plate driving the formation of the CAA and the ECLA, and to the east beneath northwestern South America (Fig. 2.6; e.g. George et al., 2021; Jaramillo et al., 2017; Zapata-Villada et al., 2021). The remnant ocean associated with the divergent subduction of the Farallon plate was closed by ~75-65 Ma when the ECLA (the northeasternmost arc spontaneously formed at ~100-90 Ma; Fig. 2.6) was accreted/subducted beneath the northern Andes causing crustal thickening, surface uplift, deformation/metamorphism and post-collisional arc magmatism (George et al., 2021; León et al., 2021a; Zapata-Villada et al., 2021).

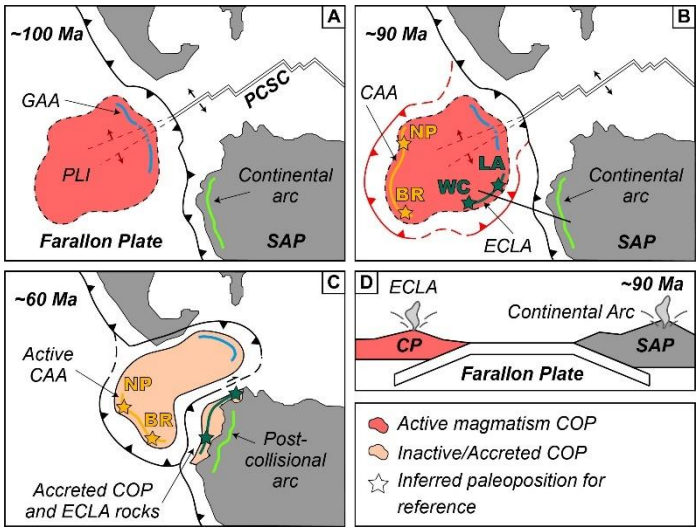

Figure 2.6. Proposed Cretaceous tectonic evolution for the Caribbean, from the integration of our new results and previous models, showing the location of intra-oceanic arcs (thick black lines). A) Plume-lithosphere interaction (PLI) and subduction of the proto-Caribbean spreading center (PCSC) beneath the "Greater Antilles Arc" (GAA; e.g. Pindell and Kennan, 2009); contemporaneous continental arc in the NW South-American plate (SAP). B) Plume-induced SI in the SW proto-Caribbean and formation of the Central American (CAA) and Ecuadorian-Colombian-Leeward Antilles (ECLA) arcs, and birth of the Caribbean plate (CP). Thin black line denotes the location of the cross-section provided in D). C) Closure of the remnant ocean between the continental margin and the ECLA. BR=Baudó Range, LA=Leeward Antilles, NP=Nicoya Peninsula, WC=Western Cordillera. D) Schematic cross-section showing the divergent double subduction of the Farallon plate between ~90-70 Ma.

Although the ECLA and the CAA could have simultaneously formed by spontaneous plume-driven SI, as suggested by the overlap of our new ~98-87 Ma arc-related zircon U-Pb ages for the CAA and previously reported ages for the ECLA (~95-75 Ma; e.g. Pardo-Trujillo et al., 2020a; Thompson et al., 2004; Vallejo et al., 2006; Villagómez et al., 2011; Weber et al., 2015; Wright and Wyld, 2011), their lateral continuity seems unlikely. We consider this hypothesis because the CAA (the southwesternmost arc spontaneously formed at ~100-90 Ma; Fig. 2.6) collided with South America ~50 Myr later than the ECLA (at ~20-15 Ma; León et al., 2018), which had already collided with the continental paleomargin by ~75-65 Ma (Vallejo et al., 2006). The provenance of the newly analyzed Oligocene-middle Miocene strata, showing mixed CAA- and continent-derived provenance, supports the early Miocene interaction between the CAA and the South American margin, as previously suggested from sedimentological and thermochronological constraints (Lara et al., 2018; León et al., 2018). We consider that the CAA and ECLA were probably separated by an along-strike gap related to lateral variations of the subduction configuration or formed in disconnected subduction zones. This would challenge the configuration of a single-slab geometry predicted for plume-related SI involving thick oceanic crust under tectonic extension (Baes et al., 2020).

2.6. Conclusions

Neogene strata exposed along the northern Pacific coast of Colombia were mostly sourced by Cretaceous to Eocene rocks of Caribbean-derived intra-oceanic arcs that are currently part of the Colombian Andes, with contribution of the pre-Cretaceous north Andean continental basement. Oligocene to Miocene sedimentary rocks are being recycled through minor rivers draining the central-southern Baudó Range towards the Pacific Ocean, as evidenced by our provenance analyses of modern sediments of the Tribugá Gulf.

Conversely, detrital zircon petrochronology of modern sediments of the northern Pacific coast of Colombia (Cupica Gulf) are probably derived from ~100-84 Ma arc-related magmatic rocks exposed in the northern Baudó Range. Trace element composition of Upper Cretaceous zircons is characterized by relative depletion in HFSE such as Nb and Ti, enrichment in incompatible elements (e.g. U and Ce), and shows positive Ce and Eu anomalies, which together with low Hf and total REE abundances, arguably indicates a

derivation from mafic-intermediate subduction-related rocks, with minor contribution of mantle-related signatures. These rocks might correlate with the Upper Cretaceous units of the Central American arc (CAA), which could have formed as a consequence of plume-related subduction initiation at ~100 Ma along the southwestern proto-Caribbean region, together with the Ecuadorian-Colombian-Leeward Antilles arc (ECLA), onto the Caribbean Oceanic Plateau (COP). North- to northwestward subduction initiation beneath plateau-like rocks along the southwestern proto-Caribbean by plume-lithosphere interaction at ~100-90 Ma could have led to the birth of the Caribbean plate from former Farallon lithosphere. Coeval east-dipping subduction of the Farallon plate beneath northwestern South America could have resulted in a divergent double subduction setting, represented by opposite-dipping subduction at the edges of the Farallon oceanic lithosphere. The associated remnant ocean was closed by ~70 Ma where the intra-oceanic Caribbean arcs (i.e. ECLA) began to collide with the northwestern South-American continental margin.

CHAPTER 3

3. Initial accretion of Caribbean-derived intra-oceanic arcs and the onset of topographic growth of the Colombian Andes during the Late Cretaceous-Paleogene

3.1. Introduction

The process of mountain building is a key factor shaping Earth's landscape, climate and biodiversity (Blisniuk et al., 2006; Rahbek et al., 2019). In subduction-related orogens such as the Andes, crustal growth and landscape evolution are mostly determined by changes in plate coupling, driven by the convergence velocity and obliquity, and subduction angle (e.g. Horton, 2018b). However, the collision of highly buoyant intra-oceanic arcs or plateaus can drastically modify the upper-plate deformational regime and its subsequent topographic evolution (Montes et al., 2019).

The onset of the Andean orogeny has been interpreted as the consequence of a margin-scale transition towards a strongly compressional regime triggered either by the accelerated westward drift of South America or by slab anchoring in the lower mantle that promoted upper-plate contraction and uplift (Faccenna et al., 2017; Horton, 2018b). In the northern (Ecuadorian and Colombian) Andes, the earliest mountain building is attributed to the Late Cretaceous-Paleocene collision of an island arc built on the Caribbean oceanic plateau, against the northwestern margin of the South-American plate (Bayona, 2018; Pardo-Trujillo et al., 2020a; Villagómez and Spikings, 2013). This collision seems to have triggered the nascent topography of the Central Cordillera of Colombia together with the formation of syn-orogenic basins both in the collisional front and the foreland (Bayona et al., 2020; Pardo-Trujillo et al., 2020a). The magnitude of this earliest uplift of the Colombian Andes has been indirectly estimated from the stratigraphic and erosional record (Horton, 2018a), as material suitable for a quantitative paleoaltimetry analysis such as pollen or stable isotopes has not been found (Garzione et al., 2008; Saylor and Horton, 2014).

Here, we apply a new paleoaltimetry technique that uses the geochemistry of arc-related magmatic rocks (Hu et al., 2020) to provide for the first time quantitative estimates of the early topographic growth of the northern Colombian Andes during the Cretaceous to Eocene (~97-53 Ma). Our results demonstrate the value of the magmatic record as a proxy to assess the long-term topographic evolution of convergent margins and highlight the ability of the collision of thick and buoyant oceanic crust to trigger kilometer-scale orogenic uplift.

3.2. Geological Background

The Central Cordillera in the Colombian Andes is characterized by a rugged morphology in its southern segment (~1°N to 5°N) with elevations up to ~5,300 m.a.s.l., and a large topographic plateau with an average elevation of ca. 2,500 m.a.s.l. in its northern segment (~5°N to 7.5°N). Its basement is mostly composed of Jurassic and older low- to medium-grade metamorphic rocks (see a summary in León et al., 2019) which are intruded by arc-related units spanning the Jurassic to early Eocene (Leal-Mejía et al., 2019), and the modern volcanic arc. The preserved sedimentary record within the Cordillera is scarce but includes Upper Cretaceous marine strata (Sarmiento-Rojas, 2019), and minor continental Upper Cretaceous and Neogene deposits located on its western flank (Lara et al., 2018; Pardo-Trujillo et al., 2002). These sequences overlie Lower to mid-Cretaceous back-arc basin deposits (Avellaneda-Jiménez et al., 2020; Zapata et al., 2019).

The Central Cordillera lithotectonic domain is sutured to the west by the Romeral Fault System (RFS; Fig. 3.1) with the Cretaceous oceanic plateau-arc system that forms the basement of the Western Cordillera (Kerr et al., 1997), which started colliding with northwestern South America at ca. 70 Ma (Pardo-Trujillo et al., 2020a; Vallejo et al., 2006). Relicts of two Meso-Cenozoic magmatic arcs in the South-American plate are found in the Central Cordillera: a Cretaceous pre-collisional arc (PRC) product of the subduction of the proto-Caribbean lithosphere, and a Paleogene post-collisional arc (POC) product of the oblique subduction/accretion of the Caribbean oceanic plateau (Fig. 3.1; Bustamante et al., 2017; Cardona et al., 2018).

The Santa Marta Range (SMR) in northernmost Colombia is one of the highest coastal mountains on Earth reaching ~5,800 m.a.s.l. (Fig. 3.1). It is an isolated massif composed of

Proterozoic and Paleozoic medium- to high-grade metamorphic rocks, intruded by Jurassic and Paleogene arc-related units (Tschanz et al., 1974), which are genetically related to coeval intrusives of the Central Cordillera (Montes et al., 2019, 2010). The SMR was likely part of the Central Cordillera until Eocene-Oligocene times, as suggested by structural and geochronological constraints (Montes et al., 2010; Mora-Bohórquez et al., 2017), when it started migrating to its present position, thus sharing similar geodynamic and magmatic histories during the Cretaceous and early Paleogene.

3.3. Methods

We applied a novel method (Chapman et al., 2015; Hu et al., 2020; Profeta et al., 2015) that uses trace elements abundances (e.g. Sr, La, Y and Yb) of subduction-related magmatic rocks to estimate the ancient crustal thickness and isostatically compensated paleoelevations of the Colombian Central Cordillera and the SMR from available geochemical datasets. This method relies on: i) the stability of garnet at high-pressure conditions and its ability to fractionate Y and heavy rare earth elements (HREE; Mamani et al., 2010), and ii) the assumption that the long-wavelength topography of most orogenic systems is isostatically compensated (Lee et al., 2015; Zhu et al., 2017). The prevalence of Airy isostasy is a reasonable assumption as demonstrated by the close relationship between crustal thickness and elevation at most (>2 km-high) mountain belts, as shown by Lee et al. (2015) using data from global crustal models. Recent crustal thickness estimates for the Colombian Andes also suggest a good correlation between high elevations and thick crust, supporting Airy isostasy at present-day for the region (Poveda et al., 2015).

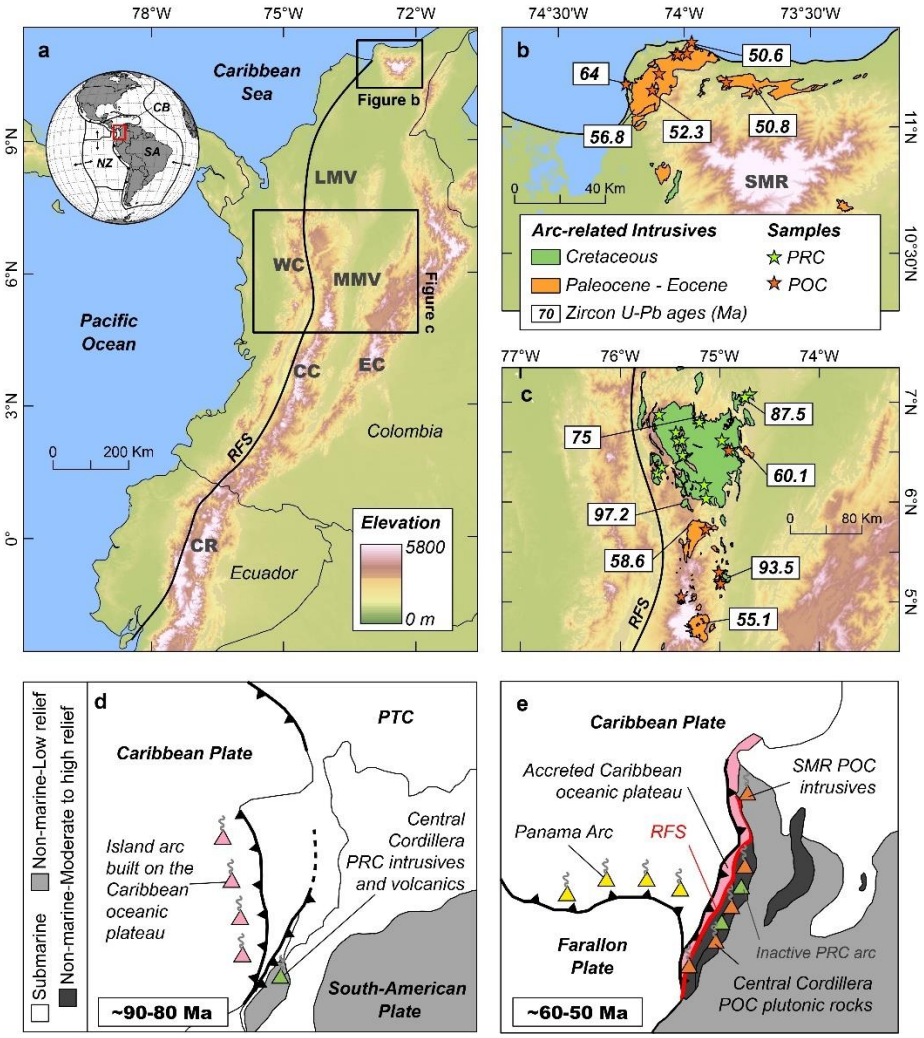

Figure 3.1. Location of the northern Andes and spatial distribution of geological units discussed in this work. a) Regional map showing the main topographic features of the Colombian and Ecuadorian Andes. b) and c) Exposure area of Cretaceous (PRC) to Eocene (POC) plutonic rocks in the SMR and the northern Central Cordillera, respectively; from Gómez-Tapias et al. (2015), with location of samples used for estimations of crustal thickness and paleoelevations, and some zircon U-Pb ages. d) and e) Simplified paleogeography of the northwestern Andes and the southern Caribbean region for the mid- to Late Cretaceous and the Paleogene, respectively; modified from Bayona (2018) and Montes et al. (2019). Abbreviations are CB = Caribbean plate, CC = Central Cordillera, CR = Cordillera Real, EC = Eastern Cordillera, LMV = Lower Magdalena Valley, MMV = Middle Magdalena Valley, NZ = Nazca plate, PRC = Pre-collisional arc, POC = Post-collisional arc, PTC = Proto-Caribbean, RFS = Romeral Fault System, SA = South-American plate, SMR = Santa Marta Range, WC = Western Cordillera.

A valuable contribution of this empirical calibration, compared to conventional isostatic analyses (Zhu et al., 2017), is that by directly correlating Sr/Y and $(La/Yb)_N$ with elevation, assumptions regarding crustal or mantle density values, whose estimation could be problematic and may introduce large uncertainty into (paleo)altimetric calculations (Gvirtzman et al., 2016; Hu et al., 2020), are avoided. This can also account for the potential effects of the thickening of the lithospheric mantle (i.e. attenuation of isostatic uplift), which is likely to occur in tune with crustal thickening (Molnar et al., 1993).

We compiled 122 whole-rock geochemical, and 56 isotopic (Sr-Nd-Pb) analyses of intermediate-acidic intrusives from both mid- to Upper Cretaceous (PRC; ~97-73 Ma) and Paleocene to Eocene arcs (POC; ~60-53 Ma) in both the Central Cordillera and SMR. Our dataset was extracted from (Leal-Mejía et al., 2019) and references therein, and additional sources (Almeida and Villamizar, 2012; Cardona et al., 2020, 2014, 2011; Duque-Trujillo et al., 2019; Jaramillo et al., 2017; Ordoñez et al., 2001). We only used samples with SiO2 = 55-70 wt%, MgO < 6 wt%, and Rb/Sr = 0.05-0.20, following the protocols of Hu et al. (2020) in order to eliminate the effects of highly fractionated rocks (Chapman et al., 2015). Sr/Y and $(La/Yb)_N$ outliers were identified using the Tukey's method (Tukey, 1977), and excluded from crustal thickness and paleoelevation calculations and graphs.

Crustal thickness and paleoelevation estimates are reported with the associated 1σ error resulting from propagating the uncertainty of the empirical equations of Hu et al. (2020) and the standard deviation of each dataset used for calculations. A Mann-Whitney U-test was used to assess the significance of the differences in the distributions of PRC and POC geochemical and isotopic data (Mann and Whitney, 1947), and all analyses were done with R (R Development Core Team, 2017).

3.4. Results

3.4.1. Geochemical constraints of pre- and post-collisional magmatic rocks

The Ba/La and Th/La values of both the PRC and POC datasets range from ~9 to 220 and ~0.1 to 0.5, respectively. Ratios of high field strength elements (HFSE) are also similar for both magmatic suites, which plot together in the Nb/Yb (~0.5 to 11.5) vs Zr/Yb (~15 to 240)

diagram (Fig. 3.2). Sr/Y values of PRC (two outliers excluded) span from 6.5 to 56.5 with a median value of 18.9, whereas they range between 22.7 and 63.4 for POC (four outliers excluded), yielding a higher median of 40.5; the distribution in the two groups differed significantly (Mann-Whitney U = 115, $p<0.005$). Likewise, $(La/Yb)_N$ ratios (normalized to the chondrite composition of McDonough and Sun (1995) span from 2.1 to 14.3 for PRC (no outliers), with a median of 6.0, whereas they range from 5.3 to 16.7 for POC (three outliers excluded), yielding a median value of 11.2; the difference in the distributions of the two groups was found to be significant (Mann-Whitney U = 86, $p<0.001$; Fig. 3.2).

Initial $^{87}Sr/^{86}Sr$ ratios of PRC and POC range from 0.702916 to 0.709461, and from 0.703092 to 0.710654, respectively independent of the Sr (ppm) concentration, and yielded median values of 0.704194 (PRC) and 0.704953 (POC); the distribution of the two datasets differed significantly (Mann-Whitney U = 115, $p<0.05$). Initial $^{143}Nd/^{144}Nd$ isotopic ratios span from 0.512544 to 0.513039 for PRC (εNd_i from -1.0 to +8.3), with a median of 0.512722, whereas they range between 0.512020 and 0.512808 for POC (εNd_i from -10.7 to + 4.8), yielding a lower median value of 0.512576; the distribution of the two datasets differed significantly (Mann-Whitney U = 98, $p<0.001$; Fig. 3.2).

3.4.2. Crustal thickness and paleoelevation estimates

The PRC crustal thickness values estimated using the Sr/Y range between ~15 and 70 km, with a median value of 29.0 $\pm$ 19.1 km (1σ), whereas they span from ~33 to 79 km for POC estimates, yielding a median of 53.0 $\pm$ 11.7 km (1σ). Similar results were obtained using the $(La/Yb)_N$, with PRC crustal thickness ranging from ~16 to 57 km, yielding a median of 38.4 $\pm$ 13.9 km (1σ), and POC values spanning from ~36 to ~60 km with a higher median value of 51.8 $\pm$ 11.1 km (1σ).

Sr/Y-derived PRC paleoelevation ranges from ~0.2 to 4.9 km with a median value estimated at 1.3 $\pm$ 1.6 km (1σ), whereas it spans from ~1.7 to 5.6 km for POC, yielding a median of 3.4 $\pm$ 1.0 km (1σ). Likewise, PRC paleoaltimetry estimations from the $(La/Yb)_N$ ratios span between -0.5 and 4.1 km, which yielded a median of 2.0 $\pm$ 1.3 km (1σ), whereas POC paleoelevations range from ~1.7 to 4.5 km with a median value of 3.5 $\pm$ 0.8 km (1σ; Fig. 3.3).

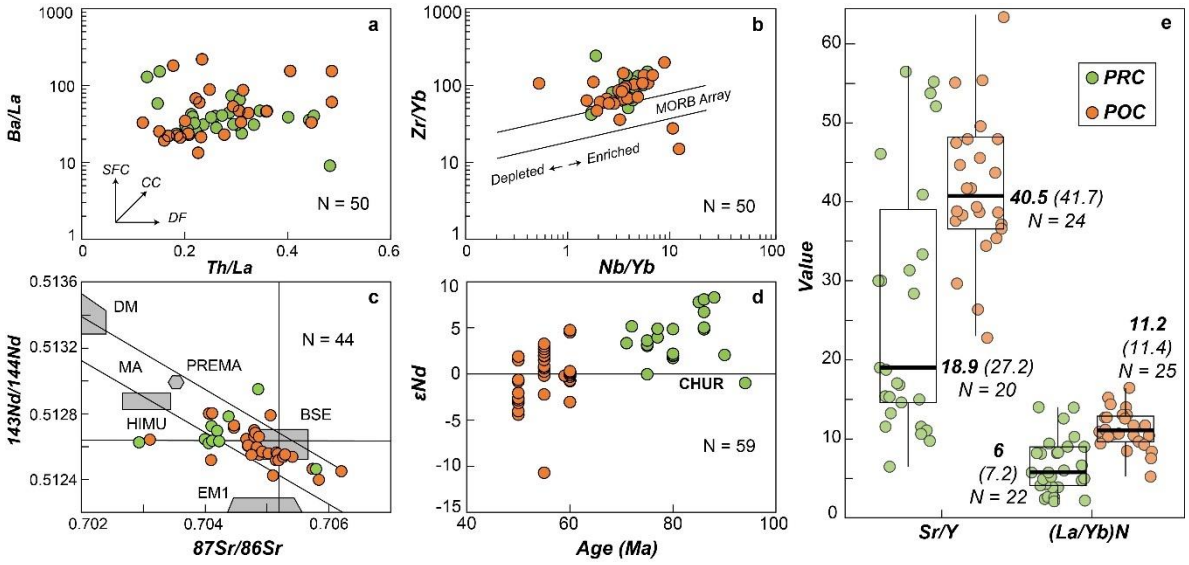

Figure 3.2. Geochemical features of compiled samples from PRC and POC plutonic rocks of the northern Central Cordillera and the SMR. a) Th/La versus Ba/La diagram to evaluate the nature of the slab-derived components; CC = Crustal contribution, DF = Differentiation, SFC = Subduction fluid component. b) Nb/Yb versus Zr/Yb ratios used to assess the compositional nature (i.e. enrichment) of magma sources after Pearce and Peate (1995). c) Sr-Nd isotopes diagram showing the mantle signature and the contribution of evolved reservoirs for PRC and POC magmas; BSE = Bulk Silicate Earth, DM = Depleted Mantle, EM1 = Enriched Mantle '1', HIMU = high 238U/204Pb, MA = Mantle Array, PREMA = Prevalent Mantle (Zindler and Hart, 1986). d) Age versus εNd diagram showing the major transition towards more radiogenic signatures after ~70 Ma; CHUR is the chondritic uniform reservoir. e) Boxplot diagram, after removing outliers, for the Sr/Y and (La/Yb)N ratios of PRC and POC rocks, showing the estimated median (bold numbers) and mean (regular numbers) values. N is number of samples.

3.5. Discussion

3.5.1. Subduction-related origin for both PRC and POC intrusives

The trace element paleoaltimetry method applied here was developed to be used in subduction-related or collisional magmatic rocks (Hu et al., 2020). Multiple lines of evidence indicate that both PRC and POC rocks were originated from subduction-modified mantle sources, including depletion in high field strength elements (HFSE) such as Nb and Ti, and relative enrichment in large ion lithophile elements (LILE) and light REE (Fig. 3.2; Pearce et al., 1984). Both PRC and POC follow the mantle array composition in the Sr-Nd isotopic diagram, also showing the contribution of isotopically evolved materials (Fig. 3.2). The nature of such evolved components could be related either to assimilation or the contribution of melts or fluids from the subducting slab (Mibe et al., 2011).

The largely variable abundance of Ba (175-2072 ppm), Sr (215-1147 ppm) and Pb (0.6-25.2 ppm) of both PRC and POC rocks is akin to the interaction of slab-derived fluids with the magma source and host-rock assimilation rather than the contribution of slab melts, as shown by the high Ba/La ratios (~10-220.4) and low Th/La values (0.1-0.5, Fig. 3.2; (Mibe et al., 2011). Thus, the adakite-like high Sr/Y and relative depletion in heavy REE (HREE; e.g. Y, Yb) values is a consequence of high-pressure differentiation under garnet and/or amphibole stability conditions, as previously interpreted (Bustamante et al., 2017; Cardona et al., 2018). Available petrographic and geochemical constraints for POC rocks allow neglecting the presence of plagioclase-rich cumulates, which could alternatively explain the high Sr/Y ratios due to the ability of plagioclase to incorporate Sr at low pressure conditions (Chapman et al., 2015). The evolved Sr isotopic composition of both the PRC and POC arcs further supports the contribution of crustal assimilation, which seems to have been more effective for the POC arc, as indicated by the more radiogenic initial $^{143}Nd/^{144}Nd$ and associated εNd_i (Fig. 3.2; e.g. DePaolo et al., 2019).

3.5.2. Surface uplift of the northern Colombian Andes during the early Paleogene

Sr/Y and $(La/Yb)_N$ of the here analyzed PRC and POC rocks are dispersed, resulting in a high uncertainty for the paleoaltimetry and crustal thickness estimations (Figs. 3.2 and 3.3). Nevertheless, the results of the Mann-Whitney U-test performed for comparison, showed that

the distributions of PRC and POC data differed significantly, indicating higher Sr/Y and $(La/Yb)_N$ POC ratios, as well as more evolved Sr-Nd isotopic signatures, which we arguably interpret as regional crustal thickening of the Colombian Andes and associated kilometer-scale isostatic surface uplift of the nascent Central Cordillera and the SMR. We combine our paleoaltimetry estimations with up-to-date sedimentological and thermochronological constraints from the Cretaceous to Paleogene north Andean hinterland and foreland systems to discuss on a plausible scenario for the early topographic growth.

Regional stratigraphic reconstructions suggest that the elevated areas of the proto-Central Cordillera that had a relatively low median elevation of ~1.3 km, as estimated here (Fig. 3.3), were mostly surrounded by a shallow-marine platform during the Cretaceous (Bayona, 2018; Sarmiento-Rojas, 2019). The presence of Early to mid-Cretaceous relief and relatively low topography is further supported by the quartz-rich composition of coeval shallow-marine to deltaic strata preserved in the hinterland and foreland basins, which has been interpreted as the record of intense chemical weathering and reworking of older sedimentary sequences in subaerially exposed areas of the proto-Central Cordillera (Cardona et al., 2020; Duarte et al., 2018).

Limited Early Cretaceous topography recorded in the northern Andes also likely persisted in the central and southern Andes, as suggested by the dominance of shallow-marine depositional settings and the provenance from easterly intra-plate sources (i.e. limited sediment dispersal from the growing hinterland), together with the presence of a thin (~20 km-thick) crust (e.g. Gianni et al., 2020; Horton, 2018a; Hurtado et al., 2018). Such scenario was probably associated to margin-scale extensional tectonics and the formation of back-arc and intra-arc basins, which shifted to a compressional-neutral regime between ~120-90 Ma in response to the northward propagation of the opening of the Atlantic Ocean and subsequent westward drift of South America (Gianni et al., 2020). However, as suggested from the stratigraphic record and our paleoelevation estimates, this continental-scale tectonic reorganization seems not to have largely contributed to the topographic growth of the Andes.

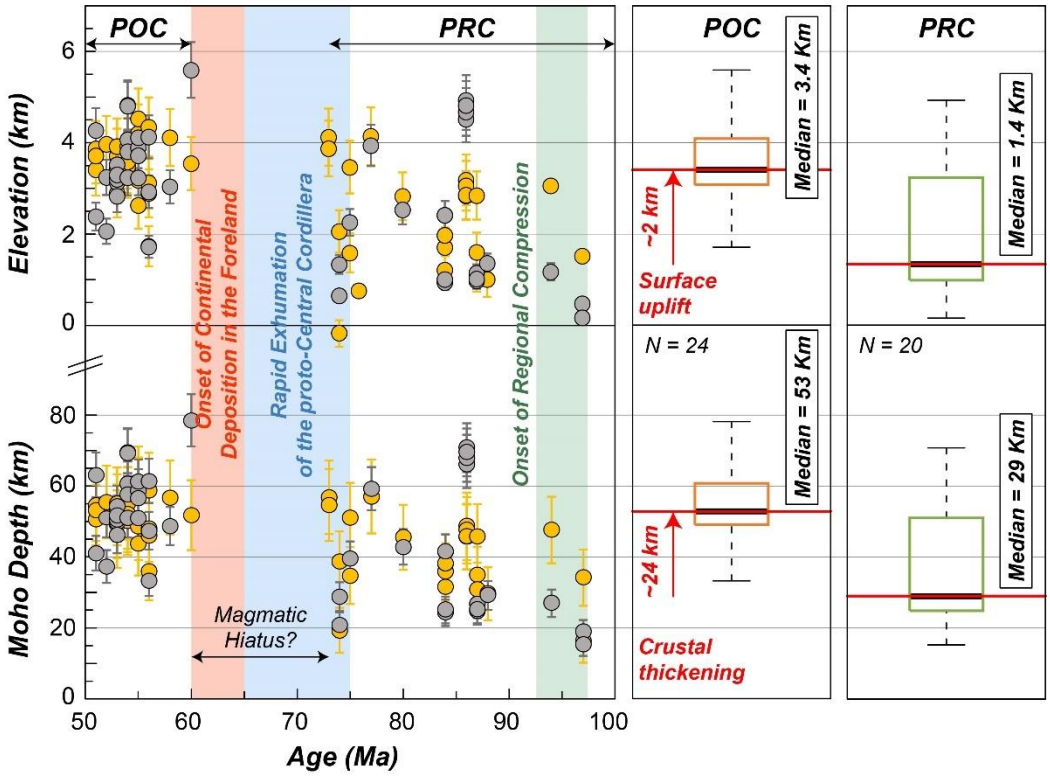

Figure 3.3. Results of the Cretaceous-Paleogene crustal thickness and paleoelevation estimates. Left panel shows the age versus estimated Moho depth (bottom) and paleoelevation (top) plots after removing outliers, estimated from Sr/Y (gray circles) and (La/Yb)N ratios (yellow circles). Error bars are from the upper and lower values obtained from the empirical equations of Chapman et al. (2015) and Profeta et al. (2015) for crustal thickness (Sr/Y and (La/Yb)N, respectively), and from Hu et al. (2020) for paleoelevation. Right panel shows boxplots for PRC and POC estimated crustal thickness (bottom) and paleoelevation (top) from the Sr/Y ratios. Red horizontal lines indicate median values for each dataset.

There is a regional transition towards a strongly compressional tectonic regime accompanied by a shift from marine to continental environments during the Late Cretaceous-Paleogene in the northern Andes. This transition is recorded in the northern Colombian basins, which was coeval with an increase of sediment influx from the Central Cordillera into the adjacent Middle Magdalena Basin concomitant with accelerated flexural subsidence (Bayona et al., 2008; Gómez et al., 2003, 2005), and rapid cooling of pre-Upper Cretaceous volcaniclastic and intrusive rocks during ca. 70-60 Ma (Villagómez and Spikings, 2013; Zapata et al., 2020).

The acceleration of the exhumation rates of the proto-Central Cordillera and the Ecuadorian Andes farther to the south, and the coupled evolution of adjacent sedimentary basins have been attributed to the collision of the Caribbean oceanic plateau (Montes et al., 2019; Pardo-Trujillo et al., 2020a; Vallejo et al., 2019), which however, does not imply surface uplift, especially at tropical latitudes where high rates of weathering and erosion could keep up with rock uplift (England and Molnar, 1990). Our results suggest that there was indeed an isostatic topographic uplift up to 2 km of the northern Central Cordillera of Colombia driven by the collision of the Caribbean oceanic plateau reaching a median elevation of 3.4 km by the Paleogene (Fig. 3.3), which could have also extended into the Ecuadorian Andes given their similar Cretaceous-Paleogene erosional exhumation and tectono-stratigraphic history (Montes et al., 2019; Spikings and Simpson, 2014). These estimates correspond to the isostatic component of the paleoelevation and do not consider the possible presence of residual topography, which could be in the order of -1 km to 1 km (Rutledge and Mahatsente, 2017; Yarce et al., 2014), values that are within the associated error range of our calculations.

In spite of the buoyancy of the Caribbean oceanic plateau, and hence its resistance to subduction (Cloos, 1993), numerical models and geological observations from analogue scenarios have demonstrated that thick oceanic crust (e.g. island arcs, ridges or plateaus) can be either accreted and/or sunk beneath active continental margins, triggering arc-related magmatism and kilometer-scale uplift of the overriding plate (Tetreault and Buiter, 2012; Timm et al., 2014; Vogt and Gerya, 2014). It seems that the Late Cretaceous collisional episode in the northern Andes involved both accretion and subduction of the Caribbean plateau. This could be attributed to the combined effect of the negative buoyancy of the old

oceanic lithosphere surrounding the plateau (>120 Ma; Boschman et al., 2019), and the presence of lithospheric weaknesses or a detachment layer due to either formational residual heat or intra-oceanic hydrothermal activity, which prevented the complete subduction of the plateau-like crust (Vogt and Gerya, 2014).

Collision of oceanic plateaus may involve underplating and subsequent slab break off of the subducting lithosphere, which could result in voluminous magmatism as a consequence of melting of either the sinking slab or the lowermost crust of the overriding plate due to thermal perturbance by asthenospheric upwelling (Davies and von Blanckenburg, 1995; Vogt and Gerya, 2014). This seems not to be the case for the Late Cretaceous collision of the Caribbean oceanic plateau against northwestern South America because: i) PRC and POC rocks are likely derived from typical subduction-related melts associated to high-pressure differentiation, and ii) there is no evidence for a post-collisional increased magmatic input. Instead, there was an apparent magmatic lull shortly after or during the collision of the plateau (Duque-Trujillo et al., 2019; Jaramillo et al., 2017), followed by vanishing and widening of the arc together with widespread deformation of the upper plate (Bayona et al., 2020, 2012; Bustamante et al., 2017), consistent with a scenario of slab flattening caused by buoyancy of the oceanic plateau and its complicated subduction (Rosenbaum and Mo, 2011).

3.5.3. Onset of topographic growth and evolution in the northern Andes

The along-strike segmentation of the Andes, represented by an accretionary and a subduction-dominated orogen in the northern and central-southern segments, respectively, may involve distinct tectonic drivers of mountain uplift that could operate simultaneously at different temporal and spatial scales (e.g. Ramos, 2009). Despite large-scale plate kinematic and/or mantle-related processes likely contributed to the earliest topographic growth in the central and southern Andes (Faccenna et al., 2017; Gianni et al., 2020; Horton, 2018b), abundant tectono-stratigraphic and magmatic evidence supports the major role of the Late Cretaceous-Paleogene collision of the oceanic plateau on the earliest growth of the northern Andes (Montes et al., 2019).

For instance, a northward topographic growth of the Central Cordillera during the Maastrichtian-Paleocene is suggested by integrated stratigraphic, provenance and structural constraints of foreland deposits (Bayona, 2018). This spatial trend is consistent with

paleogeographic reconstructions proposing the northward advance of the Caribbean plateau collision since ca. 75 Ma (Montes et al., 2019), which strengthens the interpretation of the collisional episode as the main driver of early surface uplift in the northern Andes. This collision-driven POC topography, was similar to the modern average elevations of the Central Cordillera, which could have either remained constant over the past ~50 Myr or diminished via erosion and subsequently regained by the contribution of the Cenozoic collision- and subduction-related tectonics (León et al., 2018).

On the other hand, several lines of evidence suggest that the modern elevations of the Eastern Cordillera, were only reached during the late Miocene-Pliocene as a consequence of increased crustal shortening (Mora et al., 2020). However, sedimentological and thermochronological constraints allowed documenting the presence of isolated uplift events related to an unquantified growing topography since the Paleocene-Eocene, which were likely related to the widening of the northern Andes in response to the shallow subduction of the Caribbean oceanic plateau (Bayona et al., 2020; Parra et al., 2012). Recent geodetic studies have estimated modern shortening rates of ca. 4 mm/yr, which are inconsistent with a very recent (~6-3 Ma) origin of the Eastern Cordillera topography as suggested from paleobotanical constraints, and instead favor an Eocene-Oligocene age for the onset of mountain building (Mora-Páez et al., 2016).

The potential existence of mid- to high-elevation areas along and across the Andes since the Paleogene, as a consequence of subduction- and collision-related tectonic mechanisms, would challenge the widely accepted monotonic uplift-driven late Neogene neotropical biodiversification (Baker et al., 2014). This would require additional but not exclusive climate phenomena and/or the presence of latitudinal structural and morphological discontinuities and disparate topographic growth of the Andean mountain chain, which have been indirectly suggested from the along-strike segmentation of the Cenozoic erosional exhumation history (Horton, 2018a; Spikings and Simpson, 2014).

3.6. Conclusions

The trace-element composition (e.g. Sr/Y and La/Yb ratios) of mid-Cretaceous to lower Eocene arc-related rocks exposed along the northern Central Cordillera of Colombia, suggest a ca. 20 km crustal thickening in response to the collision of the Caribbean oceanic plateau against the continental paleomargin during the Late Cretaceous-Paleogene. Available tectono-stratigraphic data indicate that this collisional episode resulted in a regional shift from marine to deltaic and continental accumulation settings in foreland basins, which may suggest the occurrence of accelerated topographic growth across the north-Andean region.

Despite the large uncertainty of our paleoaltimetry estimations, we provide a first-order quantitative approximation of up to 2 km of surface uplift of the proto-Central Cordillera during the early topographic growth of the northern Andes that is in good agreement with available tectono-stratigraphic constraints from hinterland and foreland systems. This kilometer-scale surface uplift of the northern Colombian Andes, in response to the plateau collision, is consistent with constraints from numerical modeling and geological observations from similar tectonic settings (e.g. southern Alaska), and therefore demonstrates the primary role that the collision/subduction of thickened oceanic features play on the mountain building history along convergent margins.

CHAPTER 4

4. From collision to subduction: Neogene tectonostratigraphic evolution of the northern Colombian forearc basin

4.1. Introduction

In this chapter, we combine new structural, stratigraphic and multi-proxy provenance data of Oligocene to Pliocene strata and modern sediments of the northern Colombian forearc (Atrato Basin; AB) with a review of previous cartographic, stratigraphic, structural, thermochronological and biogeographic data to reconstruct its Neogene deformational history and topographic growth. Our goal is to provide a tectonostratigraphic framework related to the coupled evolution of depositional settings and source areas of forearc basins in accretionary orogens during the transition from collision to subduction. The chapter is organized in such a way that, first, we provide a description of the Neogene tectonic and geologic setting of the Colombian Andes, followed by a review of the available stratigraphic and paleogeographic history of the AB and the nearby suture basin, which are complemented with new regional field observations from the Quibdó, Cupica, and Tribugá study areas. Then, we present new stratigraphic constraints, together with new provenance data and structural observations, which we therefore integrate with published sedimentological and thermochronological data to reconstruct the timing and nature of changes in the source-to-sink systems and correlate them with the deformational record and the subsidence/uplift history in a regional geodynamic context.

4.2. Neogene tectonics and regional geology of the northwesternmost Andes

4.2.1. Tectonic evolution

The Oligocene-Miocene to present-day tectonic activity along the northwesternmost Andes has been shaped by the interaction between the Caribbean, Farallon/Nazca and South-

American plates (Echeverri et al., 2015b; León et al., 2018; Montes et al., 2019; Wagner et al., 2017). Such interactions involved multiple geodynamic processes, including arc-continent collision, collision/subduction of aseismic ridges, subduction (re)initiation, and slab flattening, which seemingly provided first-order controls on the upper-plate deformational, tectonostratigraphic and magmatic evolution.

Nowadays, the Colombian western continental margin is tectonically segmented along-strike, with a shallow (~10-15°) subduction regime north of ~5°N, and a steep (~20-30°) slab to the south (Fig. 4.1; Chiarabba et al., 2016; Syracuse et al., 2016). This segmentation is interpreted to be caused by the tearing of the young Nazca slab (Lonsdale, 2005) at ca. 5°N, which is supported by the absence of active volcanoes north of this latitude and a ~250 km right-lateral offset of deep seismicity (Ojeda and Havskov, 2001). Despite the precise timing and drivers for the modern tectonic segmentation of the Colombian Andes (i.e. tearing of the Nazca plate and establishment of a flat slab subduction north of ~5°N) are still matters of debate, it seems that such configuration was established shortly after the early-middle Miocene collision of the intra-oceanic Cretaceous-Eocene CAA (Chiarabba et al., 2016; Wagner et al., 2017). This island arc evolved during the Cretaceous to Oligocene as a consequence of the north-northwestward subduction of the Farallon plate beneath the trailing edge of the Caribbean plate.

After this collisional episode, the subduction of the buoyant Nazca plate was (re)initiated beneath northwestern South America at ~14-12 Ma, causing the emplacement of post-collisional arc-related (sub)volcanic and plutonic rocks mostly along the suture zone (Fig. 4.2; León et al., 2018; Rodríguez and Zapata, 2012). Subsequently, the arc front apparently migrated ~30 km eastward to the intervening Cauca Valley that lies between the Western and Central Cordilleras, and finally widened as far as to the Eastern Cordillera and vanished as a consequence of slab flattening during the latest Miocene (Jaramillo et al., 2019; Monsalve et al., 2019; Wagner et al., 2017).

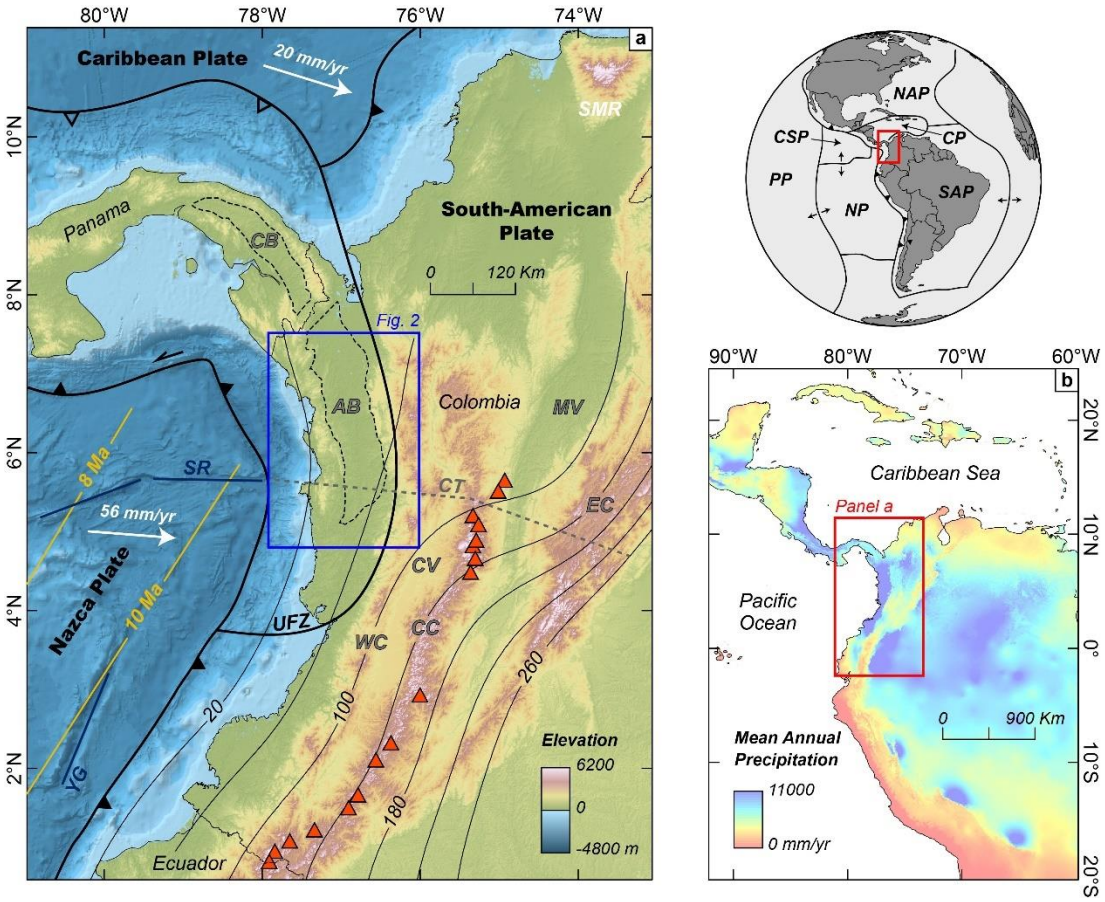

Figure 4.1. Regional map showing the main tectonic and morphological features of the Colombian Andes and the location of the study area. a) Slab-depth contours from Hayes et al. (2018), age of the oceanic plate from Müller et al. (2008), and relative motion vectors from Mora-Páez et al. (2019). Red triangles represent Holocene volcanoes. AB=Atrato Basin, CB=Chucunaque Basin, CC=Central Cordillera, CT=Caldas Tear, CV=Cauca Valley, EC=Eastern Cordillera, MV=Magdalena Valley, SMR=Santa Marta Range, SR=Sandra Ridge, UFZ=Uramita Fault Zone, WC=Western Cordillera. b) Map showing the location of panel a) and the mean annual precipitation for northwestern South America, Central America and the Caribbean region Fick and Hijmans (2017).

4.2.2. Geology of northwestern Colombia

The northwesternmost Colombian Andes mainly comprise accreted rocks of the CAA and its plateau-like basement (Barbosa-Espitia et al., 2019; Cardona et al., 2018; Kerr et al., 1997), together with a pre- to post-collisional sedimentary cover. This formerly intra-oceanic arc is composed of Cretaceous to Eocene-Oligocene volcaniclastic and intermediate intrusive rocks exposed from northwestern Colombia to central-eastern Panama (Cardona et al., 2018 and references therein). Oligocene-lower Miocene to Pliocene marine to fluvial strata of the correlatable Chucunaque (eastern Panama) and Atrato (northwestern Colombia) basins overly the CAA, which, together with the infill of a suture-related basin (Figs. 4.2 and 4.3), preserve both the pre- and post-collisional sedimentary and deformational record associated with the accretion of the island arc to northwestern South America and subsequent subduction-related tectonics (Coates et al., 2004; Duque-Caro, 1990b). According to available paleogeographic and tectonic reconstructions (e.g. Coates et al., 2004; Montes et al., 2019), it seems that the AB evolved from an oceanic intra- or back-arc to a post-collisional continental forearc basin (Fig. 4.4), as apparently occurred during Paleozoic arc-continent collisional episodes in the Appalachians and the southern Urals (Brown et al., 2001; Zagorevski et al., 2009).

The easternmost (inland) limit (suture) of the CAA is defined by the Uramita Fault Zone (UFZ; Figs. 4.2 and 4.3). The UFZ is a ~10 km-wide deformation zone that juxtaposes Cretaceous-Paleogene siliciclastic and hemipelagic rocks of the Western Cordillera of Colombia and its associated plateau-like basaltic basement representing the continental paleomargin (Pardo-Trujillo et al., 2020a), with allochthonous Eocene-Oligocene volcaniclastics of the CAA (Fig. 4.3; León et al., 2018). The southernmost limit of the latter is represented by the Istmina Hills (also known as the Istmina deformed zone; Duque-Caro, 1990a), which are closely related to the occurrence of accreted lower Miocene mafic-ultramafic rocks of the Condoto and Viravira complexes interpreted as formed in an extensional supra-subduction setting (Fig. 4.2; Tistl et al., 1994). Recently gathered provenance and thermochronological constraints from Cretaceous-Eocene and Miocene rocks exposed near the suture between the CAA and the continental paleomargin have been used to propose an early to middle-Miocene age for the arc-continent collision (Lara et al., 2018; León et al., 2018). Syn-to post-collisional lower Miocene shallow-marine and upper

Miocene to Pliocene fluvial coarse-grained rocks were accumulated along the northernmost suture zone (Dabeiba area; Fig. 4.3; León et al., 2018; Rodríguez et al., 2016), and their tectonostratigraphy will be discussed in conjunction with that of the AB in the context of the Neogene collisional and subduction-related tectonics of the northwesternmost Andes.

4.3. Data and methods

In this work, we review available biostratigraphic data of Neogene rocks of the Atrato and surrounding sedimentary basins (i.e. suture-related basin; Figs. 4.2, 4.3 and 4.4), which we combine with new stratigraphic, structural and multi-proxy provenance data to reconstruct the tectonostratigraphic evolution during the Neogene transition from collision to subduction in the northwesternmost Andes. We analyzed Oligocene to Pliocene strata and modern sediments, including bulk sandstone petrography, heavy minerals counting, detrital zircon U-Pb geochronology, Hf isotopes and trace elements geochemistry, and detrital clinopyroxene geochemistry. The multi-proxy provenance data were obtained in order to identify changes in the configuration of source areas and correlate them with the occurrence of deformational events and associated modifications of the depositional settings, which were identified from stratigraphic constraints and the history of tectonic subsidence reconstructed through a 1D backstripping analysis (Allen and Allen, 2013). Additionally, we performed a topographic lineament analysis of the major morphological domains of the northern Colombian forearc basin to study the most recent tectonic and structural configuration, expanding on the previous findings of León et al. (2021b).

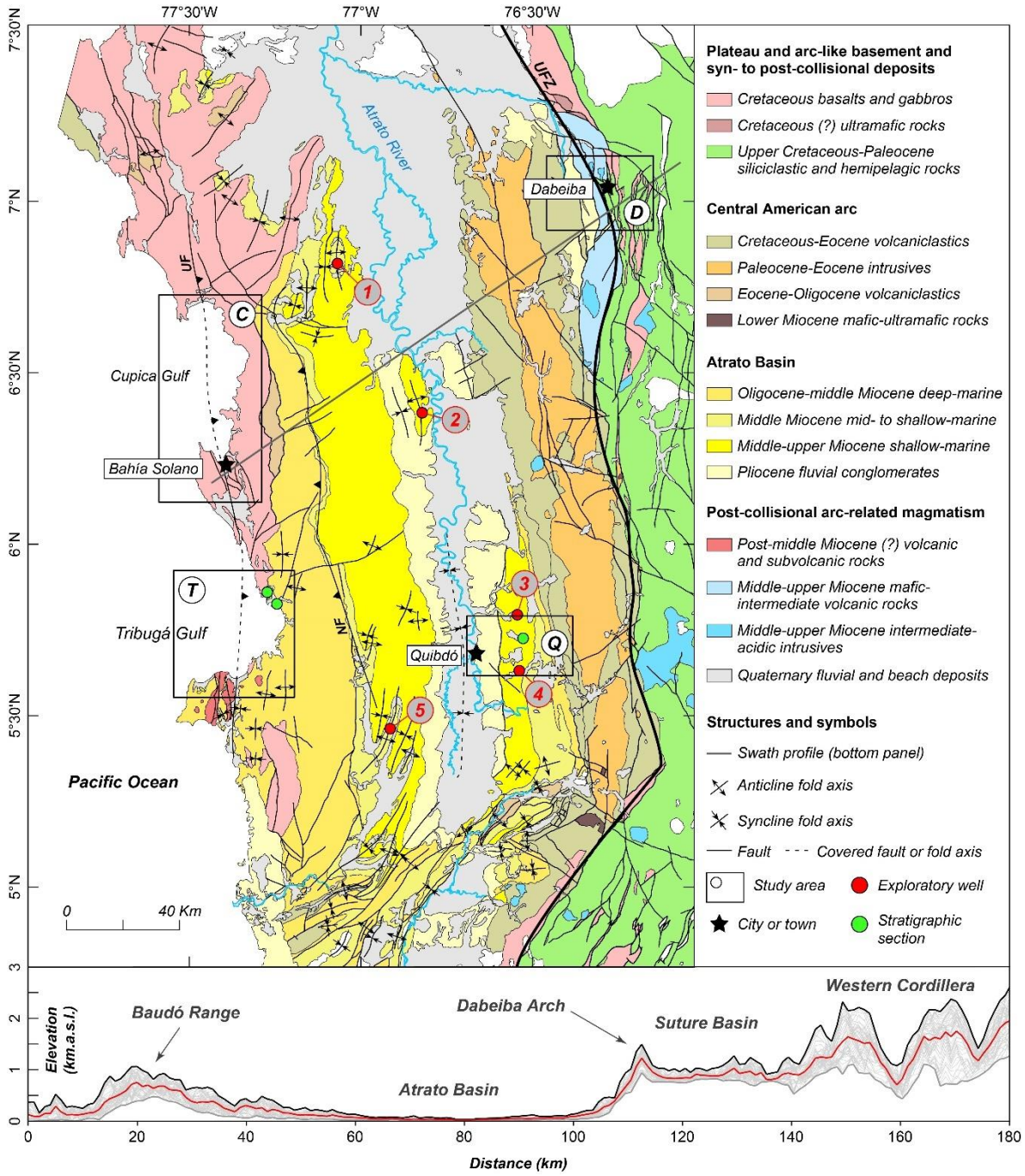

Figure 4.2. Geological map of the northern Colombian forearc basin, modified from Gómez-Tapias et al. (2017). Black rectangles delineate the different study areas; C=Cupica Gulf, D=Dabeiba, Q=Quibdó, T=Tribugá Gulf. The bottom figure is a topographic swath profile showing the main morphological elements of the forearc region, whose location is represented in main figure by the gray line.

4.4. Overview of the northern Colombian forearc and its Eocene to Recent paleogeographic evolution

4.4.1. Geology, stratigraphy and paleogeography of the AB

The AB is a nearly N-S-oriented depression located in the northern Colombian forearc region (Chocó region; ~5°-8°N), which hosts one of the wettest and most biodiverse tropical rainforest on earth (Fig. 4.1; Myers et al., 2000; Poveda and Mesa, 2000). It is flanked by the northwestern slope of the Colombian Western Cordillera to the east and the coastal Baudó Range to the west (Figs. 4.1 and 4.2), and is represented by a well-defined negative Bouguer anomaly (-25 to -20 mGal; National Hydrocarbons Agency of Colombia, 2010). The basement of the AB is composed of arc-related mafic-intermediate volcano-plutonic and volcaniclastic rocks of the CAA (Barbosa-Espitia et al., 2019; Cardona et al., 2018). This intra-oceanic arc that seemingly formed by plume-driven subduction of the Farallon plate beneath the southwestern proto-Caribbean region at ca. 100 Ma (Boschman et al., 2019; León et al., 2022; Whattam and Stern, 2015), experienced multiple shifts in the location of the main volcanic front as a consequence of changes in the subduction dynamics during the Cretaceous-Paleogene (Buchs et al., 2019a, 2010; McGirr et al., 2020; Whattam et al., 2020, 2012). For instance, after an apparent magmatic quiescence between ~40-30 Ma, a trenchward migration (southeastward displacement on present-day coordinates) of the magmatic arc is thought to have occurred at ca. 30-20 Ma coeval with either the subhorizontal tearing and steepening of the subducting Farallon/Nazca slab or with a sharp increase of the convergence obliquity at the trailing edge of the Caribbean plate (Buchs et al., 2019a; Whattam et al., 2012).

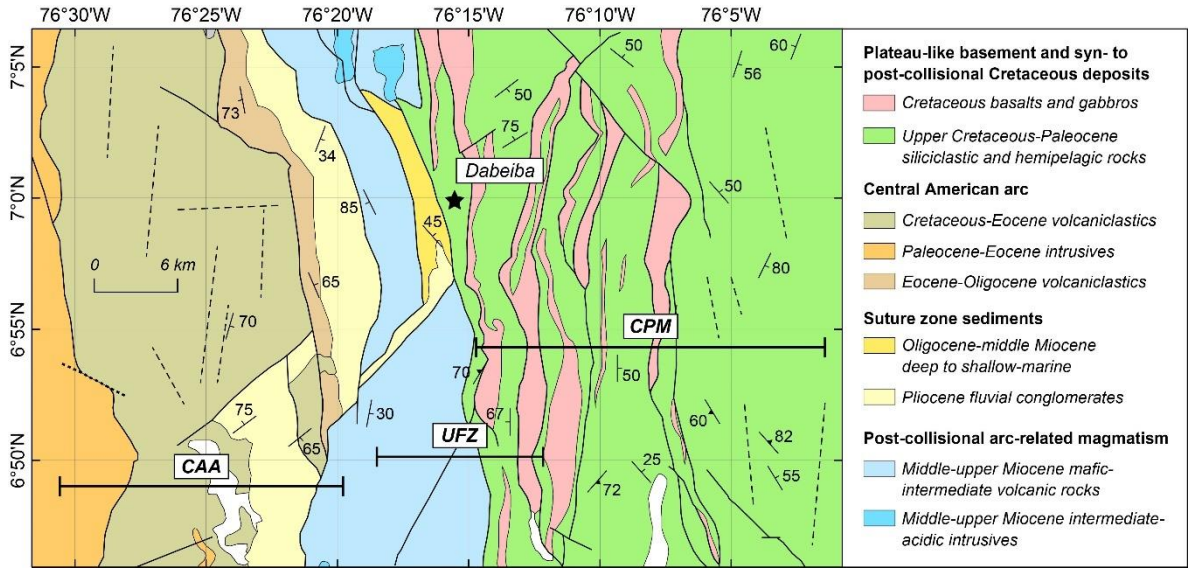

Figure 4.3. Local geological map of the suture zone between the Central American arc and Cretaceous-Paleogene strata of the Western Cordillera, representing the continental paleomargin, and some structural features such as bedding planes, faults and lineaments; from Gómez-Tapias et al. (2017) and Zapata)2000). CAA=Central American arc, CPM=Continental paleomargin, UFZ=Uramita Fault Zone.

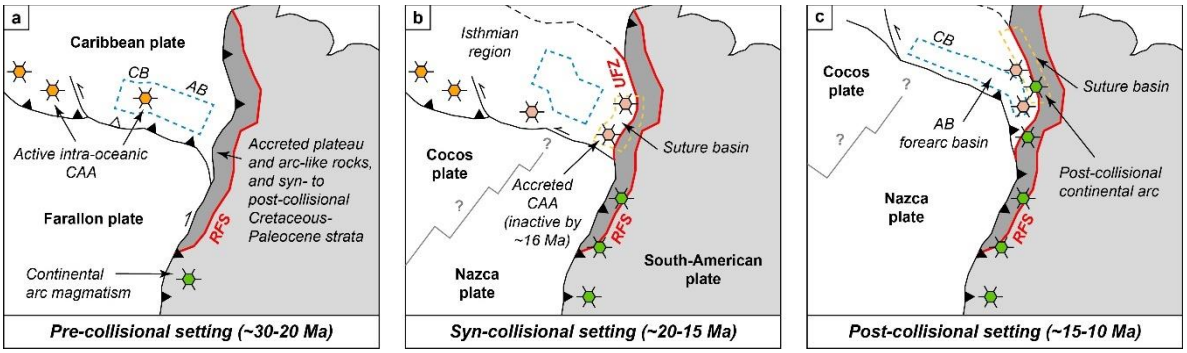

Figure 4.4. Schematic illustration showing the Neogene paleogeography of northwestern South America and southeastern Central America, modified from Montes et al. (2019) and Coates et al. (2004).

Regardless the tectonic processes involved in the Eocene-Oligocene episode of arc migration, which are beyond the scope of this work, the Oligocene-early Miocene period seems to have been dominated by extensional tectonics that prompted deepening of arc-related marginal basins (Buchs et al., 2019b; Coates et al., 2004; Montes et al., 2012), probably representing the earliest evolution of the Chucunaque and Atrato basins in an intra-oceanic (either back-arc or intra-arc) pre-collisional scenario. The sedimentary record of the pre-collisional stage of basin evolution is represented by arc-related middle Eocene to middle-upper Oligocene deep-water siliceous and calcareous strata associated with mafic volcaniclastic and volcanic rocks (Montes et al., 2012), included within the Darién and Porcona Formations in eastern Panama (i.e. Chucunaque Basin; Coates et al., 2004), as well as the Salaquí and Cruces Formations and the informal Tripogadí and Triganá units in northwestern Colombia (i.e. Atrato and suture basins; e.g. Haffer, 1967; León et al., 2018; Rodríguez and Sierra, 2010; Zapata, 2000). These units seem to have accumulated in open-water deep- to shallow-marine conditions in a back- or intra-arc setting during a regional marine transgression across partially emerged oceanic islands attributed to the early emergence of the Isthmus of Panama (Buchs et al., 2019b; Jaramillo, 2018; Montes et al., 2012; and references therein).

The syn- to post-collisional infill of the AB is represented by an upper-Oligocene to Pliocene shallowing-upward sequence that is thought to record the progressive Miocene to present-day rise of the Isthmus of Panama (Coates et al., 2004; Duque-Caro, 1990b), which constitutes one of the most striking paleogeographic and biogeographic events of the Cenozoic era (see a review in Jaramillo, 2018). The upper-Oligocene to middle Miocene Uva Formation is composed of deformed pelagic to hemipelagic fossiliferous limestones, and calcareous mudstones and sandstones with thin tuffaceous beds (Fig. 4.5), which apparently accumulated in a shelf-slope setting at lower-upper bathyal depths (Duque-Caro, 1990b; Haffer, 1967), and have an average thickness of ~1500 m that increases from north to south (Haffer, 1967). Clastic dykes of fine-grained litharenites are commonly found in the Uva Fm, which may suggest ongoing tectonic activity during or shortly after sediment accumulation (Fig. 4.5; e.g. León et al., 2021b). This unit seems to represent the late stages of a paleogeographic scenario characterized by open-water conditions, where a deep connection between the Pacific Ocean and the Caribbean Sea prevailed in a landscape dominated by

partially emerged volcanic islands across the proto-isthmian region (Buchs et al., 2019b; Jaramillo, 2018), similar to what is observed nowadays in the Kuril Islands in the northwestern Pacific.

Lower-middle Miocene siliciclastic rocks of the Napipí Formation and the informal lower Chorí unit (Zapata, 2000), unconformably overly the pelagic to hemipelagic rocks of the Uva Fm. (Fig. 4.5), from which are separated by a short-lived hiatus between ~16 and 15 Ma (Duque-Caro, 1990b; Haffer, 1967). The Napipí Fm. is 700 m-thick in average and is mostly composed of tilted and faulted hemipelagic calcareous mudstones, limestones and fine-grained sandstones, which are thought to have accumulated in organic-rich deep-intermediate water settings (Duque-Caro, 1990b). It seems that the Napipí Fm. deposited in open water conditions after an interruption of the deep connection between the Pacific and the Caribbean probably associated to a short-lived basin uplift that caused a shallowing of accumulation depths across the proto-isthmian region (Duque-Caro, 1990b). The upper-Oligocene to middle Miocene strata of the Uva and Napipí formations had been interpreted as the pre-collisional sedimentary record of the AB (Coates et al., 2004; Duque-Caro, 1990b, 1990a). Nevertheless, our new provenance data and structural observations allowed us to interpret these units as representing syn-collisional stages during the accretion of the CAA against northwestern South America, which will be discussed in section 4.6.

The middle-upper Miocene Sierra Formation unconformably overlies the Napipí Fm. and is composed of slightly deformed thick strata of organic matter-rich calcareous mudstones, and interlayered fine- to medium-grained sandstones with minor conglomerates, which combined reach an average thickness of ~2.000 m (Duque-Caro, 1990b; Haffer, 1967). After a stratigraphic hiatus between ~13 and 12 Ma, the AB recorded a major pulse of tectonically-driven uplift that caused a ~1000 m shallowing of accumulation depths and is associated with the occurrence of a regional middle Miocene unconformity on top of which the Sierra Fm. accumulated (Duque-Caro, 1990b, 1990a; Haffer, 1967). Such period of basin inversion was coeval with the near disappearance of the connection between the Pacific and Caribbean (e.g. closure of the Central American Seaway; CAS), which was limited to shallow and spatially restricted waters (Duque-Caro, 1990b; Jaramillo, 2018; Montes et al., 2015; and references therein). The uppermost part of the Sierra Fm., also referred as the upper Miocene Munguidó Formation (Duque-Caro, 1990b), seems to be separated from the underlying strata by an

unconformity and an associated short-lived sedimentary hiatus (~7 to 6 Ma), which was coeval with shallowing of accumulation depths to nearshore (< 150 m) conditions (Duque-Caro, 1990b; Zapata, 2000).

The youngest sedimentary unit of the AB is the Quibdó Formation, a ~800 m-thick slightly to non-deformed unit composed of mottled mudstones, sandstones and poorly consolidated polymictic conglomerates (Fig. 4.5), which is thought to unconformably overly the Munguidó Fm. (Duque-Caro, 1990b; Haffer, 1967). These rocks are only exposed in the Quibdó area and are interpreted as accumulated in high-energy fluvial systems, representing the establishment of fully terrestrial conditions in northwestern Colombia during the latest Miocene to Pliocene (Haffer, 1967), which was probably correlated with the final emergence of the Isthmus of Panama (Coates et al., 2004; Duque-Caro, 1990b; Jaramillo, 2018; O' Dea et al., 2016). This major environmental transition towards terrestrial settings was seemingly a consequence of widespread post-late Miocene uplift in northwestern Colombia that resulted in a major topographic uplift of the coastal Baudó Range (i.e. outer forearc high), which in turn, caused the fragmentation of the AB into an inner and outer (coastal) segments (León et al., 2021b). Yet, the drivers of uplift and basin fragmentation had remained unexplored.

Overall, the stratigraphy and paleogeography of Neogene strata of both the AB and its Panamanian correlate, the Chucunaque Basin, are well-known. As described above, this sedimentary record preserves the imprints of a highly changing landscape and environmental configuration during the middle Eocene to Pliocene that led to the progressive rise of the Isthmus of Panama and the topographic growth of northwesternmost Colombia (Jaramillo, 2018). Nevertheless, the tectonic drivers of the landscape perturbations and the associated changes in the configuration of sediment source areas and depocenters (i.e. source-to-sink system) remain barely known, since no attempt to link the stratigraphic evolution of the AB to the regional collisional and subduction-related tectonics had been made to date.

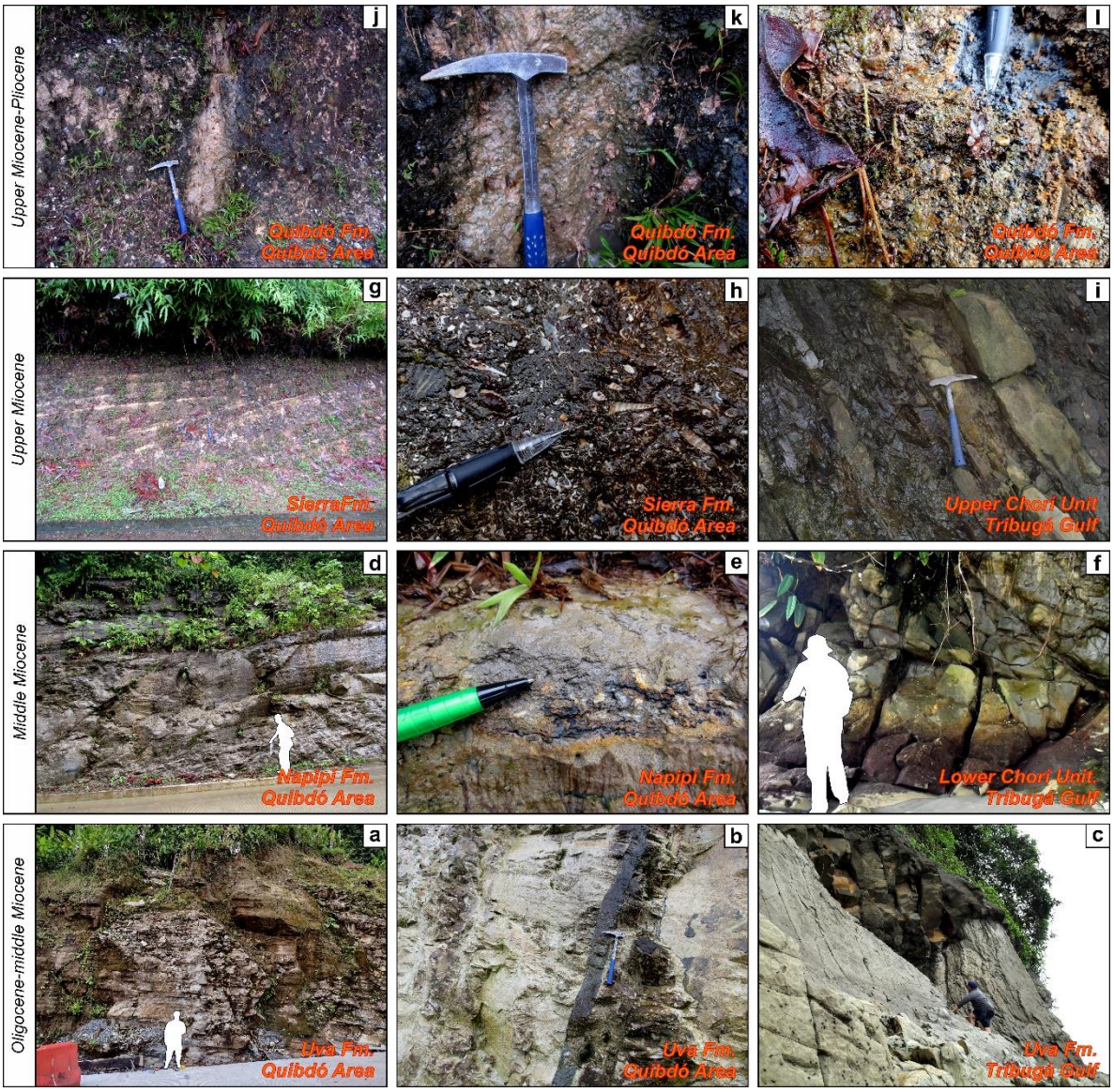

Figure 4.5. Field photographs of the main Neogene geological units representing the infill of the Atrato Basin. a) Subhorizontal, highly fractured tabular limestones and marls. b) Clastic dyke of litharenite intruding marls. c) Angular unconformity between nearly vertical limestones of the Uva Fm. and overlying calcareous sandstones of the lower Chorí unit. d) Massive calcareous sandstones gently dipping westward. e) Organic-rich medium- to coarse-grained beds. f) Massive and highly fractured calcareous sandstones. g) Growth strata of fine-grained sandstones and mudstones. h) Fossil-rich coarse-grained deposits. i) Calcareous sandstone beds interlayered with highly fractured organic-rich mudstones. j-l) Highly weathered outcrops of massive polymictic conglomerates.

4.4.2. Miocene to Pliocene sedimentary record of the suture zone

Shallow-marine to continental rocks of unknown thickness outcrop along the northern segments of the suture zone between the CAA and the continental paleomargin (Uranite Fault Zone; Fig. 4.3). The lower-middle Miocene Beibaviejo Formation is composed of deformed fine-grained calcareous sandstones and mudstones, and minor limestones and distal tuffaceous rocks, which apparently accumulated in shallow-marine settings (León et al., 2018; Rodríguez et al., 2013). The Beibaviejo Fm. is intruded by middle-upper Miocene mafic-intermediate plutonic and subvolcanic rocks thought to represent the post-collisional continental magmatic arc (León et al., 2018; Rodríguez and Zapata, 2012). Tilted strata of massive conglomerates and sandstones of the Guineales Formation represent the youngest sedimentary record of the suture zone, for which a late Miocene maximum depositional age has been proposed from detrital geochronological and thermochronological data (León et al., 2018; Rodríguez et al., 2016). This unit is interpreted as accumulated in high-energy fluvial systems and, together with coarse-grained fluvial deposits of the AB (Quibdó Fm.), represents the sedimentary record of the post-late Miocene shift to fully terrestrial conditions in northwestern Colombia. The paleogeography and paleoecology of the lower Miocene and younger strata of the suture basin remain barely known and will be discussed elsewhere.

4.5. New stratigraphic, provenance and structural constraints of the Neogene infill of the Atrato Basin

4.5.1. Stratigraphy of the northern Tribugá Gulf (northern Colombian Pacific coast) and the Quibdó area

Here we present new lithostratigraphic constraints from two sections measured in the northern Pacific coast of Colombia (Tribugá Gulf; Fig. 4.2), and from additional nearby sampling/description sites, which allowed us to complement the general stratigraphic observations of Oligocene-Miocene strata of the AB provided in section 4.4.1. These rocks probably represent the outermost (oceanward) sedimentary record of the AB, which was structurally disrupted from the innermost region (e.g. Quibdó Area) by the late Miocene to Recent uplift of the Baudó Range (see a discussion in section 4.6.3). Additionally, we present a description of a composite stratigraphic section measured in the Quibdó area, which was

constructed from very discontinuous and poorly preserved outcrops, given the intense humidity and rock weathering, found along roadcuts at the eastern flank of the AB (Fig. 4.2). A detailed facies analysis is beyond the scope of this work, as we are interested in the broad environmental significance of Neogene strata and their associated deformational record. The measured stratigraphic sections were also sampled for provenance analyses, whose results are presented in section 4.5.3.

4.5.1.1. Descriptions of measured stratigraphic sections of the Tribugá Gulf

Measured sections are mostly composed of tabular strata with sharp planar contacts of calcareous mudstones and sandstones, with minor conglomerates of the informal middle-upper Miocene Chorí unit that is informally divided into a lower and an upper member, which are tentatively correlatable with the Napipí and/or Sierra formations. These rocks are in faulted contact and overly in angular unconformity Oligocene-middle Miocene silty limestones of the Uva Fm. (León et al., 2021b; Zapata, 2000). The latter is represented by nearly vertical medium-bedded (0.1-0.3 m) tabular strata of limestones with thin (< 0.1 m) lenses of fine-grained mostly euhedral clastic fragments, which may indicate contemporaneous volcanic activity, as previously suggested from the presence of interlayered thin tuffaceous beds (Duque-Caro, 1990b). The Uva Fm. also includes massive calcareous litharenites and marls of undetermined thickness with common dissolution structures, which are found as isolated outcrops along rivers draining the Baudó Range into the Pacific Ocean. These rocks are composed of abundant bioclasts, with minor euhedral feldspar, amphibole, pyroxene, quartz and biotite.

The informal Chorí unit is represented by thick to very thick (> 0.3 m) east-dipping (~20-50°) beds of fine- to coarse grained (0.1-0.5 mm) sandstones showing parallel, wave-ripple, and flaser lamination, and less frequently, current-ripples and cross-bedding structures (Fig. 4.6). These rocks are composed of mostly subangular and poorly to moderately sorted fragments of feldspar and quartz, volcanic and minor sedimentary lithics, with abundant bioclasts, embedded within calcareous cement. Sandstones also include detrital amphibole, biotite, clinopyroxene, chlorite, epidote-group minerals, and glauconite, and seem to preserve a reduction in grain size and thickness, together with an increase in the mud/sand ratio, which are tentatively interpreted as representing the limit between the informal lower and upper

Chorí units (Fig. 4.6). Thick to very thick beds of grayish calcareous mudstones, which become more abundant towards the upper Chorí unit, show flaser lamination and, occasionally, convolute bedding structures (Fig. 4.6). The presence of disordered strata and clastic dykes in the upper Chorí unit indicates ongoing tectonic activity during sediment accumulation.

4.5.1.2. Descriptions of the stratigraphic section of the Quibdó area

The stratigraphic section is mainly composed of fossil-rich calcareous sandstones and mudstones of the Uva, Napipí and Sierra formations, which increase their abundance of siliciclastic material and the mud/sand ratio from base to top and are characterized by tabular strata gently dipping to the west (~10-15°). It is worth mentioning that given the discontinuity of the measured section and the lack of detailed biostratigraphic control, the boundaries of each stratigraphic unit, following the nomenclature of Duque-Caro (1990b), were inferred based on the occurrences of major lithological changes, indicated by abrupt increase/decrease of the mud/sand ratio and/or the proportion of carbonate/siliciclastic components. At the base, the Uva Fm. comprises thin- to medium-bedded tabular strata (~15-30 cm) of fine-grained wackestones and calcareous mudstones with sharp planar contacts, showing parallel and wave ripple lamination, and characterized by the presence of clastic dykes of lithic-rich sandstones (Fig. 4.7). Carbonate rocks of this unit also include minor siliciclastic and terrigenous components, such as quartz, feldspar, amphibole, volcanic lithics and remains of organic matter.

The overlying Napipí Fm. is composed of very thick-bedded tabular strata (> 1 m) of fine- to medium-grained calcareous sandstones gently dipping westward (~10°), which show wave-ripple lamination and fining-upward gradational structures and are interlayered with thick-bedded (~0.3-1 m) calcareous mudstones (Fig. 4.7). Sandstones are mostly composed of poorly to moderately sorted, subangular fragments of quartz, feldspar, mafic minerals and lithics, together with relatively abundant bioclasts and remains of organic matter. Thick beds (> 0.3 m) of massive sandstones and thin lenses (< 0.1 m) of conglomeratic sandstones with less abundant carbonate components predominate towards the top of the Napipí Fm., where siliciclastic components become more abundant.

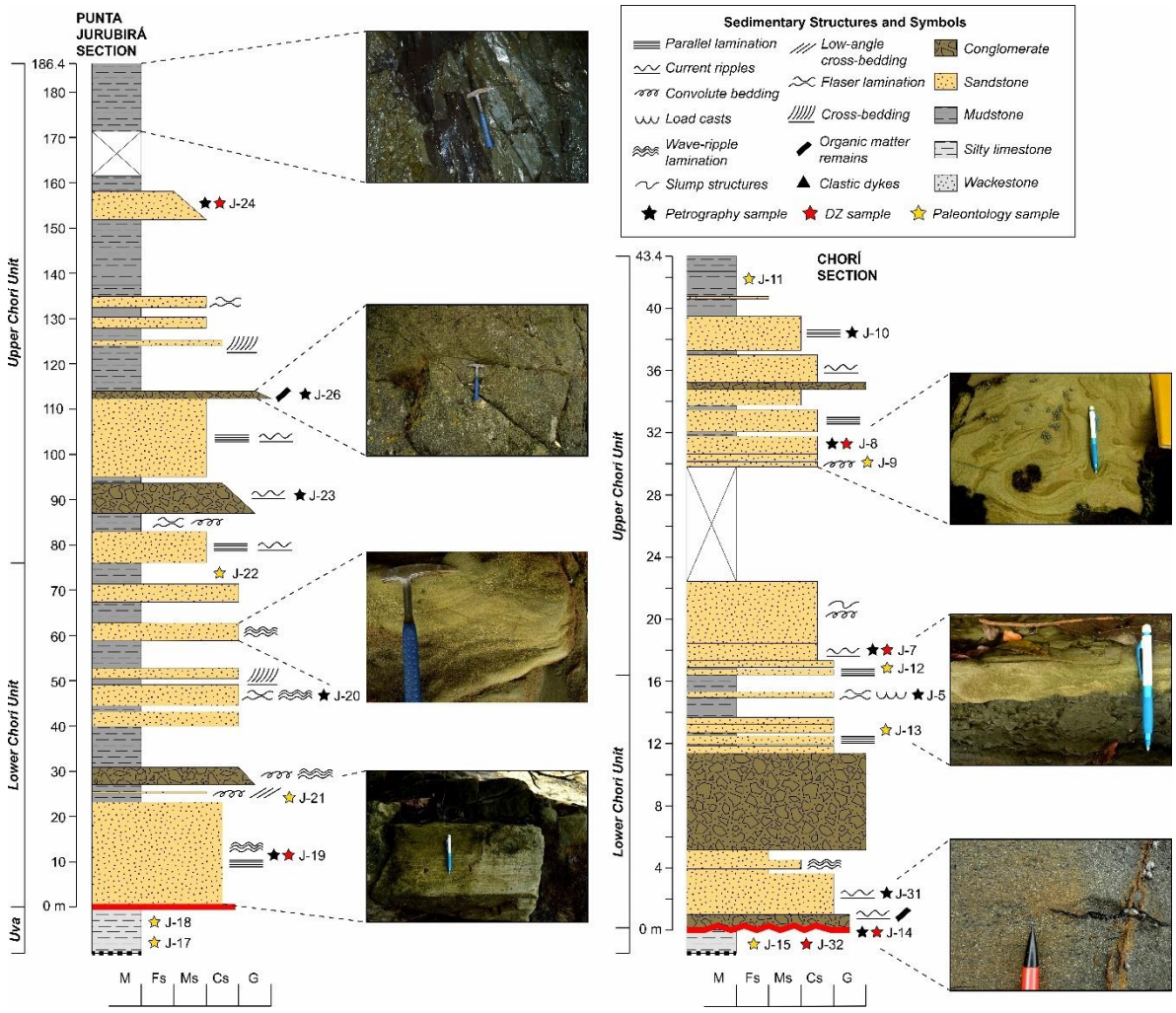

Figure 4.6. Stratigraphic sections measured in the Tribugá Gulf, showing the main lithological and structural features of the outcropping rocks, together with some representative photographs of observed sedimentary structures, and the location of analyzed samples.

Most of the middle-upper part of the measured section seems to be represented by the Sierra Fm. that is composed of tabular strata of mudstones, fine- to coarse-grained sandstones and minor conglomerates with sharp planar contacts. Thick tabular beds (~0.3-1 m) of grayish mudstones, which are associated toward the top with coarse-grained fossil-rich deposits (see a field photograph in Fig. 4.5), show parallel and wave-ripple lamination and low-angle cross-bedding structures (Fig. 4.7). Medium-bedded tabular strata of sandstones show parallel and wave-ripple lamination and are composed of mostly subangular fragments of quartz, feldspar, lithics and mafic minerals with remains of organic matter. Less abundant thick-bedded (< 1m) polymictic matrix-supported conglomerates are also observed and composed of subangular-subrounded clasts of quartz, feldspar and fine-grained lithics. The presence of growth strata may indicate ongoing tectonic instability of the basin during the accumulation of the Sierra Fm. (Fig. 4.5).

4.5.1.3. Interpretation of Miocene accumulation settings

Our new lithostratigraphic observations and the revision of available paleobathymetry constraints (Table 1) allowed us to propose that the Oligocene-middle Miocene Uva Fm. likely correspond to pelagic-hemipelagic deposits accumulated in a distal platform or open shelf setting at middle-lower bathyal depths. Therefore, regularly bedded thin to medium-thick tabular limestones of the Uva Fm. with massive structures found in the Tribugá Gulf were probably formed by pelagic settling of abundant planktonic foraminifera, with minor contribution of distal airfall deposits, as suggested by the presence of thin layers of volcaniclastic material (Stow and Smillie, 2020; Stow et al., 1996), which were likely transported by wind and low-energy surface currents from the nearby locally active volcanoes (i.e. Oligocene-lower Miocene CAA; see discussion in section 4.6.1). This is consistent with the greater abundance of tuffaceous deposits interlayered with foraminifera-rich mudstones and limestones of the correlatable middle-upper Oligocene Porcona Fm. and lower-middle Miocene Clarita Formation of the Chucunaque Basin, which, according to available paleogeographic reconstructions, accumulated in lower- to middle-bathyal depths, closer to the active volcanic front (Fig. 4.4; e.g. Coates et al., 2004; Montes et al., 2019).

Conversely, fine- to medium-grained wackestones and interlayered calcareous mudstones of the Uva Fm. observed along the Quibdó area, show wave-ripple and parallel lamination and relatively greater abundance of terrigenous material including siliciclastic fragments and organic matter remains, which may indicate accumulation in higher energy settings under the influence of bottom currents in relative proximity to emerged landmasses (Stow et al., 1996).

The overlying middle Miocene Napipí Fm. and the lower Chorí unit, are characterized by interlayered calcareous sandstones, limestones and mudstones, with the latter being virtually more abundant in the measured sections of the Tribugá Gulf than in the Quibdó area (Figs. 4.6 and 4.7). Calcareous sandstones present wave-ripple and flaser lamination, cross- and convolute-bedding, as well as load and slump structures (Figs. 4.6 and 4.7), and also show an increase in the proportion of siliciclastic components when compared with the underlying Uva Fm., accompanied by the regular appearance of glauconite (see a detailed description of petrographic features in section 4.5.3.), which may indicate accumulation in organic-rich waters at shallower depths than previously proposed (Odin and Matter, 1981). This, together with our revision of the paleobathymetry from the benthic foraminiferal fauna (Table 1), suggest that the Napipí Fm. and the lower Chorí unit were likely deposited in a tectonically active organic-rich slope-shelf setting at upper bathyal to outer neritic depths influenced by intermittent turbidity currents (Arnott, 2010; Stow et al., 1996), after a short-lived period of basin uplift (~1 Myr; Duque-Caro, 1990b). In such scenario, the mud-dominated sequence of the lower Chorí unit (Tribugá Gulf), and the laterally continuous sandstone levels, probably represent more distal deposition in an unconfined proximal shelf influenced by episodic turbidity currents with associated hemipelagic settling. On the other hand, the sand-dominated strata of the Napipí Fm. of the Quibdó area may represent higher energy deposits related to proximal slope settings with minor contribution of background hemipelagic deposition (Stow and Smillie, 2020).

Table 1. Results of the revision of the taxonomy of benthic foraminifera and previous interpretations of accumulation depths for Neogene rocks of the Atrato Basin

Stratigraphic unit	**Accumulation age (Duque-Caro, 1990b)**	**Previously proposed accumulation depth (Duque-Caro, 1990b)**	**Revised accumulation depth ranges**	**Benthic foraminifera**
Uva Formation	Oligocene-middle Miocene (biozones P.21 to N.9 of Blow, 1969)	Open-water conditions at depths greater than 2000 m	Lower-middle bathyal depths (~2000-600 m)	*Cibicidoides mexicanus* (Nutall), *Heterolepa perlucida* (Nutall)
Napipí Formation	Middle Miocene (biozones N.9 to N.11 of Blow, 1969)	Organic-rich settings at depths of 2000 m or greater	Middle-upper bathyal depths (~1500-750 m)	e.g. *Bulimina striata* (d'Orbigny), *Martinottiella communis* (d'Orbigny), *Uvigerina carapitana* (Hedberg)
Sierra Formation	Middle-late Miocene (biozones N.13 to N.17 of Blow, 1969)	Upper bathyal depths with very low oxygen conditions	Upper bathyal to shallow-marine (~750-200 m)	e.g. *Buliminella elegantissima* (d'Orbigny), *Cancris auricula* (Fichtel & Moll), *Valvulineria araucana* (d'Orbigny), *Eubuliminella subfusiformis* (Cushman)
Munguidó Formation	Late Miocene-early Pliocene (biozones N.17 to N.18 of Blow, 1969)	Outer shelf-nearshore environments (< 150 m) with poorly oxygenated waters	Not revised	N/A

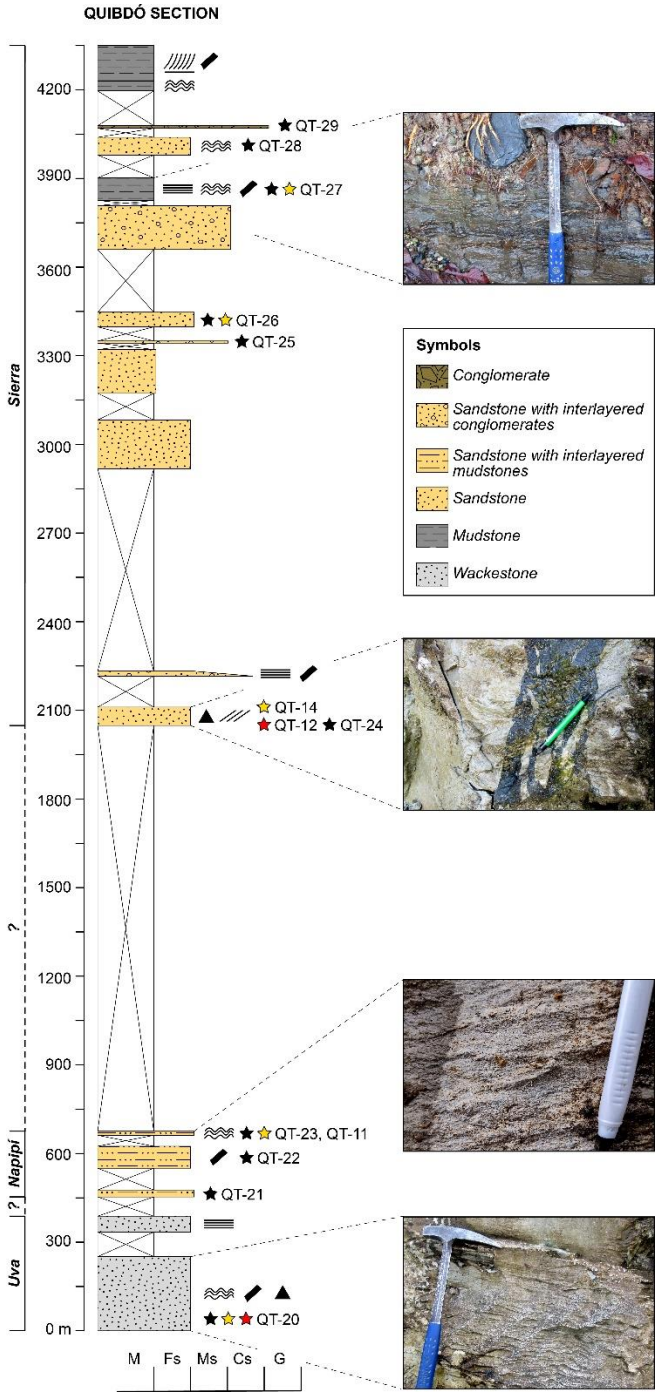

Figure 4.7. Composite stratigraphic section measured in the Quibdó area, showing the main lithological and structural features of the outcropping rocks, together with some representative photographs of observed sedimentary structures, and the location of analyzed samples. Not shown symbols as in Figure 4.6

The upper-Miocene Sierra Fm. and the upper Chorí unit are characterized by the dominance of mudstones over fine- to coarse-grained sandstones that prevailed during the deposition of the Napipí Fm., which is more evident in the Punta Jurubirá section measured in the Tribugá Gulf (Figs. 4.6 and 4.7). Calcareous mudstones are interlayered with fossil-rich fine- to medium-grained sandstones showing wave ripple, current ripple and flaser lamination, and with conglomerate beds showing normal gradational structures (Fig. 4.6). These features, together with available paleobathymetry constraints that suggest that the Sierra Fm. was probably accumulated at shallow depths after a major event of kilometer-scale basin uplift (Table 1; Duque-Caro, 1990b), may indicate that deposition mostly occurred in a mud-dominated tidal flat system (Dalrymple, 2010; Johnson and Baldwin, 1996). Although the prevalence of the above-mentioned characteristics for the Sierra Fm. in the measured section of the Quibdó area, located ~80 km landward (eastward in present-day coordinates), may suggest lateral continuity of accumulation environments, we claim that both sections represent different depositional settings within a wide shallow-marine shelf, since such an accumulation system is expected to be laterally heterogeneous over the scale of tens of kilometers (Dalrymple, 2010; Johnson and Baldwin, 1996; Plint, 2010). Yet, the discrimination of the architecture of the upper-Miocene shallow-marine depositional system of the AB is beyond the focus of this work.

4.5.2. Tectonic subsidence and uplift

The tectonic evolution of the northern Colombian forearc basin can be envisioned as the product of two contrasting regimes: an intra-oceanic pre- to syn-collisional scenario where Oligocene-middle Miocene rocks formed in an intra- or back-arc setting, and a post-collisional regime where middle-upper Miocene and younger strata accumulated in continental forearc and suture-related basins and were subsequently deformed. In this section, we summarize the results of a 1D backstripping analysis of available stratigraphic data for syn- to post-collisional units (Uva, Napipí and Sierra formations) from exploratory boreholes drilled nearby the Quibdó area (see location in Fig. 4.2) and studies on the recovered Neogene foraminiferal fauna (Cediel et al., 2009; Duque-Caro, 1990b; Haffer, 1967). As mentioned in section 4.5.1., we revised the taxonomic nomenclature of reported benthic foraminifera and their paleoenvironmental significance to better estimate the

accumulation paleobathymetry, following Hayward et al. (2001), Holbourn et al. (2013), and Jones (1994). Obtained results are provided in Table 1 together with a comparison with previously proposed interpretations of paleobathymetry constraints (Duque-Caro, 1990b). To consider the large uncertainty with the estimated accumulation depth from the benthic foraminifera of Neogene strata of the AB, we provide both minimum and maximum tectonic subsidence curves (Fig. 4.8), reconstructed following the procedure of Allen and Allen (2013). We focused on the syn- to post-collisional history of the AB, as proper information on the thicknesses and biostratigraphy of older pre-collisional strata from compiled data is lacking (Cediel et al., 2009).

Despite the minor differences among the recovered stratigraphic record from each of the five exploratory boreholes used for the subsidence analysis, similar patterns can be observed. The interval between the late Oligocene and the middle Miocene (up to ~16 Ma), during the accumulation of the Uva Fm., was marked by slow subsidence (<50 m/Myr) and low sedimentation rates (<100 m/Myr; Fig. 4.8), prior to the occurrence of an early-middle Miocene (~16-15 Ma; Duque-Caro, 1990b) unconformity. The latter was accompanied by a short-lived period of initial basin inversion with moderate uplift rates (~250 m/Myr), and then followed by slow subsidence (< 100 m/Myr) and moderate-high sedimentation rates during the accumulation of the Napipí Fm. (up to ~400 m/Myr; Fig. 4.8). Subsequently, the middle Miocene unconformity between the Napipí and Sierra formations (~13-12 Ma; Duque-Caro, 1990b) was accompanied by moderately rapid uplift (~300 m/Myr), which was followed by a period of relative basin stability and a considerable reduction of sedimentation rates to less than ~230 m/Myr that prevailed until ~7 Ma (Fig. 4.8).

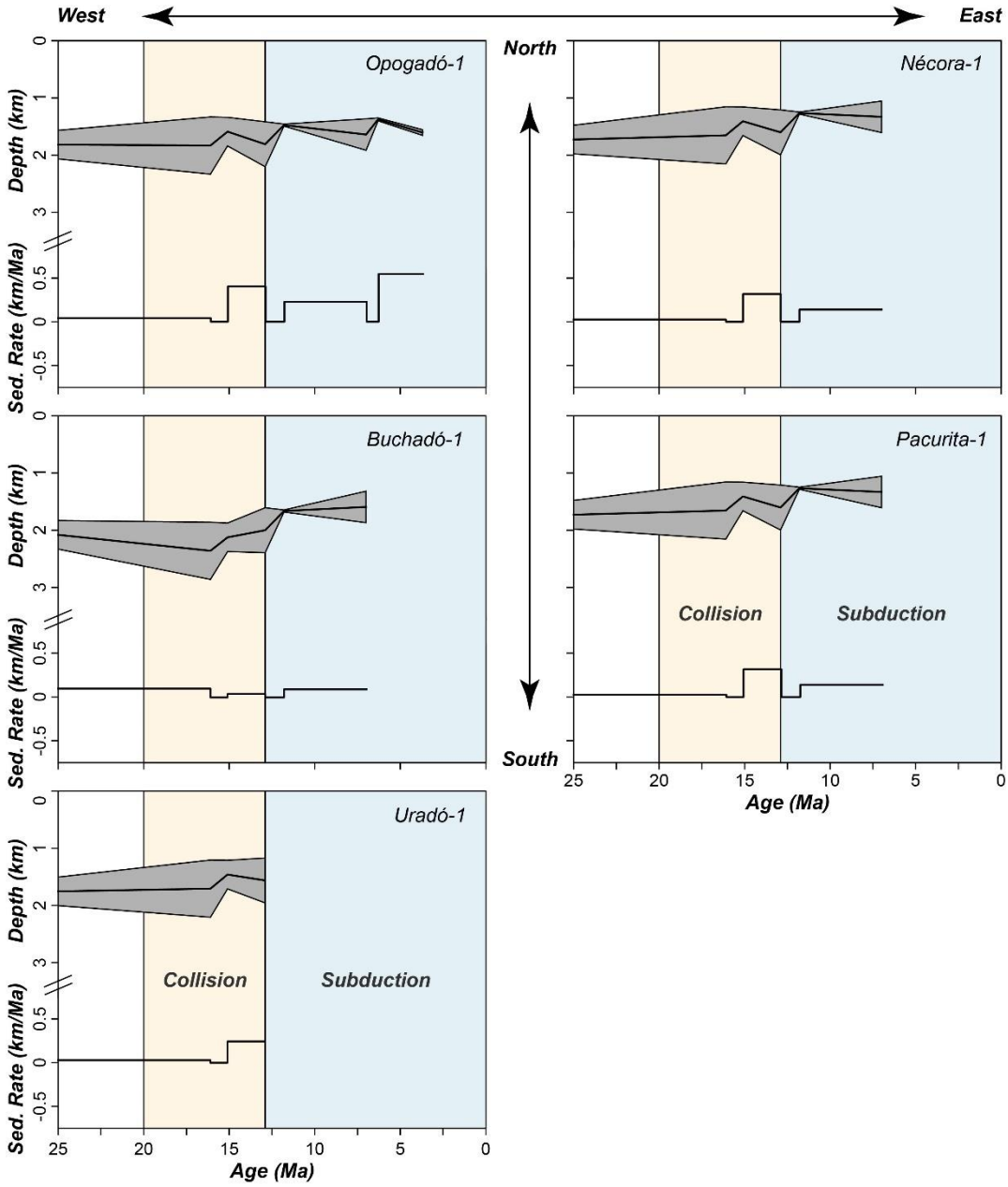

Figure 4.8. Tectonic subsidence and sedimentation rates curves derived from our results of the 1D backstripping analysis. Dark-gray shades represent the uncertainty related to the accumulation paleodepth, whereas thick black lines denote the average tectonic subsidence.

It is worth mentioning that the sedimentation rates during the accumulation of the Sierra Fm. (~12-7 Ma) might be overestimated as available data from exploratory boreholes do not differentiate between this unit and the unconformably overlying Munguidó Fm., whose thickness remains undetermined for most of the available boreholes and surface stratigraphic sections (Cediel et al., 2009; Duque-Caro, 1990b; Zapata, 2000). This means that, whatever the thickness of the Munguidó Fm., it is being added to the Sierra Fm., and thus, the estimated decompacted thickness and sedimentation rates between ~12-7 Ma could be actually lower. Only the northernmost borehole (Opogadó-1) allowed differentiating between the Sierra and the Munguidó Fm. (Duque-Caro, 1990b). There, the upper-Miocene unconformity (~7-6 Ma) that separates the latter units was coeval with basin uplift at moderate rates (~400 m/Myr), which was followed by low subsidence (<100 m/Myr) and moderate-high sedimentation rates (~550 m/Myr) during the accumulation of the Munguidó Fm. (Fig. 4.8).

4.5.3. Sedimentary provenance constraints

Most of the analyzed samples selected for provenance analyses were collected from measured sections in the Tribugá Gulf, where there is a stronger stratigraphic control; however, as discussed in the following sections, new and previous provenance constraints from the Quibdó area are used for comparison and correlation, which aid us to provide basin-scale representativeness.

4.5.3.1. Results of petrographic, geochronological, isotopic and geochemical analyses of Neogene strata from the Tribugá Gulf

The upper Oligocene-middle Miocene Uva Fm. is mostly composed of fossil-rich (up to ~75%) wackestones and packstones with minor terrestrial input that includes subangular biotite, amphibole, pyroxene, quartz and euhedral feldspar (Fig. 4.9). A total of 63 individual zircon U-Pb ages were obtained from sample J-32, collected at the base of the southernmost stratigraphic section measured in the Tribugá Gulf, below the angular unconformity that separates the Uva Fm. and the overlying Chorí informal unit (Fig. 4.6). Over 22% of the analyzed grains yielded ages older than 100 Ma, corresponding to Permian, Carboniferous, and Neoproterozoic to Paleoproterozoic ages (Fig. 4.10). However, most of the dated zircons yielded Eocene (~56-41 Ma; 47%), Late Cretaceous (~90-74 Ma, 17%), and early Miocene (~19-17 Ma; 8%) age peaks. From the latter, a maximum depositional age of 17.6 $\pm$ 0.3 Ma

was estimated according to the Maximum Likelihood Age (MLA) algorithm of Vermeesch (2021), which is considerably younger than the Oligocene age suggested from the calcareous nannofossils.

Compositionally, zircons from the Uva Fm. show low concentration of Rare Earth Elements (∑REE < 2000 ppm), Lu (< 260 ppm) and Ti (< 6 ppm), and variable contents of Hf (~6.000-11.000 ppm) and Y (~300-3.600 ppm), with no apparent trend with age. Zircons show both positive and negative Eu anomalies (Eu/Eu* ~0.2-2.5), positive Ce anomalies (Ce/Ce* ~2-130; after Loader et al., 2017), and U/Yb and Nb/Yb ratios shifting from 0.05 to 1.8, and from 0.002 to 0.034, respectively (Fig. 4.10). The latter elemental ratios, allow analyzed zircons to follow the magmatic arc trend, partially overlapping the mantle array field in the discrimination diagram of Grimes et al. (2015; Fig. 4.10). Permian and older zircons are isotopically evolved with εHf_i between -15.6 and +1.7, whereas Cretaceous and younger grains are more juvenile with εHf_i ranging from +8.7 to +15.1 (Fig. 4.10). No detrital pyroxenes from the Uva Fm. were recovered for geochemical analyses given the low abundance of siliciclastic material.

Calcareous sandstones from the lower Chorí unit (samples J-14, J-19, J-31) are fine- to coarse-grained texturally immature feldspathic and lithic arkoses (Fig. 4.9), composed of subrounded fragments of monocrystalline and minor polycrystalline igneous quartz, feldspar, volcanic lithics with microlithic and lathwork textures, and sedimentary lithics mainly represented by siliceous mudstones (Fig. 4.9). Detrital biotite, clinopyroxene, amphibole, chlorite and epidote-group minerals are also found. Bioclastic materials mostly include algae, foraminifera and mollusks. Minor glauconite (~1%) was identified in all analyzed samples. A total of 197 individual zircon dates were obtained from samples J-14 and J-19, 28-52% of which are older than 100 Ma and cluster at Triassic-Permian, Devonian-Silurian, and Neoproterozoic to Paleoproterozoic age peaks (Fig. 4.11). As in sample J-32 from the Uva Fm., most of the analyzed zircons from the lower Chorí unit are Eocene (~56-40 Ma; 39%), Paleocene (~57-63 Ma; 13%) and Late Cretaceous (~92-69 Ma, 8%) in age. Since the youngest dated zircons yielded Eocene ages, we did not estimate a maximum accumulation age for the lower Chorí unit as it would be significantly older than the expected Neogene ages according to published biostratigraphic constraints (Duque-Caro, 1990b; Haffer, 1967; Zapata, 2000).

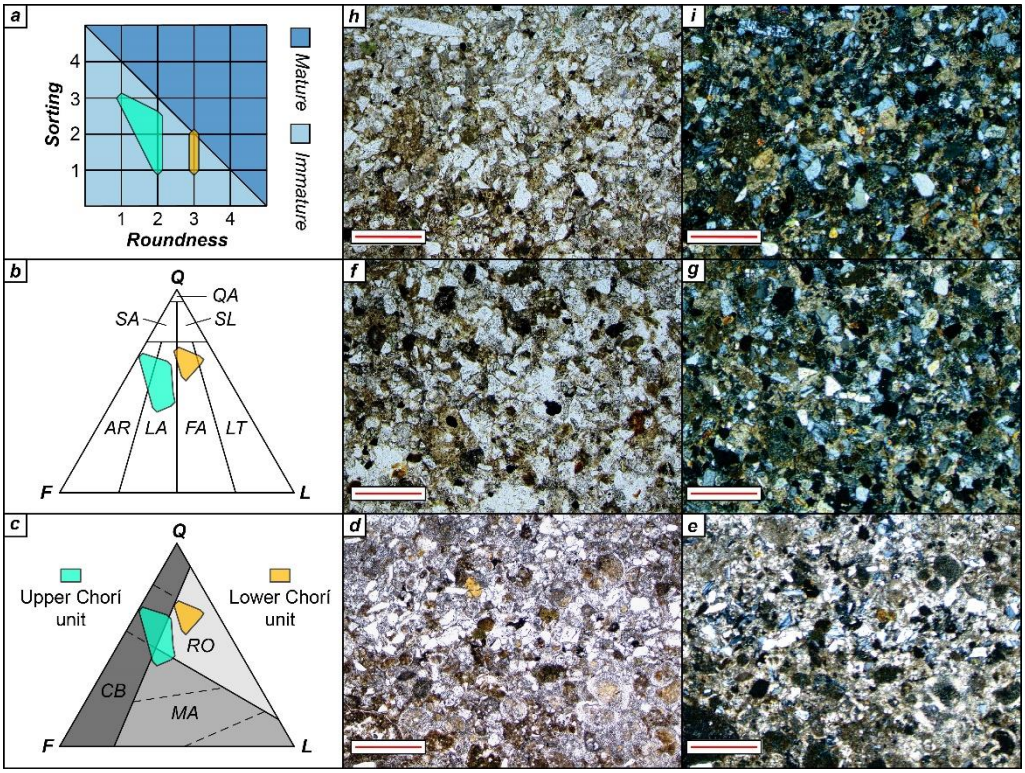

Figure 4.9. Summary of the results of our petrographic analyses showing the main textural and compositional features. a) Diagram showing the textural maturity by means of the roundness and sorting of clastic components of the Chorí unit. b) Q-F-L classification diagram of Folk (1980). c) Discrimination diagram of Dickinson (1985).

Dated zircons from sample J-19 have low concentrations of REE (∑REE < 1.400 ppm), Lu (< 130 ppm), Y (~300-1.750), Ti (5-5.5 ppm), and moderate abundance of Hf (~8.000-11.000 ppm), with no apparent trend with age. Negative and positive Eu anomalies (Eu/Eu* ~0.2-1.7), and slightly to well defined positive Ce anomalies (Ce/Ce* ~1-124; after (Loader et al., 2017) were observed in the analyzed zircons, which have U/Yb and Nb/Yb ratios shifting from 0.09 to 1.6, and from 0.002 to 0.014, respectively (Fig. 4.11). The latter ratios, allow analyzed grains to plot following the magmatic arc trend, with a partial overlap with the field of mantle-derived zircons in the discrimination diagram of Grimes et al. (2015; Fig. 4.11). Results from the Hf isotope analysis showed that old zircons (Proterozoic) are isotopically evolved with εHf_i ranging between -4.3 and +8.1, whereas Cretaceous and younger zircons are juvenile with εHf_i shifting from +13.5 to +15.8 (Fig. 4.11).

Detrital clinopyroxenes from sample J-19 from the lower Chorí unit have diopside to augite compositions, with Mg# shifting from 57 to 70 [Mg# = Mg/(Mg + Fe)], which decreases as Ti content increases (Fig. 4.12). Most of the analyzed grains are Ti- and Cr-poor (Ti < 0.02 and Cr < 0.001, c.p.f.u.) and have moderately high abundances of Na (~0.02-0.04 c.p.f.u.), Ca (~0.84-0.91 c.p.f.u.), and Al (~0.03-0.21 c.p.f.u.). Accordingly, clinopyroxenes from sample J-19 have geochemical affinity with subalkaline-alkaline tholeiitic arc settings (Fig. 4.12; after Leterrier et al., 1982).

Calcareous sandstones from the upper Chorí unit (samples J-5, J-7, J-8, J-10, J-20, J-23, J-24, and J-26), are represented by fine- to coarse-grained texturally immature arkoses and lithic arkoses, composed of subangular monocrystalline and polycrystalline igneous quartz, feldspar, plutonic and volcanic (mostly with microlithic and lathwork textures) lithic fragments, and siliceous mudstone lithics (Fig. 4.9). Detrital amphibole and pyroxenes are moderately abundant (~7-17%), and are accompanied by minor chlorite, epidote-group minerals, biotite, muscovite, and glauconite. Bioclastic fragments are mostly represented by foraminifera, algae and mollusks. A total of 298 individual ages were obtained from samples J-7, J-8 and J-24, only less than 2% of which, unlike samples from the Uva Fm. and the lower Chorí unit, are older than 100 Ma. Most analyzed grains yielded Eocene ages (~56-35 Ma; 91%), although minor lower Miocene zircons (~18-17 Ma; 2%) were also found (Fig. 4.13).

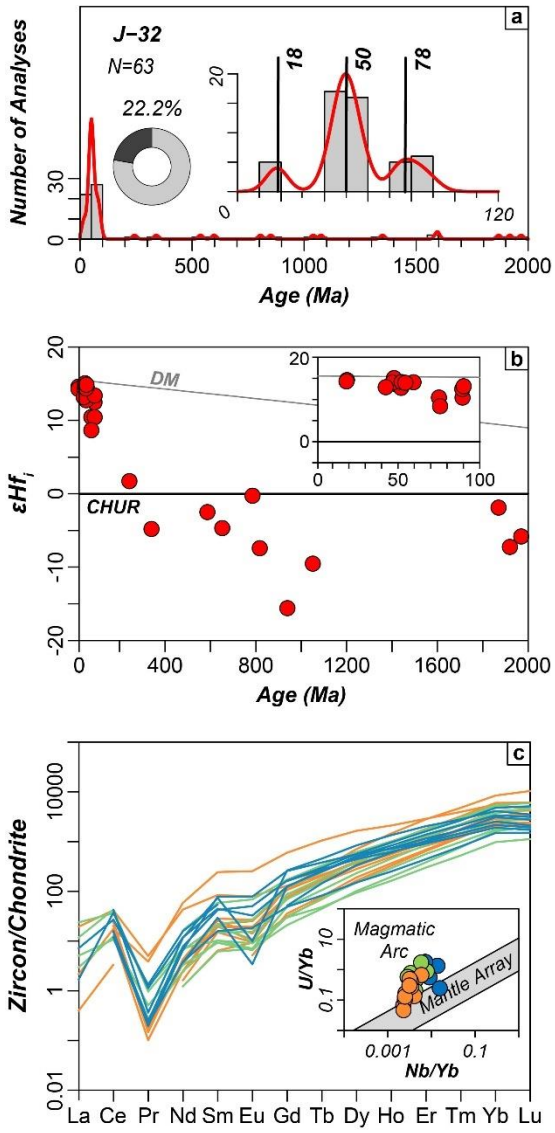

Figure 4.10. Summary of the provenance analysis for the Uva Fm. a) KDE of detrital zircon U-Pb ages showing the main peaks (thick black lines) and the proportion of ages older than 100 Ma (dark portion of the pie diagram). b) εHfi values for analyzed zircons. c) REE diagram showing the results of the trace element analysis of dated zircons; inset showing the discrimination plot of Grimes et al. (2015).

Compositionally, dated zircons from the upper Chorí unit have low abundance of REE (∑REE < 2.400 ppm), Lu (< 165 ppm), and Ti (4.8-6.1 ppm), with variable Y and Hf, shifting from 250 to ~3.000 ppm, and from 6.700 to ~11.000 ppm, respectively, with no apparent correlation between age and trace elements concentrations. Zircons show both positive and negative Eu anomalies (Eu/Eu* ~0.6-2.1), and slightly negative to positive Ce anomalies (Ce/Ce* ~0.7-135.8; after Loader et al., 2017). U/Yb and Nb/Yb ratios vary between 0.01 to 0.9, and from 0.002 to 0.006, respectively, which allow the analyzed zircons to mainly plot following the magmatic arc trend in the discrimination diagram of Grimes et al. (2015; Fig. 4.13). Only one zircon older than 100 Ma (261.4 $\pm$ 2.1 Ma) was analyzed by Hf isotopes, which yielded a εHf_i of +1.7, whereas Eocene zircons showed isotopically more juvenile compositions with εHf_i shifting from +12.7 to +15.1 (Fig. 4.13).

Detrital clinopyroxenes from samples J-23 and J-24 of the upper Chorí unit have diopside to augite compositions with Mg# between 52 and 78, which decreases as Ti increases (Fig. 4.12). Analyzed grains are Ti- and Cr-poor (Ti < 0.02 and Cr < 0.002, c.p.f.u.), but have moderately high concentrations of Ca (~0.83-0.95 c.p.f.u.), Na (~0.01-0.09 c.p.f.u.), and Al (~0.02-0.18 c.p.f.u.). As in sample J-19 from the lower the Chorí unit, clinopyroxenes from samples J-23 and J-24 are akin to subalkaline-alkaline supra-subduction settings, probably associated to tholeiitic and in minor proportion to calc-alkaline arcs (Fig. 4.12; after Leterrier et al., 1982).

In addition to Neogene strata, we analyzed the geochemistry of detrital pyroxenes from modern sediments collected in two rivers draining the Baudó Range towards the Pacific Ocean (samples LR-6 and NG-1), including one locality previously analyzed by detrital zircon geochronology (LR-6; León et al., 2022). The latter, yielded abundant Eocene (~56-42 Ma), Cretaceous-Paleocene (~100-56 Ma), and minor Triassic to Proterozoic individual ages, which are interpreted to mainly suggest recycling of Oligocene-Miocene strata outcropping in the surrounding areas (León et al., 2022). This is supported by the results of our geochemical analysis of detrital pyroxenes, which have diopside to augite compositions and are mostly characterized by Mg# shifting from ~50 to 80, like those analyzed from the lower and upper Chorí units (Fig. 4.12). However, clinopyroxenes from modern sediments (samples LR-6 and NG-1) show two compositional domains, mostly in terms of their Ti and Cr content, since highly variable abundances of Ca (~0.50-0.92 c.p.f.u.), Na (~0.01-0.10

c.p.f.u.), and Al (~0.01-0.21 c.p.f.u.) are similar. A first group, representing ~60% of the analyzed grains, are Ti- and Cr-poor (Ti + Cr < 0.02, c.p.f.u.), and are dominantly akin to subalkaline supra-subduction settings, probably associated with tholeiitic arcs (Fig. 4.12). Conversely, the second compositional group that was not recognized in the Oligocene-Miocene strata is characterized by higher Ti and Cr (Ti + Cr ~0.02-0.04, c.p.f.u.), which are akin to subalkaline anorogenic (MORB-like) settings (Fig. 4.12).

4.5.3.2. Results of geochronological analyses of Neogene strata from the Quibdó area

One sample from the Uva Fm. (QT-20) was collected at the base of the measured section in the Quibdó area (Fig. 4.7), which is represented by a wackestone with minor siliciclastic input as suggested by the presence of moderately sorted subangular fragments of quartz, feldspar, amphibole and volcanic lithics, as well as remnants of organic matter. Only three detrital zircons were successfully dated and yielded U-Pb ages of 41.9 $\pm$ 0.8 Ma, 47.8 $\pm$ 1.2 Ma, 56.4 $\pm$ 0.6 Ma, and 90.1 $\pm$ 1.5 Ma.

Two additional samples from the Sierra and the Quibdó formations were collected in the Quibdó area and analyzed by detrital zircon U-Pb geochronology. Sample QT-12 of the Sierra Fm. was extracted from a fossil-rich fine- to medium-grained lithic arkose collected along the measured composite stratigraphic section (Fig. 4.7), which is mostly composed of moderate- to well-sorted angular to subangular fragments of quartz, feldspar, amphibole and mudstone lithics, with minor epidote and glauconite. Most of the analyzed zircons yielded Eocene (~56-41 Ma; 89%) and Paleocene (~62-57 Ma; 8%) ages, with only one grain older than 100 Ma (1123 $\pm$ 71 Ma). Conversely, over 30% of the 104 analyzed zircons from sample QT-3 of the Quibdó Fm., collected in an isolated outcrop of a highly weathered and poorly consolidated polymictic conglomerate, are older than 100 Ma, yielding Triassic, Neoproterozoic to Paleoproterozoic age peaks (Fig. 4.14). Most of the analyzed zircons yielded Late Cretaceous (~92-66 Ma; 34%) and Eocene (~52-43 Ma; 13%) ages, although a major middle-late Miocene age peak was also observed (15-10 Ma; 20%). From the latter, we estimated a maximum depositional age of 10.1 $\pm$ 0.1 Ma (after Vermeesch, 2021).

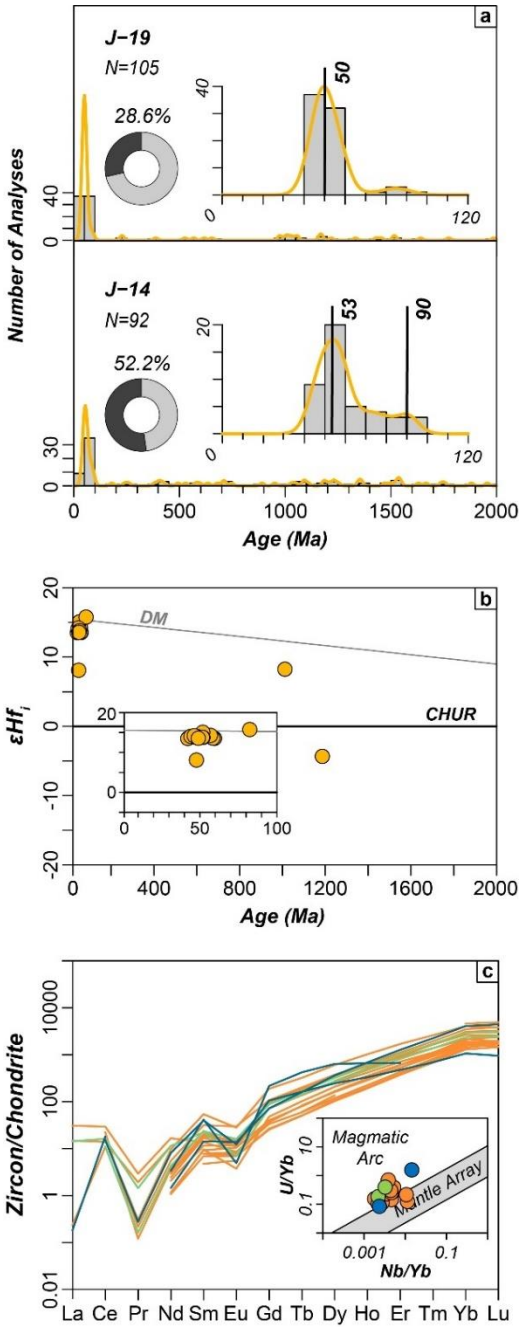

Figure 4.11. Summary of the provenance analysis for the lower Chorí unit. a) KDE of detrital zircon U-Pb ages showing the main peaks (thick black lines) and the proportion of ages older than 100 Ma (dark portion of the pie diagram). b) εHfi values for analyzed zircons. c) REE diagram showing the results of the trace element analysis of dated zircons; inset showing the discrimination plot of Grimes et al. (2015).

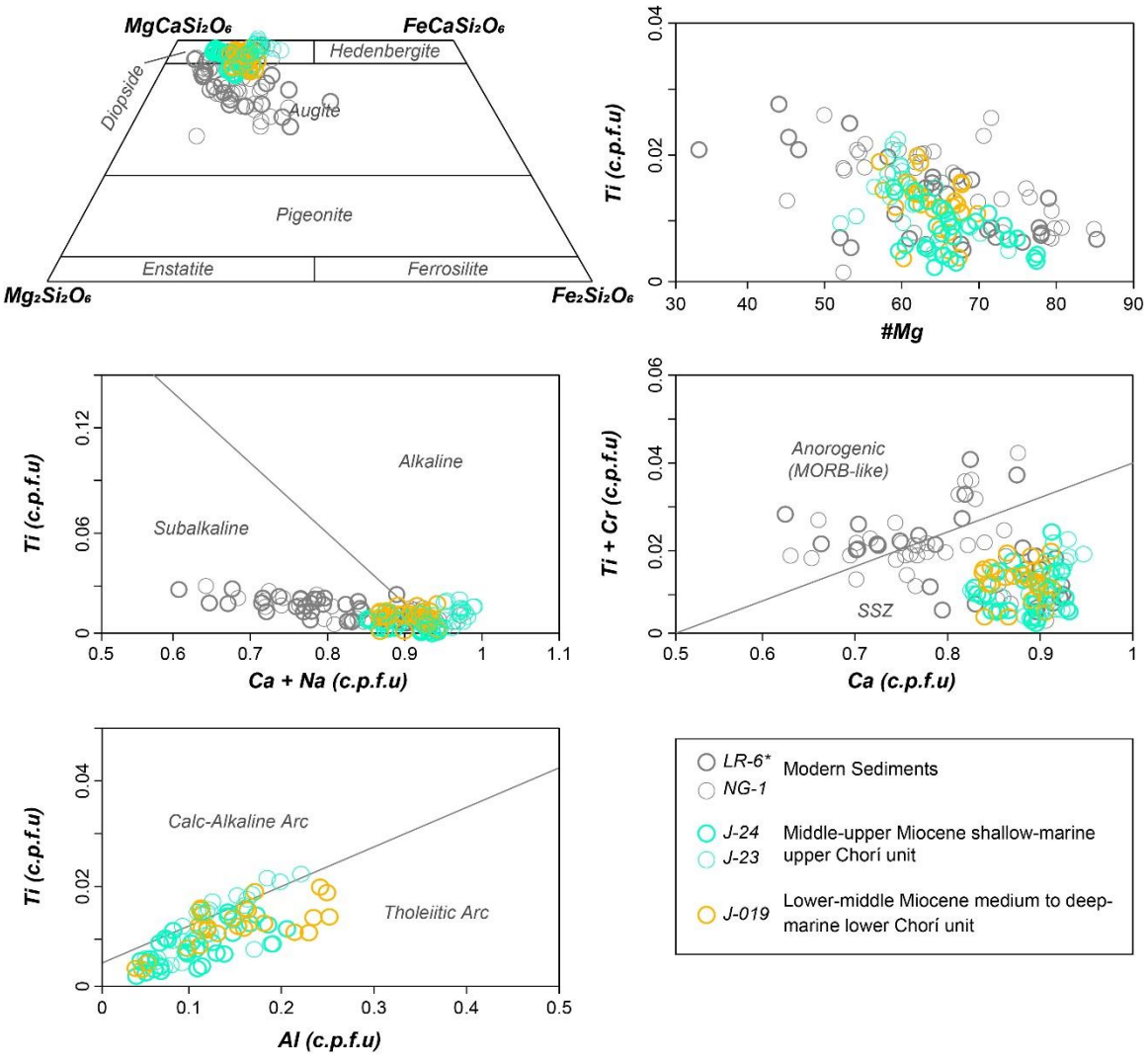

Figure 4.12. Discrimination diagrams for clinopyroxenes after Leterrier et al. (1982), showing the results of the detrital geochemical analysis.

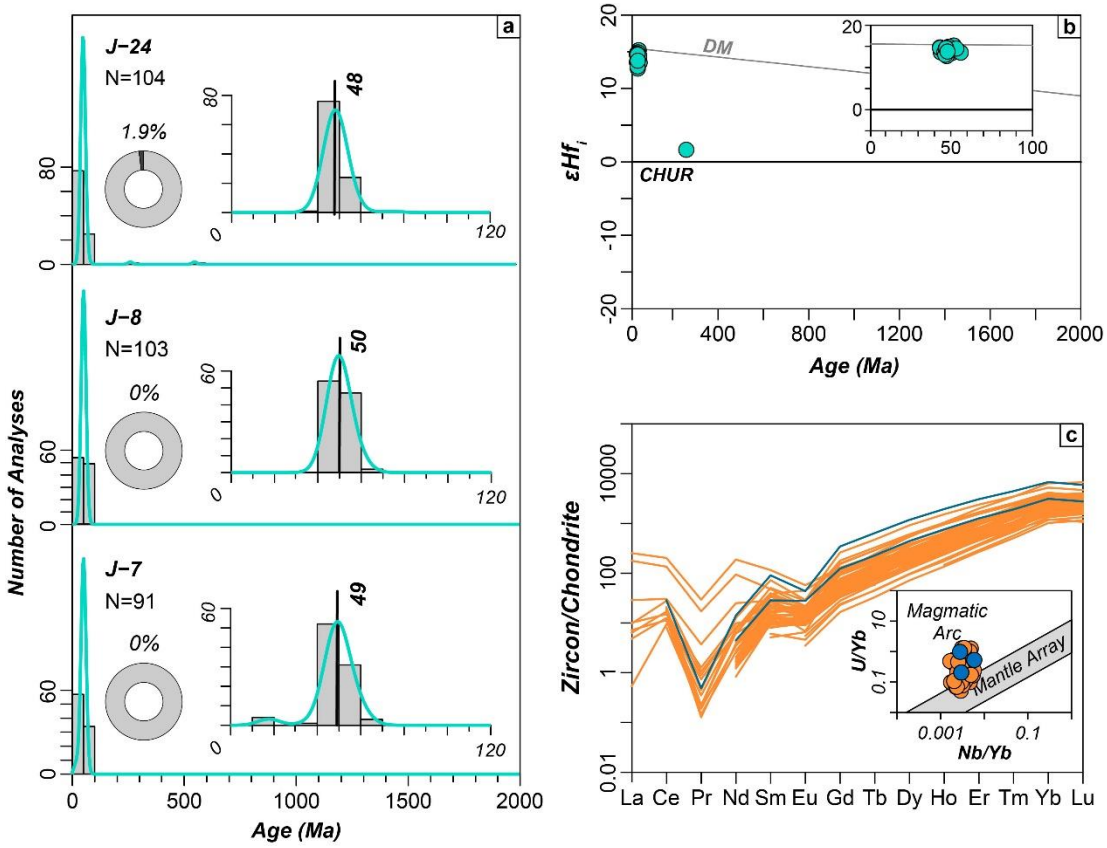

Figure 4.13. Summary of the provenance analysis for the upper Chorí unit. a) KDE of detrital zircon U-Pb ages showing the main peaks (thick black lines) and the proportion of ages older than 100 Ma (dark portion of the pie diagram). b) εHfi values for analyzed zircons. c) REE diagram showing the results of the trace element analysis of dated zircons; inset showing the discrimination plot of Grimes et al. (2015).

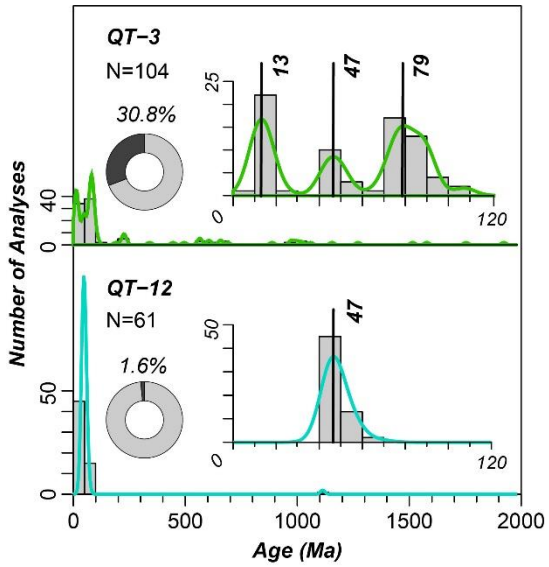

Figure 4.14. KDE of detrital zircon U-Pb ages showing the main peaks (thick black lines) and the proportion of ages older than 100 Ma (dark portion of the pie diagram) for analyzed samples of the Sierra Fm. (bottom) and the Quibdó Fm. (top) collected in the Quibdó area.

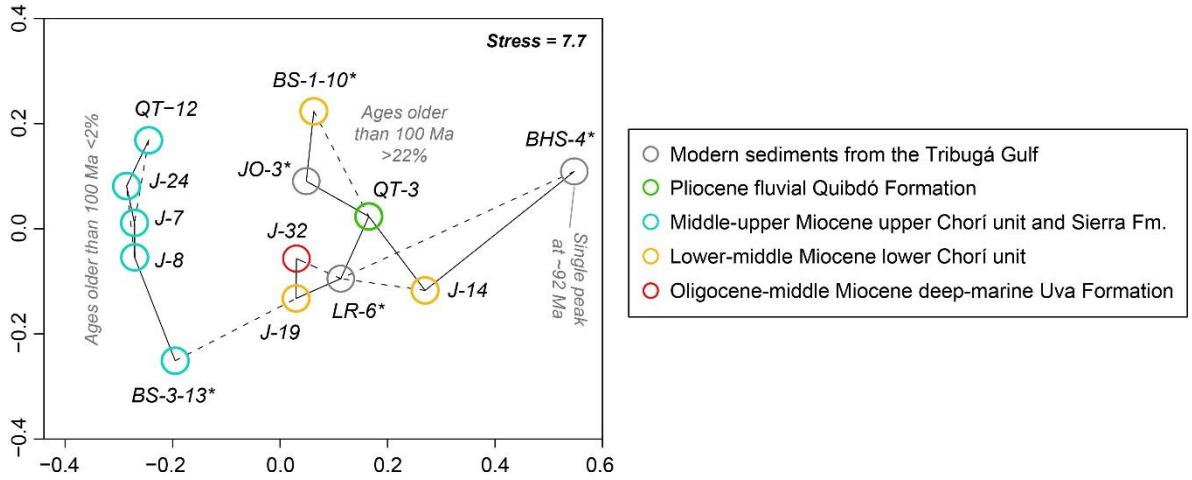

Figure 4.15. Non-metric multidimensional scaling (MDS) showing the dissimilarity between detrital zircon age populations of the Neogene strata of the Atrato Basin.

4.5.3.2. Source areas interpretation

The observed textural immaturity of Neogene strata indicates short residence in the sedimentary systems, which is coherent with their rapid syn-tectonic deposition. Compositionally, these rocks were likely sourced from mixed mafic-intermediate crystalline rocks and reworked siliciclastic strata, as suggested by the presence of relatively abundant amphibole, pyroxene and epidote-group minerals, and lithic fragments of sandstones and mudstones. The results of our provenance analysis suggest the dominance of Paleocene-Eocene sources for the analyzed Oligocene to Miocene strata, which are probably related to isotopically juvenile magmatic arcs, as suggested by the Hf isotopes and the geochemistry of detrital clinopyroxenes (Figs. 4.10 to 4.14). Such compositional and age constraints are strongly consistent with a provenance from the remnant CAA, as indicated by available petrological data for the latter (Barbosa-Espitia et al., 2019; Buchs et al., 2019a; Cardona et al., 2018; Wegner et al., 2011), and previous interpretations for middle-upper Miocene strata of the Atrato and the suture-related basins (León et al., 2018; Rodríguez et al., 2016). Early Miocene zircon U-Pb ages found in the Oligocene-middle Miocene Uva Formation are probably derived from distal air-fall deposits related to subaerial pyroclastic activity of the Oligo-Miocene CAA (e.g. Buchs et al., 2019b), for which ~30-20 Ma U-Pb ages have been documented (e.g. Montes et al., 2012; Rooney et al., 2011; Whattam et al., 2012). This is further supported by the presence of thin tuffaceous beds interlayered with pelagic carbonates of the Uva Fm. (Duque-Caro, 1990b).

Conversely, detrital zircon ages older than 100 Ma, which apparently represents the oldest magmatic activity of the CAA (León et al., 2022; Whattam and Stern, 2015), are interpreted to reflect provenance from reworked continental-affinity domains that according to tectonic and paleogeographic reconstructions are represented by Cretaceous-Paleogene siliciclastic strata of the Colombian Western Cordillera (León et al., 2018; Pardo-Trujillo et al., 2020a). These rocks are thought to preserve the syn- to post-collisional sedimentary record of the Cretaceous collision of the leading edge of the Caribbean oceanic plateau against northwestern South America (Pardo-Trujillo et al., 2020a), and were primarily sourced by Upper Cretaceous magmatic units from either the basement of the Western Cordillera and/or the Central Cordillera, and by Lower Cretaceous strata and Triassic and older metamorphic

rocks of the latter (see a review of the potential source areas of the Central Cordillera in León et al., 2019).

We interpret the CAA and the Cretaceous-Paleogene strata of the Western Cordillera, as the primary sedimentary sources for the Oligocene to middle-upper Miocene Uva, Napipí and Sierra formations, and the correlatable Chorí unit. The near disappearance of the Cretaceous and older detrital zircon U-Pb ages in the Sierra Fm. suggest a major reorganization of the source areas during the middle-upper Miocene (Fig. 4.15), whose origin is probably attributed to the uplift of the CAA near the collisional front (suture zone) that prevented the passage of easterly sediments derived from the continental paleomargin (discussion in sections 4.6.2 and 4.6.3). Previous work on the sedimentary provenance of the middle-upper Miocene strata of the AB had interpreted the Sierra Fm. as sourced from recycled Cretaceous-Paleogene strata of the Western Cordillera, according to the presence of Triassic-Permian and older detrital zircon U-Pb ages (León et al., 2018). Nevertheless, in the light of our new comprehensive tectonostratigraphic and provenance analysis of the AB, we consider that samples analyzed in the work by León et al. (2018) were likely collected from the Quibdó Fm. rather than from the underlying Sierra Fm. as previously thought, which however, do not disagree with proposed tectonic interpretations regarding the early-middle Miocene collision of the CAA (see a discussion below in sections 4.6.1 and 4.6.2).

The late Miocene-Pliocene Quibdó Formation records a second period of reorganization of source areas, as indicated by the reappearance of abundant detrital zircons older than 100 Ma (Fig. 4.15). We interpret this change in the provenance of rocks from the AB as associated with intense reworking of older strata (i.e. Uva and Napipí formations), which is further supported by the high abundance of conglomerate clasts of calcareous litharenites and mudstones. As discussed below, this reorganization of the source-to-sink systems is probably related to the establishment of fully terrestrial conditions and the formation of a dominantly longitudinal drainage system like the modern Atrato River, which would have favored the incorporation of recently exhumed older strata.

An additional observation allowed from our multi-proxy provenance analysis is the strong similarity between the Napipí and Sierra formations with the informal lower and upper Chorí units, respectively, which we use to tentatively correlate them (see discussions in sections

6.2 and 6.3). This interpretation is further supported by our new and previous stratigraphic constraints, which may suggest that the above-mentioned units were likely accumulated in spatially correlatable depositional settings in organic-rich mid- to shallow-marine conditions and share similar biostratigraphic signatures represented by middle-late Miocene foraminifera assemblages (Zapata, 2000).

4.5.4. Present-day structural and morphological configuration of the forearc

The modern physiographic configuration of the northern Colombian forearc basin can be divided into an inner domain represented by the flat-lying recent deposits of Atrato River overlying the above-described Oligocene-Pliocene strata of the AB, and an outer region including the coastal Baudó Range and the narrow shelf of the northern Colombian Pacific coast (Fig. 4.16). This structural fragmentation of the AB into an inner and outer (coastal) segments seemingly occurred as a consequence of the post-late Miocene emergence of the Baudó Range that was associated with widespread uplift and rapid exhumation of the northwesternmost Andes (León et al., 2021b, 2018). Nowadays, the inner AB is bounded to the east by the foothills of the Western Cordillera, to the south by the Istmina Hills, and to the west by the Baudó Range (Fig. 4.16). Each of these four regions defines an independent morpho-structural domain characterized by contrasting terrain morphology, as suggested by the highly variable Terrain Ruggedness Indices (TRI: mean of the absolute differences between the elevation value of a cell and the values of its eight surrounding cells; Riley et al., 1999; Fig. 4.16).

The inner AB is a nearly N-S-oriented narrow (< 50 km-wide) depression with an average elevation of less than 500 m.a.s.l, which extends ca. 300 km northward from the Istmina Hills (~5°N) to the Colombia-Panama border (~8°N). It is characterized by a smooth relief and lacks topographic lineaments. Conversely, both the Western Cordillera and the Baudó Range are characterized by steeper slopes and a rougher relief and show widespread topographic lineaments with a dominant NNW trend (N5-10°W, 14-20%), followed by subordinate lineaments preferentially striking NE (N20-60°E, 5-11%) and WNW (N50-80°W, 3-8%; Fig. 4.16). These observations allow extending the results of León et al. (2021c), who studied the structural patterns of the outermost (coastal) forearc region and found a similar distribution of the main trends of topographic lineaments. The Istmina Hills, represents a deformation

(suture) zone more than 40 km wide that mostly affects Oligocene to middle Miocene strata, and is thought to represent the southernmost limit of the accreted CAA (Duque-Caro, 1990a). This domain shows a contrasting structural pattern when compared with the Baudó Range and the Western Cordillera (Fig. 4.16), with topographic lineaments mainly striking NE (N40-70°E, ~30%).

The spatial distribution of precipitation across the northern Colombian forearc basin is closely related to the structural and morphological fragmentation of the AB, as suggested by the drastic drop of mean annual precipitation from 6.000-7.000 mm/yr to ~2.000 mm/yr at the western slopes of the Western Cordillera (Fig. 4.16; Fick and Hijmans, 2017). This suggests that there might be a causal relationship between the uplift history of the northern Colombian forearc, particularly the northwestern flank of the Western Cordillera (i.e. Dabeiba Arch; Duque-Caro, 1990a), and the constitution of its extremely humid rainforest that hosts the Chocó biodiversity hotspot (Myers et al., 2000), which we further discuss in section 4.7.

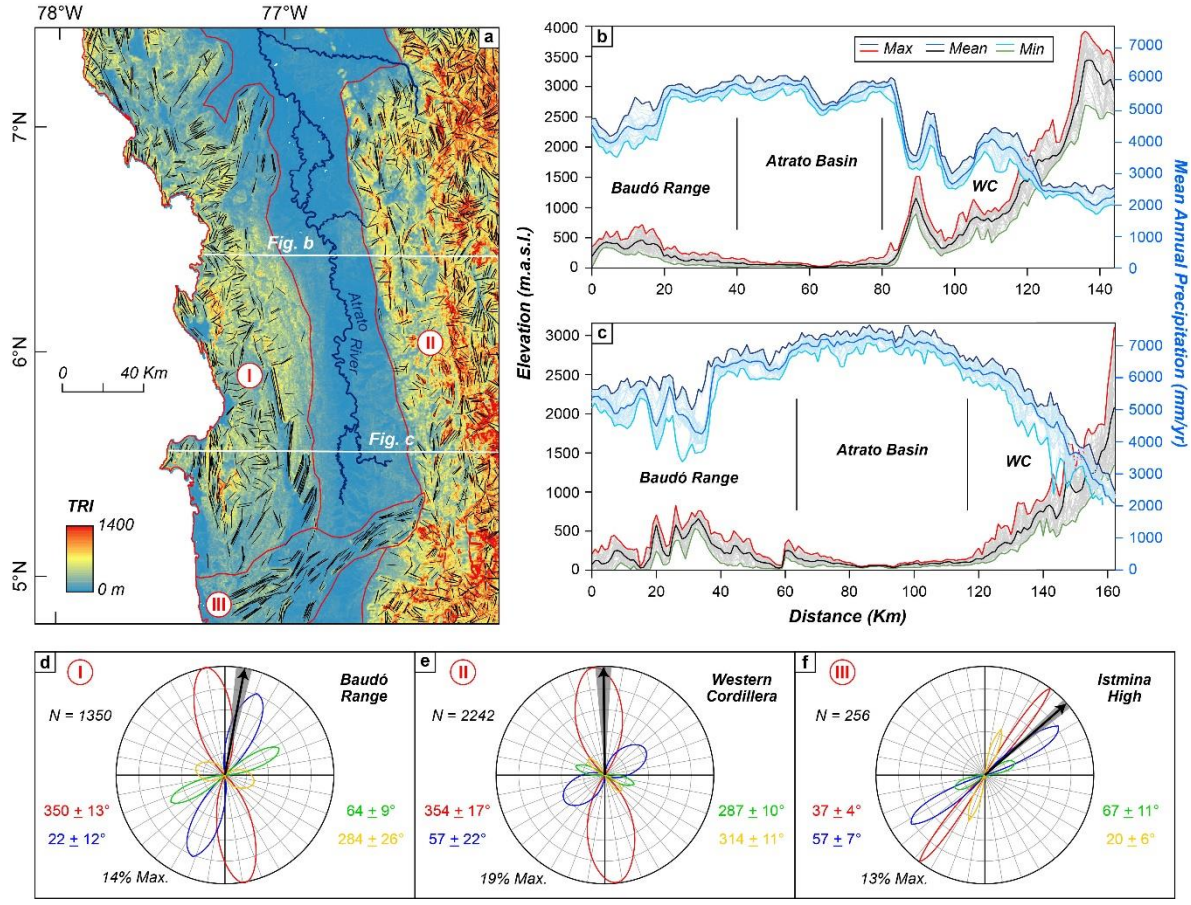

Figure 4.16. Summary of the morphological and structural analyses of the northern Colombian forearc basin. a) Terrain Ruggedness Index (TRI) values showing the presence of three contrasting domains; I=Baudó Range, II=Western slope of the Western Cordillera, III=Istmina Hills; and topographic lineaments. b) East-west swath profiles showing the topography and mean annual precipitation across the forearc basin. c) Rose diagrams showing the main azimuthal trends of topographic lineaments; black arrow show the mean azimuth of lineaments and the gray-shaded region the associated uncertainty. N=number of lineaments.

4.6. Neogene tectonostratigraphic evolution of the Atrato forearc basin

4.6.1. Early-middle Miocene collision of the CAA and associated intra- or back-arc basin

According to available biostratigraphic and paleogeographic reconstructions, the youngest strata of the Chucunaque and Atrato basins likely accumulated in an intra- or back-arc setting related to an extensional tectonic phase during the growth of the CAA (e.g. Coates et al., 2004; Montes et al., 2012). In this scenario, Eocene-Oligocene strata probably accumulated in deep marine conditions and were mostly sourced from partially emerged and volcanically active islands with a Cretaceous volcano-plutonic substratum (Montes et al., 2012; Ramírez et al., 2016), which were far from the South-American paleomargin, as suggested by the virtual lack of terrestrial input with continental affinity (Coates et al., 2004; Ramírez et al., 2016). Yet, the drivers of extensional tectonics in the CAA and the subsequent formation of marginal basins remain barely explored. An existing model tentatively proposes an eastward propagation of a subhorizontal tear in the Farallon slab (Nazca slab after the ~25 Ma fission of the Farallon lithosphere; Lonsdale, 2005), associated with the emplacement of ~30-20 Ma adakite-like rocks in a high heat-flow regime, which was accompanied by steepening of the subducting slab (Whattam et al., 2012). This may have resulted in a dominantly extensional or transtensional regime in the upper-plate that allowed the formation of marginal intra- and/or back-arc basins Nakakuki and Mura, 2013; Sdrolias and Müller, 2006; Uyeda and Kanamori, 1979), such as the Chucunaque and Atrato basins, and also pull-apart basins (e.g. Canal Basin in central Panama; Ramírez et al., 2016).

The presence of lower Miocene (~20 Ma) mafic-ultramafic units in western Colombia nearby the southeastern limit of the CAA (e.g. Condoto and Viravira complexes), interpreted as formed in an extensional supra-subduction setting (Tistl et al., 1994), further supports the above interpretation. This, because the lower Miocene magmatic units are represented by high MgO and silica-poor basalts and ultramafic rocks, apparently formed by intense (~20%) partial melting of a depleted mantle source modified by metasomatic subduction-related fluids under highly extensional tectonics (Tistl et al., 1994), and could therefore represents an accreted fragment of an oceanic back-arc unit associated with the CAA system (Fig. 4.17).

The Oligocene to the earliest Miocene period of intra-oceanic extensional tectonics in which the Chucunaque and Atrato basins seemingly formed, was partially contemporaneous and shortly followed by the initial collision of Cretaceous to Eocene rocks of the remnant CAA against northwestern South America, whose sedimentary record is represented by the Uva Formation (Fig. 4.17). By this time, the steepening of the subducting slab would had split the CAA into a remnant (inactive) pre-Eocene segment and an active Oligo-Miocene volcanic arc (Fig. 4.17), which as discussed above, could have been associated with the opening of marginal basins, as seemingly occurred during the late Miocene to present-day growth of the Lau Basin in the southwestern Pacific Hawkins Jr., 1995). The mixed provenance of the Uva Fm., including young Eocene and Miocene arc-related components, and pre-middle Cretaceous (Triassic and older) detrital material of continental affinity, suggest sedimentary input from both the remnant and the active segments of the CAA, which were partially emerged (Buchs et al., 2019a, 2019b; Montes et al., 2012; Ramírez et al., 2016), and the South-American paleomargin, which may indicate spatial proximity between colliding blocks (Fig. 4.17). Available detrital zircon U-Pb constraints from early-middle Miocene shallow-marine strata accumulated near the proto-suture zone (Beibaviejo Fm.), also suggest a mixed provenance from the remnant CAA and recycled Cretaceous-Paleogene siliciclastic units representing the northwestern South-American paleomargin (León et al., 2018). This, together with the appearance of tuffaceous layers within the Beibaviejo Fm. that could represent distal air-fall deposits derived from the active Oligo-Miocene CAA, supports the interpretation above.

The Uva Fm. was deposited during a period of slow subsidence and low sedimentation rates in a wide distal shelf, as suggested by our new and previous stratigraphic constraints and the results of our backstripping analysis, which could have been associated with extensional tectonics and/or thermal subsidence during pre- to syn-collisional basin evolution (Fig. 4.17). In such a geodynamic setting, ongoing slab steepening and subsequent increased trenchward suction, and upper-plate dragging by induced toroidal mantle flow could have triggered the observed slow tectonic subsidence during the pre- to syn-collisional intra- or back-arc stage of the AB (e.g. Cassel et al., 2018; Chen et al., 2017; Heuret and Lallemand, 2005). Thermal contraction is also a feasible driver of subsidence, since recent reconstructions of the evolution of the CAA suggest a trenchward migration and considerable

reduction of magmatic activity between ~30-20 Ma and its final cessation by ~18-16 Ma along the region where the Chucunaque and Atrato basins were located (central-eastern Panama and northwestern Colombia in present coordinates; Buchs et al., 2019a; Whattam et al., 2012).

On the other hand, the presence of sandy clastic dykes intruding the carbonate rocks of the Uva Fm., observed around the Quibdó area (i.e. innermost AB), suggests tectonic activity during and/or shortly after sediment accumulation, which we interpret as a consequence of the initial arc-continent collision. The lack of evidence for intense and widespread deformation of the AB, which were apparently focused along its innermost (inland) segment during the Oligocene-middle Miocene, and the apparent continuation of slow subsidence and low sedimentation rates during the accumulation of the Uva Fm., suggest that this period was marked by a "soft" collisional setting, as it apparently did not involve considerable crustal thickening and associated uplift of colliding blocks (Zagorevski and van Staal, 2011). Ongoing deposition in deep- to shallow-marine settings may indicate that this initial collision of the CAA did not contribute considerably to the topographic growth of the northwesternmost Andean and proto-isthmian region.

Available thermochronological constraints suggest that during the early-middle Miocene initial collision, Eocene volcaniclastic rocks of the remnant CAA exposed near the suture zone were slightly buried/heated to temperatures below the apatite fission-track partial annealing zone (~60-120°C; Reiners and Brandon, 2006), whereas Cretaceous-Paleogene strata representing the continental paleomargin were being cooled/exhumed at moderately rapid rates (León et al., 2018). This evidence is consistent with a soft collision scenario, where allochthonous intra- or back-arc strata (e.g. Uva Fm. and underlying volcaniclastic basement) and mafic-ultramafic rocks (e.g. Condoto and Viravira complexes), were barely deformed/uplifted during its accretion to the continental margin. Such geodynamic setting is similar to that proposed for the growth of the Annieopsquotch accretionary tract (AAT; Central Newfoundland, eastern North America) as a consequence of Ordovician collisions between peri-Laurentian and peri-Gondwanan intra-oceanic and microcontinental terranes in the northern Appalachians (Zagorevski et al., 2009; Zagorevski and van Staal, 2011). In this setting, intra-oceanic rocks, such as the Lloyd's River ophiolite in the AAT (Zagorevski et

al., 2009), frontally accreted and/or partially underthrust the continental margin during collision without experiencing intense deformation or high-grade metamorphism.

The middle Miocene stratigraphic hiatus (~16-15 Ma) that separates the Uva Fm. from the overlying Napipí Fm. and the lower Chorí unit was accompanied by a period of basin inversion and shallowing to upper bathyal-outer neritic depths, deformation, and disruption of the deep connection between Pacific and Caribbean waters across the proto-isthmian region, which together indicate increased tectonic activity and initial topographic uplift of the collisional front and surrounding areas. This period was coeval with the onset of exhumation of the remnant CAA nearby the suture zone, as suggested from previous inverse thermal modeling (León et al., 2018), and the subsequent increase of sedimentation rates from <100 m/Myr to ~400 m/Myr and input of siliciclastic material into the AB. The Napipí Fm. and lower Chorí unit show more abundant Paleocene-Eocene detrital zircon ages than the underlying Uva Fm., which is consistent with intense exhumation/erosion of volcaniclastic and plutonic rocks of the CAA. The observed middle Miocene slow subsidence could have been driven by ongoing thermal contraction of the recently extinct Oligo-Miocene magmatic arc, as proposed for the Late Cretaceous Great Valley forearc basin in western North America (Moxon and Graham, 1987).

We interpret the early-middle Miocene evolution of the AB as controlled by a harder collision of the remnant CAA and its plateau-like basement, in which the buoyant crust of the arc-back-arc system (i.e. AB) was scrapped off from the colliding/subducting plate and accreted to and/or partially underplated beneath the continental margin (Fig. 4.17). The positive buoyancy of the accreted/underplated arc-related crustal material could have promoted uplift/exhumation of the upper-plate (e.g. Clift and Hartley, 2007; Delph et al., 2021), which seems to be supported by coeval erosion driven exhumation of the northern Western Cordillera that was likely associated with topographic growth of this morphological feature and the formation of intramontane basins farther inland (Lara et al., 2018; Zapata et al., 2020). This geodynamic scenario could have been associated with the detachment of the middle-upper crust of the CAA, probably facilitated by the presence of a thick and heterogeneous crust (e.g. Boutelier et al., 2003). The lack of accreted deep crustal sections, except by the back-arc Condoto and Viravira complexes, and the expected rheological contrast between the arc-related intermediate-acidic rocks and the underlying mafic plateau-

like basement that could have provided a structural weakness (Vogt and Gerya, 2014), is in good agreement with the above interpretations.

In this case, the onset of exhumation of the easternmost (closest to the suture) remnant CAA at ~15 Ma (León et al., 2018) could have been associated with buoyancy-driven rock uplift, attributed to the loss of the slab pull once the lowermost crust and the lithosphere mantle detached from the colliding/subducting plate and continued sinking (Boutelier et al., 2003; Zagorevski et al., 2009). The subducted material, corresponding to the trailing edge of the Caribbean plate (Fig. 4.17), could eventually have broken off as a consequence of the buoyant effect of accreted rocks in the collisional front that resisted subduction (Vogt and Gerya, 2014; Zagorevski and van Staal, 2011). Yet, the fate of the subducted slab during the early-middle Miocene collision of the CAA, and the potential consequences on the upper-plate magmatic and deformational history still needs to be explored.

4.6.2. Middle-late Miocene transition from arc collision to Nazca subduction and the onset of mountain building in the northwesternmost Andean forearc

The collision of the CAA was followed by the re-establishment of an east-dipping subduction zone, in which the young oceanic Nazca plate began sinking beneath northwesternmost South America at ~14-12 Ma, causing the growth of a post-collisional continental arc (León et al., 2018; Rodríguez and Zapata, 2012). The period of transition from collision to subduction could be interpreted as the establishment of the AB as post-collisional continental forearc basin, and was marked by a stratigraphic unconformity (~13-12 Ma) between the Napipí and Sierra formations (Duque-Caro, 1990b), which was accompanied by a major (kilometer-scale) shallowing of accumulation depths to shallow-marine settings due to tectonically-driven basin inversion. Such episode was also recorded in the Chucunaque Basin, as suggested by the switch from middle bathyal to neritic depths during the accumulation of the Tapaliza and the overlying Tuira formations (Coates et al., 2004). The locus of basin deformation was apparently located along the collisional front between the CAA and northwestern South America, since evidence for stratigraphic hiatuses and/or unconformities is virtually lacking in the outermost AB (Tribugá Gulf), where sedimentation between the lower and upper Chorí units was seemingly continuous.

It is therefore reasonable to interpret the middle Miocene deformational episode as related to the final docking of the CAA, which seems to have triggered the onset of mountain building in the northwesternmost Colombian forearc, as indicated by the occurrence of a major source-to-sink reorganization during the accumulation of the Sierra Fm. and the upper Chorí unit. The results of our detrital geochronological analyses show a near disappearance of zircon U-Pb ages older than 100 Ma in the Sierra and upper Chorí units, which suggest a drastic reduction of sedimentary input from continental sources (i.e. recycled Cretaceous-Paleogene strata of the Western Cordillera; León et al., 2018; Pardo-Trujillo et al., 2020a). The observed decrease of lithic fragments and an increase in feldspar abundance in the Sierra Fm., when compared with the underlying Napipí Fm. and lower Chorí unit., also suggest a limited reworking of older strata and higher contribution of intermediate-felsic material from subvolcanic and/or plutonic rocks by progressive unroofing of the CAA that was being moderately rapid cooled/exhumed (León et al., 2018). We interpret this shift in the provenance as caused by the topographic uplift of the easternmost portion of the CAA located near the suture zone (i.e. Dabeiba Arch, western flank of the Western Cordillera; Duque-Caro, 1990a), which may have constituted a discontinuous morphological barrier for easterly sediments derived from continental-affinity domains (Fig. 4.17) that may also account for the reduction of sedimentation rates from ~400 to less than 200 m/Myr. The sedimentary record of this event in the suture-related basin is virtually lacking, which could be attributed to a transient basin inversion (no sedimentation) due to ongoing topographic uplift and deformation (Fig. 4.17).

Additional evidence for topographic uplift and drainage reorganization along northwestern Colombia and eastern Panama was the closure of the Central American Seaway (CAS, Fig. 4.17), which is thought to have occurred during the middle Miocene (~15-13 Ma), as suggested by the appearance of detritus derived from the CAA in middle-upper Miocene fluvial strata of the northern Caribbean plains of Colombia and intramontane basins (Montes et al., 2015). In such a paleogeographic setting, the Eocene detrital zircons interpreted as derived from the accreted arc could have been sourced from newly emerged areas along the suture zone, which furthers supports our interpretations.

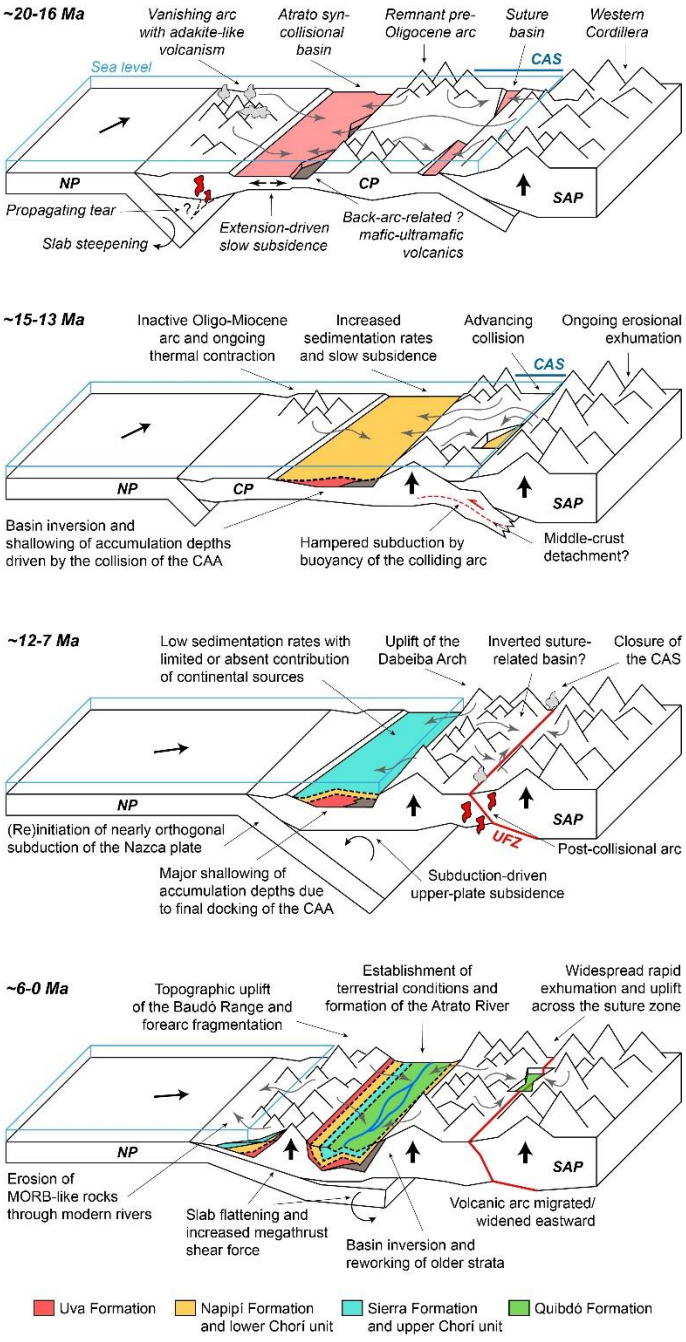

Figure 4.17. Schematic illustrations showing the Neogene tectonostratigraphic evolution of the northern Colombian forearc (Atrato) basin and the interpreted geodynamic setting and processes.

Rapid uplift of the innermost forearc region was followed by very slow tectonic subsidence of the main depocenters where the Sierra Fm. was being accumulated, probably as a consequence of the combined effects of the load of the newly emerged topography and the downward suction of the upper-plate due to the (re)initiation of the eastward subduction of the Nazca plate and the associated mantle drag (Fig. 4.17; e.g. Chen et al., 2017). This tectonic configuration seemingly prevailed until ~7-6 Ma, when the shallowing of the slab dip angle caused orogen-scale tectonic disturbances.

4.6.3. Late Miocene to Recent slab flattening

The late Miocene evolution of the northern Colombian Andes is marked by widespread topographic uplift and changes in the sedimentary patterns along intramontane and foreland basins, as suggested by moderately rapid exhumation of the Western and Eastern Cordilleras, and the accumulation of thick coarse-grained syn-orogenic deposits (León et al., 2018; Parra et al., 2009; Reyes-Harker et al., 2015; Rodríguez et al., 2016; Siravo et al., 2019; and references therein). This was also accompanied by the eastward migration and vanishing of the continental arc, which shifted its main volcanic focus from the suture zone of the CAA (Dabeiba area, northwestern flank of the Western Cordillera) towards the intervening Cauca Valley that lies between the Western and Central Cordilleras (Jaramillo et al., 2019; Wagner et al., 2017), although distal volcanism emplaced farther to the east in the northern Eastern Cordillera has been also associated with the late Miocene arc (Monsalve et al., 2019).

In the northwestern Colombian forearc, the late Miocene period was characterized by short-lived basin inversion and moderately rapid uplift between ~7 Ma and 6 Ma, associated to the occurrence of a stratigraphic unconformity that separates the Sierra Fm. from the overlying Munguidó Fm., which accumulated in nearshore to deltaic conditions (Duque-Caro, 1990b). During this time period, the suture-related basin was characterized by the accumulation of a thick conglomeratic unit interpreted as deposited in a high-energy fluvial system (Guineales Fm.; Rodríguez et al., 2016), which was contemporaneous with rapid (~1 km/Myr) exhumation of the northern Western Cordillera and the areas close to the Uramita Fault Zone (León et al., 2018). The coeval occurrence of deformation/uplift for hundreds of kilometers across the upper-plate, inversion and shallowing of forearc, hinterland and foreland basins, and increased sedimentation rates as a consequence of accelerated erosional

exhumation of source areas, together with inboard migration and vanishing of arc magmatism is consistent with a flat-slab subduction setting (e.g. Finzel et al., 2011; Perez and Levine, 2020; Ridgway et al., 2011). Thus, the observed deformational and stratigraphic patterns of the northern Colombian forearc could be explained by the flattening of the young and buoyant Nazca plate (< 12 Ma; Lonsdale, 2005; Müller et al., 2008), which seemingly began at ~10 Ma as a consequence of the subduction of thick and buoyant oceanic crust (e.g. aseismic Sandra Ridge; Chiarabba et al., 2016), as likely occurred in other flat-slab segments of the Andes (Espurt et al., 2008; Gutscher et al., 1999).

After the late Miocene tectonically driven uplift related to the onset of a flat slab subduction in northern Colombia, the AB was characterized by very slow subsidence and a major increase of the sedimentation rates from < 200 m/Myr to ~500 m/Myr. According to global stratigraphic and structural observations of forearc basins, it has been suggested that slow to very slow subsidence rates are commonly associated with tectonic erosion (e.g. Clift and MacLeod, 1999; Clift and Vannucchi, 2004; von Huene et al., 2004), which may imply the removal of the lowermost forearc crust that could be either underplated farther inland or incorporated into the arc magma sources (Stern, 2011).

A piece of evidence for the loss of lower forearc crustal material by tectonic erosion beneath the AB is the relatively thin crust along the northern Colombian Pacific region, estimated at ~20 km from seismic data (~10 km thinner than in the southern forearc region; Poveda et al., 2015), and the presence of adakite-like melts in the late Miocene volcanic arc, which may suggest the contribution of forearc-derived mafic materials into the magma sources (e.g. Jicha and Kay, 2018). Nevertheless, recent petrological analyses of ~9-5 Ma mafic-intermediate arc-related rocks outcropping along the Cauca Valley, tentatively attributes the adakite-like signature to mid- to high-pressure differentiation of mantle-derived melts emplaced onto a structurally and compositionally heterogeneous continental crust (Jaramillo et al., 2019). This may suggest that, if the lowermost crust of the northern Colombian forearc was removed by tectonic erosion, it could have been underplated farther inland below northwestern Colombia rather than incorporated into the sources of arc-related magmatism.

Although the relationship between subduction erosion and the late Miocene magmatic evolution of the northernmost Andean continental arc remains elusive, we consider that this mechanism could still account for the observed low subsidence rates of the AB and the thin forearc crust. The subduction of high bathymetric features such as the aseismic Sandra ridge could have enhanced tectonic erosion of the northern Colombian forearc since its early interaction with the continental margin that seemingly took place at ~10 Ma (Chiarabba et al., 2016), as observed in several convergent margins involving the subduction of rough oceanic crust (e.g. Central America and the Central Andes, Clift et al., 2003; Ranero and von Huene, 2000). This is supported by recently acquired bathymetric data along the central-northern Pacific coast of Colombia that shows the occurrence of active landslides at the trench-slope region, closely related to and probably triggered by the ongoing subduction of the Sandra Ridge beneath the northwestern continental margin of South America (Vargas et al., 2020), as also documented in the erosive Middle American and Peruvian margins (Ranero and von Huene, 2000).

Our stratigraphic and provenance constraints provide evidence for recent (post-late Miocene) topographic uplift across the AB after subduction erosion-driven subsidence, as indicated by the transition towards fully terrestrial conditions during the accumulation of the latest Miocene to Pliocene Quibdó Formation (Duque-Caro, 1990b) and the emergence of the coastal Baudó Range that caused the fragmentation of the forearc into an inner and outer segments (León et al., 2021b). This period of topographic growth could have been associated with the switch from a paleogeographic setting characterized by shallow-marine tidal flats mostly sourced by transversal source-to-sink systems during the early-middle Miocene (e.g. Osorio-Granada et al., 2017) towards the establishment of the modern longitudinal Atrato River along the inner forearc (Fig. 4.17). Detrital zircon geochronology of the Quibdó Fm. shows the reappearance of old (>100 Ma) sources, which however, were not likely derived from primary continental-affinity domains such as Cretaceous-Paleogene strata of the Western Cordillera but associated with reworking of older Neogene strata, as expected for ongoing exhumation/erosion of older sedimentary rocks prompted by tectonically-driven basin uplift (e.g. Ridgway et al., 2011). The recycling of Oligocene-Miocene strata (e.g. Uva, Napipí and Sierra formations) is further supported by the high content of sandstone and

mudstone clasts and the quartz-rich composition of the conglomerates of the Quibdó Fm. (Zapata, 2000).

The post-late Miocene topographic growth of the northwesternmost Andes could have resulted in the formation of orographic barriers for the westerly moisture transported from the tropical Pacific Ocean by the so-called Chocó low-level jet towards the continent (Poveda and Mesa, 2000), as suggested by the dramatic decrease in precipitation observed at the western slopes of the Western Cordillera nowadays (e.g. Dabeiba Arch; Fig. 4.17). This may have contributed to enhanced weathering of source areas and the observed increase of sedimentation rates and, as discussed below, could have played a primary role on the constitution of one of the wettest and most biodiverse tropical rainforest on Earth (Chocó region; average precipitation of > 8.000 mm/yr; e.g. Myers et al., 2000; Poveda and Mesa, 2000).

On the other hand, the results of our geochemical analysis of detrital pyroxenes suggest a major post-late Miocene change in the composition of source areas, as indicated by the appearance of MORB-like sub-alkaline to alkaline clinopyroxenes in the modern sediments of the northern Pacific coast, which were absent in adjacent Miocene strata (i.e. Chorí unit). Such Ti- and Cr-enriched clinopyroxenes akin to oceanic intra-plate magmatic rocks are similar to those reported for the Cretaceous Caribbean oceanic plateau forming the basement of the Western Cordillera (Buchs et al., 2018). Therefore, it is likely that the MORB-like clinopyroxenes of the modern sediments are being sourced from the mafic basement of the Baudó Range that is interpreted as dominantly composed of pillowed and massive basalts of the Caribbean oceanic plateau (Kerr et al., 1997), which were accreted in conjunction with the overlying CAA during the early-middle Miocene (León et al., 2022, 2018). Additional sub-alkaline to alkaline Ti- and Cr-poor clinopyroxenes with supra-subduction geochemical affinity are probably derived from reworked Miocene strata and/or from minor Upper Cretaceous arc-related intrusives that have been recently documented in the Baudó Range, which are thought to represent the early magmatic activity of the CAA (León et al., 2022; Whattam and Stern, 2015). This scenario suggests that the topographic uplift and subsequent erosional unroofing of the coastal Baudó Range mostly took place after the accumulation of the upper Miocene strata outcropping in the Tribugá Gulf.

Previous constraints on the topographic and structural features of the Colombian Pacific coast, propose that the most recent uplift of the northern forearc region, particularly along the outermost segment (i.e. Baudó Range), resulted from increased megathrust shear force (León et al., 2021b), which has been suggested to provide a first-order control on the upper plate topography at convergent margins (Dielforder et al., 2020). This in turn, has probably been a consequence of the erosive or non-accretionary nature of the margin and a wide seismogenic zone attributed to the shallow-angle subduction of the Nazca plate (León et al., 2021b). The resulting increased tectonic shortening of the forearc wedge by deviatoric stress associated with the increased megathrust shear force is probably related to a nearly trench-orthogonal transpressional stress regime that may account for the observed topographic lineaments characterized by dominant NNW and NE azimuthal trends, and shallow earthquake focal mechanisms that suggest the dominance of oblique reverse kinematics (León et al., 2021b). In this scenario, the contrasting structural arrangement of the Istmina Hills that is instead characterized by NE-oriented lineaments is likely due to the structural inheritance of the transpressional suture formed during the early-middle Miocene collision of the CAA, and recent (late Miocene and/or younger) reactivation episodes of NE-oriented steep faults and fold structures (Duque-Caro, 1990a; Haffer, 1967).

Accordingly, the pulsated Miocene to Recent topographic growth of northwestern Colombia was likely accommodated by high-angle oblique reverse faults such as the Utría and Nazca faults in the outermost AB (Fig. 4.17), which may represent former extensional features created during early stages of basin formation that were subsequently inverted and reactivated during syn- to post-collisional tectonics, similar to what has been observed in the Central Andes (Martinez et al., 2022, 2021).

4.7. Biogeographic implications of the topographic growth of the northern Colombian forearc

The northern Colombian forearc hosts one of the most biodiverse tropical rainforests on Earth, which is part of the Chocó/Darién/Western Ecuador biodiversity hotspot (Myers et al., 2000). The spectacular biodiversity of this region seemingly resulted from the combined effects of several biotic and abiotic mechanisms, including the topographic uplift of the

Baudó Range and the Western Cordillera, and the establishment of terrestrial conditions together with the final emergence of the Isthmus of Panama (Pérez-Escobar et al., 2019; Rodríguez-Olarte et al., 2011). Topographic growth along the northwesternmost Andes could have directly promoted diversification by creating corridors and/or barriers for the migration of species, and by enhancing the observed high levels of endemicity (Gentry, 1986). This is supported by the occurrence of episodic migration of plant species from Central America to the Chocó region since ~5 Ma during the progressive establishment of a fully terrestrial setting, as constrained by recently gathered phylogenetic data (Pérez-Escobar et al., 2019), and by the Pliocene colonization of Central America from northwestern South America of freshwater fishes as a consequence of the final emergence of the Isthmus of Panama (Rodríguez-Olarte et al., 2011). On the other hand, the rise of mid- to high-elevation areas may have resulted in the formation of important orographic barriers, such as the western slopes of the Western Cordillera (i.e. Dabeiba Arch), which apparently has prevented the passage of most of the moisture transported from the tropical Pacific by the Chocó low-level jet into inland regions of the northern Colombian Andes (Poveda and Mesa, 2000). This could have also promoted plant speciation as suggested by the observed positive correlation between precipitation rates and the diversity of plant communities in the Chocó region (Copete et al., 2019), which supports the primary role of collisional and subduction tectonics and subsequent topographic growth as direct and indirect drivers of biodiversification.

4.8. Summary and conclusions

Continental forearc basins have been considered key elements preserving the deformational imprints of a changing subduction system at Andean-type convergent margins, which typically lack of collisional episodes. As discussed above, the Neogene tectonostratigraphy of the northwestern Colombian forearc, initially formed as an intra-oceanic back-arc basin, was rather controlled by interspersed collisional and subduction-related tectonics, which makes it a key area to study the long-term evolution of marginal source-to-sink systems at accretionary orogens. Our results and previous work show that the early collision of the CAA during the early-middle Miocene did not involve widespread deformation and/or topographic uplift of the exotic domain but localized basin instability and

was rather accompanied by low sedimentation rates and very low subsidence that could have been triggered by thermal contraction of the arc and/or tectonic extension driven by slab steepening. The soft collision of the CAA was seemingly associated with its partial underthrust beneath the continental margin that promoted buoyancy-driven exhumation/uplift of the upper-plate nearby the collisional front. The advance of the collision hampered the subduction (i.e. underthrusting) of the buoyant CAA that was rather scrapped off through structural weaknesses or detachment layers from the subducting Caribbean plate, on which the island arc formed, causing its uplift/exhumation.

The late collision of the CAA against northwestern South America and the transition to subduction-related tectonics during the middle-late Miocene was likely accompanied by the onset of topographic growth along the northern Colombian forearc, as suggested by the occurrence of a major shallowing of accumulation depths in the AB, and the closure of the Central American Seaway across the proto-isthmian region. This episode was associated with the re-establishment of an east-dipping subduction zone in which the young Nazca plate began sinking beneath northwestern South America, causing: i) the emplacement of a post-collisional magmatic arc, and ii) constitution of the AB as a continental forearc basin. The transition from collision to subduction was coeval with a major reorganization of the source-to-sink system as a consequence of the creation of physiographic barriers along the innermost forearc basin related to topographic uplift nearby the suture zone, which isolated the main depocenters from inland source areas. Subsequently, the AB was characterized by slow subsidence arguably triggered by the combined effects of subduction-induced upper-plate dragging and tectonic loading of the newly uplifted areas along the innermost (inland) forearc.

During the late Miocene, the apparent interaction of a highly buoyant feature of the Nazca plate (e.g. aseismic Sandra Ridge), caused a shallowing of the subducting slab, which was accompanied by widespread deformation/uplift and the widening and final cessation of arc magmatism in the northern Colombian Andes. The establishment of a flat-slab subduction drove uplift and rapid exhumation across the northern Colombian forearc basin, together with the progressive continentalization of accumulation settings in the main depocenters, in which subsidence was arguably driven by tectonic erosion. The resulting dominantly erosive character of the margin (i.e. sediment-starved trench), together with the widening of the

seismogenic zone due to slab flattening, seemingly resulted in a late Miocene to present-day increase of the megathrust shear force in the forearc wedge, which drove the uplift of the coastal Baudó Range (i.e. outer forearc high) and the fragmentation of the forearc basin into an inner (inland) and an outer (coastal) segment. This late episode of mountain building in the northwesternmost Andes was accompanied by the establishment of fully terrestrial conditions and the final emergence of the Isthmus of Panama, which in turn, caused the occurrence of one of the most striking Cenozoic biogeographic events, the Great Interamerican Biotic Interchange, as well as global oceanographic and climate changes (e.g. onset of northern hemisphere glaciation). Here, we demonstrated the pulsated nature of topographic growth of the northwesternmost Colombian Andes, whose spatiotemporal evolution was strongly controlled by combined collisional and subduction tectonics, which in turn played a major role on the physiographic and biogeographic evolution of the region.

CHAPTER 5

5. Modern along-strike segmentation of the NW South American continental margin: Positive feedback between megathrust rheology and topographic uplift in the Colombian Pacific forearc

5.1. Introduction

Forearc vertical motion at convergent margins seems to reflect the signal of its erosive or accretionary nature, which in turn plays a primary role on the recycling of the Earth's continental crust into the mantle (von Huene and Scholl, 1991). Generic models of subduction erosion predict forearc deepening, as the loss of crustal root is compensated by long-term basin subsidence (Stern, 2011; Wagreich, 1995). However, even in erosive margins, episodic forearc uplift (e.g. development of an outer forearc high; Noda, 2016) can occur, as documented in the Central Andes (e.g. Clift and Hartley, 2007; Genge et al., 2020). Therefore, it seems that additional tectonic drivers must operate as first-order controls of the forearc vertical motion (Dielforder et al., 2020; Tassara, 2010), and exploring them is the main purpose of our research.

The Pacific margin of northwestern South America, considered as dominantly erosive in nature (Clift and Vannucchi, 2004), is strongly segmented by the latitudinal differences in age, thickness, buoyancy and morphology of the subducting Nazca plate (e.g. Ramos, 2009; Viveen and Schlunegger, 2018). Two contrasting geometries prevail along the Colombian Andes, a flat-slab (~10-15°) and a steep (~20-30°) subduction system, north and south of ~5°N, respectively (Ojeda and Havskov, 2001; Vargas and Mann, 2013; Yarce et al., 2014). The flat subduction regime of northern Colombia has produced an imprint in the lateral offset of deep-intermediate seismicity, the late Neogene spatiotemporal evolution of arc-related magmatism, and inland exhumation/uplift (Jaramillo et al., 2019; León et al., 2018; Siravo et

al., 2019; Wagner et al., 2017). Such flat subduction regime could increase the width of the frictional segment of the plate interface, and therefore, the megathrust shear force along the forearc region (Hayes et al., 2018; Pacheco et al., 1993; Wang and He, 1999), which would drive the most recent landscape evolution and neotectonic activity.

We integrate field, structural and topographic data of the northernmost Andean coastal forearc within the influence zone of the northern Colombia flat-slab and compare them with the southern forearc where the slab is steeper, to estimate the megathrust shear force, the crustal stress regime and their implications on the most recent landscape evolution.

5.2. Tectonic and Geological Setting of the Colombian Pacific Margin

5.2.1. Late Neogene to present-day tectonic configuration

The subduction of the young (≤ 12 Ma; Lonsdale, 2005; Müller et al., 2008) Nazca plate underneath South America has shaped the late Cenozoic tectonic evolution of the westernmost Colombian Andes (Echeverri et al., 2015b; León et al., 2018). This buoyant oceanic plate is subducting almost orthogonally at moderate rates around 54-58 mm/yr (Mora-Páez et al., 2019), and it is characterized by several relict fractures and elevated bathymetric features up to ~2 km-high above the surrounding seafloor, such as the Carnegie and Sandra ridges, which are currently colliding with the northern South-American trench (Fig. 5.1; Collot et al., 2019; Vargas et al., 2020).

Seismic observations and the evolution of the late Miocene to Recent north-Andean continental arc (Chiarabba et al., 2016; Wagner et al., 2017), evidence slab flattening and a nearly trench-perpendicular slab-tear ("Caldas Tear"; Vargas and Mann, 2013) in the Nazca plate at ca. 5°N (Syracuse et al., 2016), that separates a southern steep slab from a flat-slab regime to the north (Fig. 5.1). The existence of the latter is further supported by the absence of arc-related magmatism in northern Colombia (Wagner et al., 2017), and a ca. 250 km right-lateral offset of intermediate-deep (> 80 km) seismicity (Ojeda and Havskov, 2001; Pennington, 1981). Hereafter, we use the 5°N latitude to separate the northern (NCF) and southern (SCF) segments of the Colombian coastal forearc, according to their contrasting geology and topography (Fig. 5.2).

The SCF extends into the Ecuadorian Manglares and Borbón basins (Hernández et al., 2020), and includes Neogene to Recent deltaic to fluvial deposits associated to a low-relief morphology characterized by wide swamps and deltas (Correa and Morton, 2010), which are partially segmented by the presence of low (< 200 m) structural promontories such as the Remolinogrande-Gorgona high (Pardo-Trujillo et al., 2020b). The NCF extends to the Colombia-Panama border along the Pacific coast and includes an up to ~1000 m-high coastal range (Baudó Range), and Oligocene-Pliocene sediments and topographic lowlands of the Atrato Basin that is flanked to the east by the western foothills of the Western Cordillera (Fig. 5.1).

Receiver function analysis suggests that crustal thickness along the NCF is around 20 km, whereas along the SCF it is thicker with values up to ca. 30 km (Poveda et al., 2018, 2015). There are also high shear-wave velocities at depths between 10 and 25 km (V_s around 3.2-4.0 km/s) for the forearc region, which are more obviously and constantly observed for the northern segment, where they seem to exceed the estimated crustal thickness (Poveda et al., 2018). The northern continental margin (north of ~5°N) is sediment-starved in spite of being in the region with one of the highest precipitation rates on Earth (Poveda and Mesa, 2000), whereas the southern sector includes between 1 and 2 km-thick trench-fill deposits and a well-developed accretionary prism (Marcaillou and Collot, 2008; Mountney and Westbrook, 1997).

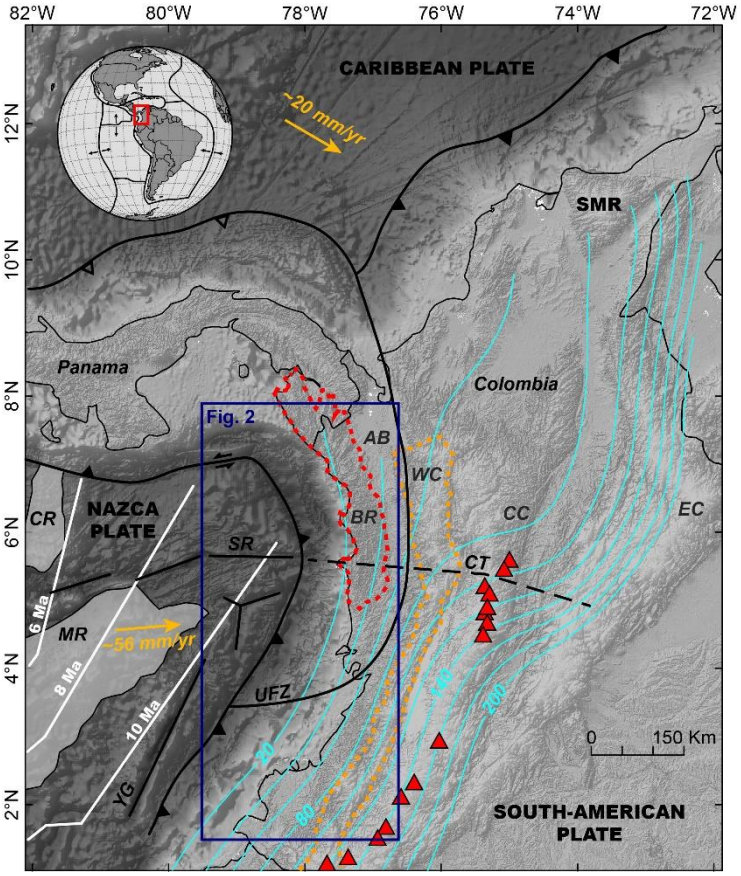

Figure 5.1. Modern tectonic configuration of northwestern South-America, showing slab-depth contours each 20 km from Hayes et al. (2018), Holocene volcanoes (red triangles), and major bathymetric features of the subducting Nazca plate. Red box in the globe shows the location of the main map. Age of the ocean floor after Müller et al. (2008); plate motion vectors relative to stable South America from Mora-Páez et al. (2019). AB=Atrato Basin, BR=Baudó Range (red dotted line), CC=Central Cordillera, CR=Cocos Ridge, CT=Caldas Tear, EC=Eastern Cordillera, MR=Malpelo Ridge, SMR=Santa Marta Range, SR=Sandra Ridge, UFZ=Uramita Fault Zone, WC=Western Cordillera, YG=Yaquina Graben.

5.2.2. Northern forearc geology

The Colombian forearc mostly comprises Cretaceous to Eocene oceanic plateau- and arc-like basement rocks (Cardona et al., 2018; Echeverri et al., 2015a; Kerr et al., 1997; Serrano et al., 2011), accreted to the South-American margin in at least two different episodes, first during the Late Cretaceous-Paleocene (León et al., 2021a; Pardo-Trujillo et al., 2020a), and the second during the early-middle Miocene (Lara et al., 2018; León et al., 2018). This volcaniclastic and plutonic oceanic basement is overlain by syn- to post-collisional Neogene shallow-marine to deltaic sedimentary rocks (Borrero et al., 2012; Duque-Caro, 1990b; Echeverri et al., 2016; Fig. 5.2), which record the erosional history of both the continental margin and the accreted terrains (Echeverri et al., 2015b; León et al., 2018).

Neogene deposits in the NCF are exposed across the low-plains of the Atrato Basin that is fault-bounded to the west by the coastal Baudó Range, which abruptly stands above the flat-lying Pacific coast (Figs. 5.1 and 5.2). These two contrasting morphological domains, the Baudó mountains and the Atrato low-plains, are characterized by strong positive (~75-120 mGal) and negative (ca. -20 mGal) Bouguer gravity anomalies, respectively (Case et al., 1971; National Hydrocarbons Agency of Colombia, 2010). The infill of the Atrato Basin is represented by Eocene-Oligocene to Pliocene mostly fine-grained siliciclastic strata, up to ca. 7-10 km thick (Case et al., 1971), which record an environmental switch from deep- to shallow-marine accumulation during the middle Miocene, and to high-energy continental conditions during the late Miocene-Pliocene (Duque-Caro, 1990b, 1990c). This was coeval with rapid exhumation of the northern Colombian Andes and could have been driven by the collision of the Panama Arc and the subsequent slab flattening of the Nazca plate (León et al., 2018). Nevertheless, the northern outermost (coastal) forearc region and its response to the most recent tectonic activity is still poorly known.

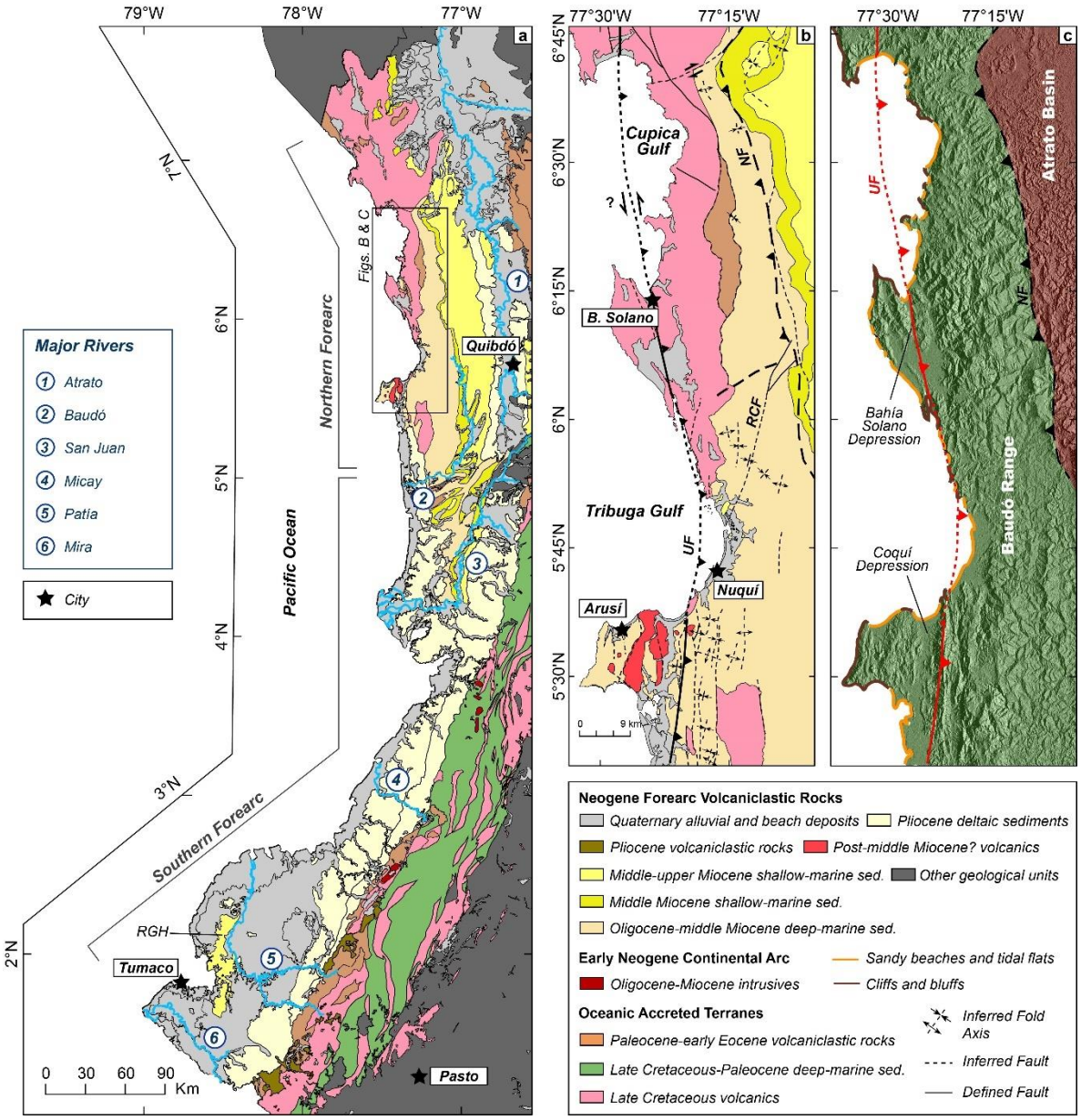

Figure 5.2. Geology of western Colombia and main morphological elements of the northern forearc region, modified from Gómez-Tapias et al. (2017). a) simplified geological map of the Colombian forearc and major river systems; RGH=Remolinogrande-Gorgona high. b) Local geology and structural features of the northern coastal forearc; NF=Nauca Fault, RCF=Rio Condotico Fault, UF =Utría Fault. c) Topography and shoreline classification of the outer segment of the northern forearc showing the main morphological elements and their inferred tectonic boundaries.

5.3. Methods

In this work, we focus on the barely studied onshore Cretaceous to Miocene volcanic and sedimentary rocks exposed along the outer NCF, as well as on its main topographic and structural features.

5.3.1. Fieldwork

We studied the lithological and structural features of the geological units exposed along the Tribugá and Cupica Gulfs on the northern Pacific coast of Colombia (Fig. 5.2), between ~5.5°N and 7°N, using streams draining the western flank of the Baudó Range, as well as cliffs along the coastline and islets on the Pacific Ocean. The extremely dense rainforest vegetation and widespread weathering of rocks due to the high humidity of the region (mean annual rainfall exceeding 7.000 mm; Poveda and Mesa, 2000), hindered finding continuous outcrops. Additional information was gathered from field, stratigraphic and structural data from the Colombian National Geological Survey (Zapata, 2000) and previously published studies (Duque-Caro, 1990b; Galvis, 1980; Kerr et al., 1997; Macía, 1985).

5.3.2. Morphometric and lineament analysis

We constructed east-west 50 km-long swath profiles (10 km-width and a sampling interval of 2.5 km), separated each 1° on latitude (from 2°N to 7°N), from a 30 m-resolution digital elevation model (DEM) derived from Shuttle Radar Topography Mission data (SRTM - https://earthexplorer.usgs.gov/). We additionally used a longitudinal swath profile at ~25 km from the coastline from 2°N to 7°N (10 km-width and a sampling interval of 2.5 km) that included topography and mean annual precipitation (Fick and Hijmans, 2017). We also estimated slope values and the Topographic Ruggedness Index (TRI; Riley et al., 1999), that is the mean of the absolute differences between the value of a cell and the value of its eight surrounding cells. The calculations were made at three different spatial resolutions to test whether the scale had an observable effect. Probability density distributions of slope and TRI values, for both NCF and SCF, were estimated from the non-filtered DEM, 3 x 3 (~100 m-cell size) and 10 x 10 cell (~300 m-cell size) resolutions, respectively. Comparison of slope and TRI of NCF vs. SCF were done by 1.000 randomized subsamples of equal length (10,000 observations). We only considered the outermost (coastal) area of the forearc, as far as 50

kilometers from the coastline to avoid the topographic signal of the adjacent Western Cordillera and inland morphological domains, as we were interested in the short wavelength morphology of the region. A two-sided t-test was used to assess the significance of differences between mean morphometric values of NCF and SCF. All analyses were performed using the R Software (R Development Core Team, 2017) and package "raster" (Hijmans, 2017).

Topographic lineaments are widely used as indicators of the presence of planar and linear geological structures such as faults and fold axes, whose spatial patterns may give insights on the orientation of active crustal stress and most recent deformational events in tectonically active areas (e.g. Oguchi et al., 2003; Wise et al., 1985). We conducted an iterative lineament analyses on shaded-relief images generated from the 30 m-resolution DEM by using different light directions (0, 45, 90 and 315° azimuth) following the procedures of (Celestino et al., 2020), aiming to reduce bias due to the choosing of lighting direction. A regional (small) observation scale of 1:250.000 was chosen, as it has been suggested that smaller scales of lineament mapping tend to better represent regional structural and geological features (Scheiber et al., 2015). We grouped observed lineaments into three categories including: i) those shorter than 5 km, ii) between 5 and 10 km, and iii) longer than 10 km, in order to explore for potential dependence of azimuthal distribution on length. The directional and length attributes of the identified lineaments were compiled into separate databases, and then analyzed by using the software Daisy 3 (http://host.uniroma3.it/progetti/fralab/; (Salvini et al., 1999). A polymodal Gaussian fit was conducted to analyze the azimuthal frequency of our data and to identify the main trends or lineament domains as proposed by Wise et al. (1985).

5.3.3. Earthquake focal mechanism analysis

We compiled the focal parameters of 54 shallow earthquakes (less than 20 km deep) located in the area between 2°N, 78°W and 8°N, 76°W, from the Global Centroid Moment Tensor (1976-2014; Dziewonski et al., 1981; Ekström et al., 2012) and the Colombian Geological Survey (2014-2020). Earthquakes were classified following the scheme of (Frohlich, 1992) to represent the focal mechanisms (i.e. reverse, normal, strike-slip) as a function of the plunge of their estimated T, P, and B axes. We then reassessed the

classification of focal mechanisms by using the FMC program developed by Álvarez-Gómez (2019), which is a Python-based script for classification and clustering of earthquake data. We focused on shallow earthquakes according to estimated crustal thickness for the northern Colombian Pacific region (Poveda et al., 2018, 2015), attempting to avoid signals from deeper regions such as the lithospheric mantle or the subducting Nazca plate. Overall, our focal mechanism analysis was conducted in order to gain insights into the regional stress field in the Colombian forearc and explore for its tectonic significance.

5.3.4. Isostasy and residual topography

Available models for crustal thickness and density structure of northwestern South America were used to assess the isostatic state of northwestern Colombia. Elevation data was gathered from the 30 m-resolution DEM used for the morphometric and lineament analysis, continental crustal thickness values were taken from recently published seismological observations (Poveda et al., 2018, 2015), and density was obtained from the CRUST1.0 global model (Laske et al., 2013). We compute the expected topography from Airy isostasy using constant lithospheric and asthenospheric mantle density values of 3250 kg/m^3 and 3203 kg/m^3, respectively, which are thought to represent reasonable values for the northern Colombian Andes (Yarce et al., 2014); we also used an average lithospheric thickness of 105 km, recently estimated for the region (Blanco et al., 2017). Residual topography was calculated as the difference between the observed and the expected isostatically compensated topography, by using 100%, 95% and 105% of the crustal density values after averaging the CRUST1.0 model (Laske et al., 2013). We also calculated the residual topography by using the 95% and the 105% of the estimated crustal thickness model of Poveda et al. (2018). This procedure was conducted to assess the sensitivity of the resulting residual topography to the selected crustal density and thickness values.

5.3.5. Megathrust shear force

We estimated the total shear force along the frictional segment of the plate interface (i.e. seismogenic zone) for both the NCF and SCF to depict the differences that arise from the contrasting subduction geometry and megathrust strength. For this, we followed the procedures of (Wang and He, 1999), and calculated the total shear force (Fs; Eq. 1) by iteratively using 100,000 combinations of values for the effective friction coefficient (μ’),

average density of the overlying wedge (ρ = 2900-3000 kg/m^3), width of the seismogenic zone (SZW), slab dip angle (θ), and the surface slope angle between the trench and the coastal area of the forearc region (α).

$$F_S = \frac{1}{2}\mu' SZW^2 \qquad (1)$$

Slab dip and the surface slope angles were determined from the Slab2 model of Hayes et al. (2018) and from the SRTM15+ global topography and bathymetry (Tozer et al., 2019). A reasonable range of values for μ' between 0.05 and 0.13 was assumed according to Gao and Wang (2014), who present global observations of megathrust strength from heat flow and force balance analyses. The width of the seismogenic zone (SZW) was taken from Hayes et al. (2018), where it is reported to vary between ~90 and 140 km for some of the major subduction zones on Earth with slabs dipping between 12 and 16°, and between ~70 and 90 km where the slab dip angle is higher than 18. We assumed the above ranges of values as representative for the flat-slab regime of the NCF and the steeper subduction beneath the SCF, given the lack of a direct characterization of the seismogenic zone.

Moreover, to assess the effects of the effective friction coefficient on the magnitude of the shear force, we estimated Fs by assuming constant values for the depth of the downdip limit of the seismogenic zone (Dd) of 30 km, surface slope angle between the trench and the coast area (α) of 2°, and an average wedge density (ρ) of 3000 kg/m^3. In this case, SZW is equal to the ratio Dd/sin(θ), which we calculated using three different slab dip angles (θ) of 15°, 20° and 30°. Similarly, we estimated the relative changes in the magnitude of Fs as a consequence of varying the dip angle with respect to a subduction setting represented by a slab dipping 20°, in order to illustrate the effects of slab shallowing.

5.4. Results

5.4.1. Geology of the northern Pacific coast

5.4.1.1. Upper Cretaceous Basaltic oceanic basement

Cretaceous basaltic rocks associated with the Caribbean oceanic plateau (COP; Kerr et al., 1997), represent the basement of the Colombian forearc. In the northern region, this unit is

mostly exposed on cliffs and along gullies on the Baudó Range foothills, as well as on islets along the Cupica and Tribugá gulfs (Fig. 5.2). It comprises fractured and altered massive and pillowed basaltic lava flows, occasionally interlayered with chert and mudstone, with 15-40° NNE-dipping bedding planes and overturned folds (Fig. 5.3). Minor gabbros and diorites are also found. Basalts show aphanitic and porphyritic, as well as less common amygdalar textures, with clinopyroxene as the most abundant phenocryst, followed by plagioclase and minor olivine. Alteration phases include epidote-group minerals, clays and chlorite. The latter is commonly found defining incipient steep foliation planes in highly sheared deformation zones dipping between 15° and 80° to the NE-SE, observed close to the main trace of the Utría Fault (UF; Fig. 5.2).

These rocks have been dated as Late Cretaceous (~73-78 Ma), and interpreted as either derived from a compositionally heterogeneous plume system associated to the southernmost fragment of an oceanic plateau forming most of the Caribbean plate (Kerr et al., 1997), or as an immature intra-oceanic arc (Whattam and Stern, 2015). Either way, these rocks were subsequently accreted to the South-American margin during the early-middle Miocene (León et al., 2018).

5.4.1.2. Oligocene-lower Miocene calcareous rocks

Fossiliferous limestones and fine-grained calcareous litharenites of the Uva Formation are widely exposed along the coastal plains of the Tribugá Gulf and in the Atrato Basin, as well as on isolated roofs along the axis and southwestern flank of the Baudó Range (Fig. 5.2). In our study area, the Uva Formation is composed of discontinuous massive fossil-rich micritic limestones with abundant dissolution structures, and minor litharenites with moderately high (≤ 25%) content of bioclasts. Medium-thin bedded (≤ 20 cm) limestones are found interlayered with clastic-rich thin (2-3 cm) layers, which define almost vertical bedding planes (Fig. 5.3). Clastic rocks are mostly fine- to medium-grained and poorly sorted, with subangular quartz, feldspar, bioclasts, and abundant lithic fragments. The Uva Formation is reported to be nonconformably overlying Cretaceous basaltic rocks (Zapata, 2000), and it is overlain by the middle-upper Miocene informal Chorí Unit in angular unconformity (Fig. 5.3).

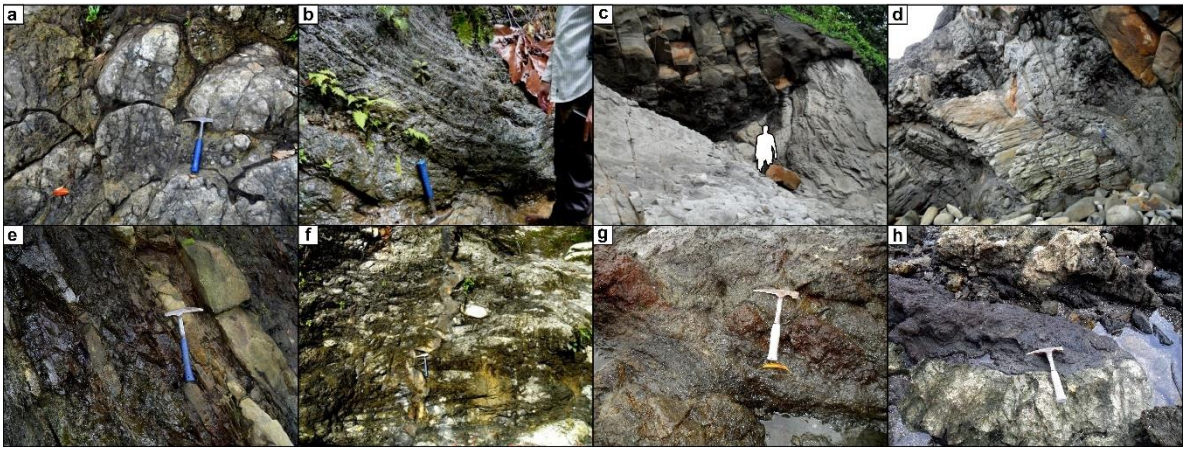

Figure 5.3. Mosaic of field photographs showing the main lithological features of the Cretaceous to late Miocene geological units exposed along the Tribugá Gulf. a-b) Basaltic pillow-lava of the Cretaceous oceanic basement and interlayered siliceous mudstones defining an overturned fold structure. c-d) Angular unconformity and highly deformed zone of the Oligocene to lower Miocene Uva Formation. e-f) Interlayered tabular strata of calcareous mudstones and calcareous litharenites, disordered strata and clastic dyke in the middle-upper Miocene informal unit Chorí Unit. g-h) Post-middle Miocene (?) basaltic rocks and fragments of recrystallized host limestones with dissolution structures.

The Uva Formation has been interpreted as Oligocene-lower Miocene deposits mostly accumulated at lower to upper bathyal depths based on the foraminifera fauna (Duque-Caro, 1990b; Zapata, 2000). It has experienced multiple deformational events, as suggested by the high density of fractures, the presence of narrow north-south striking en-echelon fold axis spatially correlated to the Nauca Fault (NF; Fig. 5.2; see discussion below), and the west-dipping angular unconformity with the overlying Chorí Unit, together with the presence of high deformation zones in which both units are tectonically mixed (Fig. 5.3).

5.4.1.3. Middle-upper Miocene siliciclastic rocks

Along the Tribugá Gulf, the informal middle-upper Miocene Chorí Unit is found forming isolated hills of medium to very thick (0.1-2 m) tabular strata of interlayered calcareous mudstones and fine- to coarse-grained calcareous litharenites, and minor conglomerates (Fig. 5.3). Litharenites are moderately sorted and mainly composed of subangular-subrounded quartz-feldspar, volcanic, sedimentary lithic and coal fragments, as well as abundant bioclasts. Available biostratigraphic constraints (i.e. planktonic foraminifera; Zapata, 2000) have been used to interpret this unit as shallow-marine deposits accumulated on proximal upper bathyal to shoreface-offshore settings during the middle-late Miocene (Duque-Caro, 1990b).

The Chorí Unit is characterized by the presence of disordered strata and chaotic sandy blocks embedded within a fine-grained matrix, as well as sandy, nearly vertical, clastic dykes (Fig. 5.3). Deformation structures are represented by eastward (landward) 15°-30° strata tilting (west-verging folding), as well as observed outcrop-scale reverse faults mostly dipping to the NE-SE and high fracture density, together with the presence of strong deformation zones where these rocks are tectonically juxtaposed with the older Uva Formation (Fig. 5.3).

5.4.1.4. Post-middle Miocene (?) basaltic rocks

Previous studies have reported the occurrence of highly altered volcaniclastic basaltic rocks including autobrecciated lavas, tuffs and agglomerates, exposed along the southernmost Tribugá Gulf, closely related to the trace of the Utría Fault (Fig. 5.2), which have been formerly interpreted as part of the Cretaceous oceanic basement (i.e. Baudó Basalts; (Kerr et al., 1997; Zapata, 2000). However, whole-rock and major oxides

geochemical data, has shown that these rocks may be compositionally different, as indicated by their more alkaline signature when compared with the plateau-like Cretaceous unit (Galvis, 1980; Macía, 1985). Basaltic rocks mostly include fine- to medium-grained massive lava flows, together with volcaniclastic units. The latter are characterized by the presence of rounded basaltic fragments with massive and porphyritic textures, embedded within a reddish or greenish altered glassy matrix (Fig. 5.3). Clinopyroxene is virtually the most abundant phenocryst found in the porphyritic fragments with minor plagioclase, whereas secondary alteration minerals include chlorite, epidote and palagonite.

We observed an intrusive relationship between brecciated lavas and fossiliferous limestones similar to those described for the Oligocene-middle Miocene Uva Formation (Fig. 5.3). Based on this cross-cutting relationship, together with the distinctive geochemical character of this unit (Galvis, 1980; Macía, 1985), it is possible that these volcaniclastic rocks are not related with the Cretaceous basement, and could rather represent a middle Miocene or younger previously unreported unit located across the southern Tribugá Gulf. If this were the case, this unit could be related to the Nazca subduction dynamics, and its connection with the arc-like rocks exposed farther inland along the flanks of the Western Cordillera (Jaramillo et al., 2019; Rodríguez and Zapata, 2012), should be explored. The petrogenesis of this unit will be discussed elsewhere.

5.4.2. Geomorphic constraints of the northern Colombian forearc

The outermost sector of the NCF is characterized by an irregular coastline located at ca. 40-60 km from the trench, and a narrow shallow-marine shelf 10 to 25 km wide, with isolated embayments limited by cliffed and bluffed promontories of either Cretaceous or post-middle Miocene (?) volcanic rocks (Fig. 5.2). Sandy beaches and sandy-muddy tidal flats are commonly observed near deltas of short rivers draining into the Pacific Ocean from the western flank of the Baudó Range. This ca. 300 km-long coastal range is north-south oriented and structurally interrupted by fault-bounded depressions (e.g. Bahía Solano and Coquí), likely controlled by the east-dipping reverse Utría Fault (Fig. 5.2). To the east, the forearc region is mostly represented by low-lands and floodplains of the Atrato River, which are probably limited to the west by the west-dipping Nauca Fault, defining the morphotectonic

limit between the rough relief and elevated surface of the coastal Baudó Range and the Atrato Basin (Figs. 5.1 and 5.2).

Elevation along the northern Pacific coast oscillates between 0 and ~1000 m.a.s.l., with the highest elevations between ~5°N and 6°N, which abruptly decrease southwards from the edge of the Baudó Range and the Istmina Hills at ca. 5°N (Fig. 5.4). This is associated to the transition from steep and rough landscapes to wide low-plains and swamp systems formed by large fluvial systems (i.e. Micay and Patía Rivers) that characterize the southern Pacific coast (Figs. 5.2 and 5.4). Mean annual precipitation along the entire coastal forearc spans from ~3.5 m/yr to ~7 m/yr, showing an irregular pattern marked by a localized peak between ~4.5°N and 5.5°N, as well as a minor increase from 3°N to 3.5°N, with no apparent correspondence of topography (Fig. 5.4).

Estimated slope values for the northern forearc are highly variable, ranging from 0° up to 85° (at the 30 m resolution), with the highest values frequently observed along both flanks of the Baudó Range, following the main trace of the Utría and Nauca faults (Figs. 5.5 and 5.6). The probability density shows a bimodal distribution that yielded a mean value of ~10.3 ± 8.3° (1σ) from the non-filtered 30 m elevation data, whereas mean slope values of 7.5 ± 6.7° (1σ) and 4.3 ± 4.3° (1σ) were estimated from the 100 m (not shown) and 300 m aggregated analyses, respectively (Fig. 5.5). Calculated TRI values follow the same spatial distribution of slope (Fig. 5.6), showing a bimodal distribution, with mean values of 4.8 ± 3.9 m (1σ), 11.4 ± 9.1 m (1σ) and 23.4 ± 20.2 m (1σ), from the non-filtered, the 100 m (not shown), and the 300 m data, respectively (Fig. 5.5).

We included for comparison the density of probability and spatial distribution of estimated slope and TRI values for both the NCF and SCF (north and south of 5°N latitude, respectively; Figs. 5.5 and 5.6), where the steeper and rougher relief of the northernmost area, independently from the scale, is easily observed. This is further supported by the results of the t-test, as after assessing the difference of the means for both the slope and TRI values, at three different scales (1.000 iterations each; 6.000 repetitions in total), the null hypothesis (H_0: there is no difference in mean values) was rejected ($p < .05$) over 95% of the cases, except for the TRI at 30 m-cell size, where only the 21.4% of the cases allowed rejecting H_0.

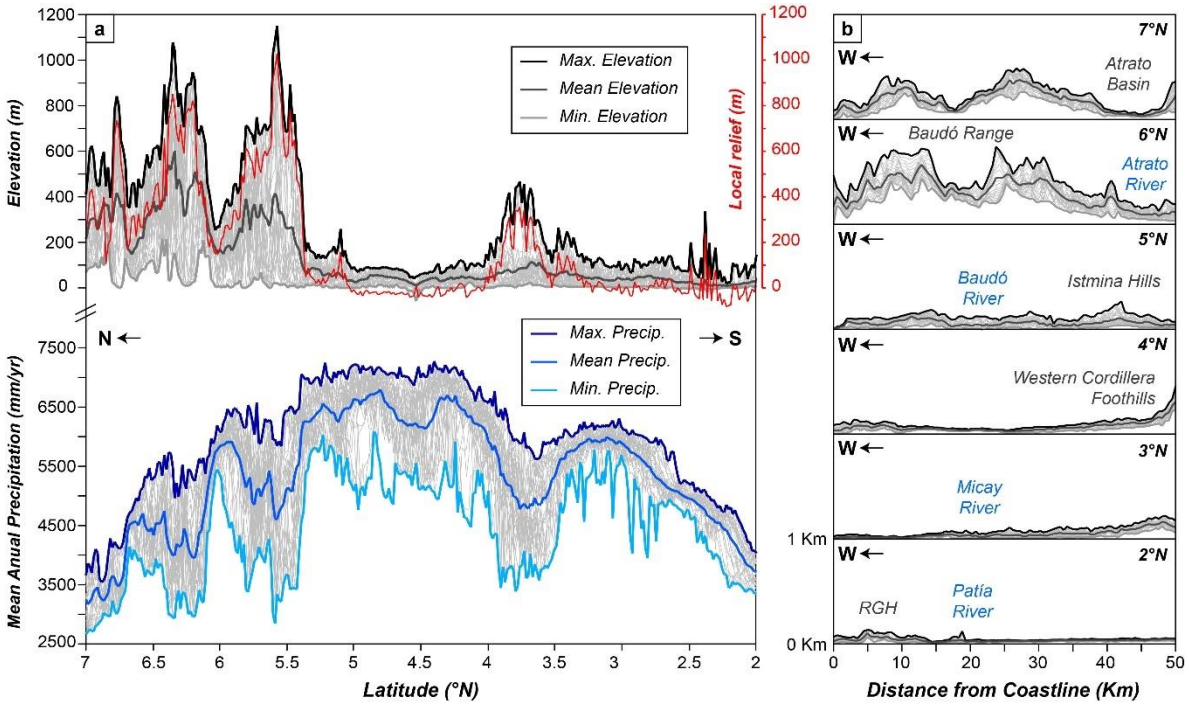

Figure 5.4. Along-strike morphology and mean annual precipitation of the Colombian coastal forearc. a) Longitudinal swath profile, from 2°N to 7°N. Red curve in the upper panel showing the local relief (maximum elevation-minimum elevation). b) East-west swath profiles, from 2°N to 7°N (separated by 1° latitude). Note the dramatic decrease in elevation and relief south of ~5.5°N, with no apparent relationship with rainfall. RGH=Remolinogrande-Gorgona structural high.

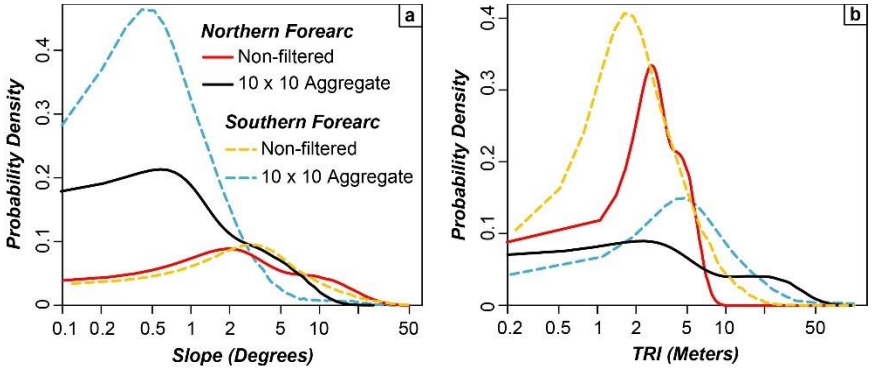

Figure 5.5. Probability density plots for slope (a) and TRI values (b), computed at 30 m- and 300 m-cell size, for both the northern (solid lines) and southern (dashed lines) forearc.

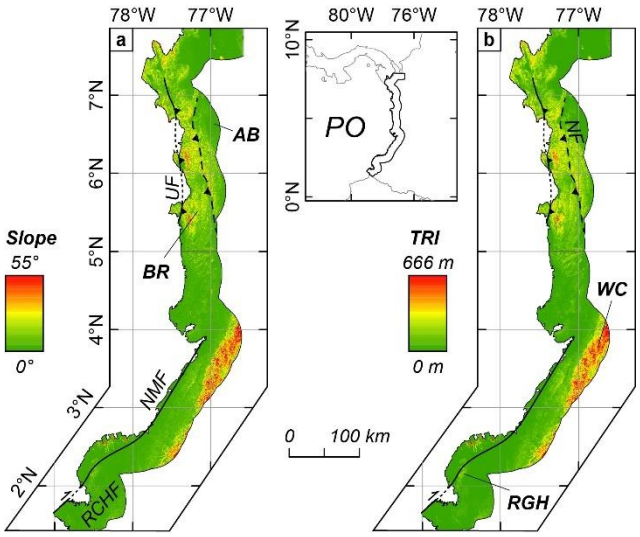

Figure 5.6. Slope and TRI maps estimated from the 10 x 10 aggregation (300 m-resolution DEM). AB=Atrato Basin, BR=Baudó Range, NF=Nauca Fault, NMF=Naya-Micay Fault, PO=Pacific Ocean, RCHF=Remolino-El Charco Fault, WC=Western Cordillera. Main trace of faults modified from Paris et al. (2000).

5.4.3. Spatial patterns of topographic lineaments

A total of 1199 topographic lineaments were identified in the costal NCF, including aligned ridges and straight valleys ranging in length from ~1.5 to ~ 26.7 km (~6.3 km in average; Fig. 5.7), which yielded a mean azimuthal direction of N3.9E ± 3.2° (Fig. 5.7). The Gaussian fitting of all identified lineaments, which consisted in the decomposition of the observed probability distribution into individual peaks associated to preferential azimuthal directions, show that the main trend has a mean azimuth of N17W ± 12° (15%), followed by a slightly different N6E ± 8° (8%) trend. Secondary lineament domains show mean azimuthal directions of N59E ± 14° (9%) and N27E ± 6° (4%; Fig. 5.7). No apparent relationship between lineament trends or spatial distribution and lithology was observed.

The azimuthal trends of lineaments shorter than 5 km are in good agreement with the general pattern and are represented by a mean direction of N11E ± 3°. Four peaks were also identified from the Gaussian fit, which yielded mean azimuths of N8E ± 11° (12%), N25W ± 16° (12%), N60E ± 9° (7%), and N35E ± 7° (4%). Lineaments between 5 km and 10 km-long yielded a mean direction of N1E ± 3°, with four peaks centered at N13W ± 12° (18%), N62E ± 30° (11%), N7E ± 7° (4%), and N28E ± 4° (2%). Lineaments longer than 10 km also follow the regional structural trend, with a mean azimuth of N3E ± 2°, and four individual peaks centered at N23E ± 6° (11%), N4E ± 3° (10%), N13W ± 3° (9%), N23W ± 3° (5%). The overall lineament analysis indicates the presence of dominant NNW-SSE and ENE-WSW structural trends.

There are well-defined en-echelon truncated structures on the southeastern flank of the Baudó Range with NE strike, similar to those observed by (Zapata, 2000) in the southern Tribugá Gulf (Fig. 5.7). The fold structures, together with the spatial distribution of aligned ridges and escarpments, can be used to infer the trace of the nearly N-S oriented Nauca Fault, which was previously observed only in the northernmost study area (Zapata, 2000). The N-S strike of the main fault traces in the study area (Utría and Nauca; Fig. 5.7), and NE-SW strike of the observed en-echelon fold-axis, are consistent with the azimuthal trends of the observed lineaments.

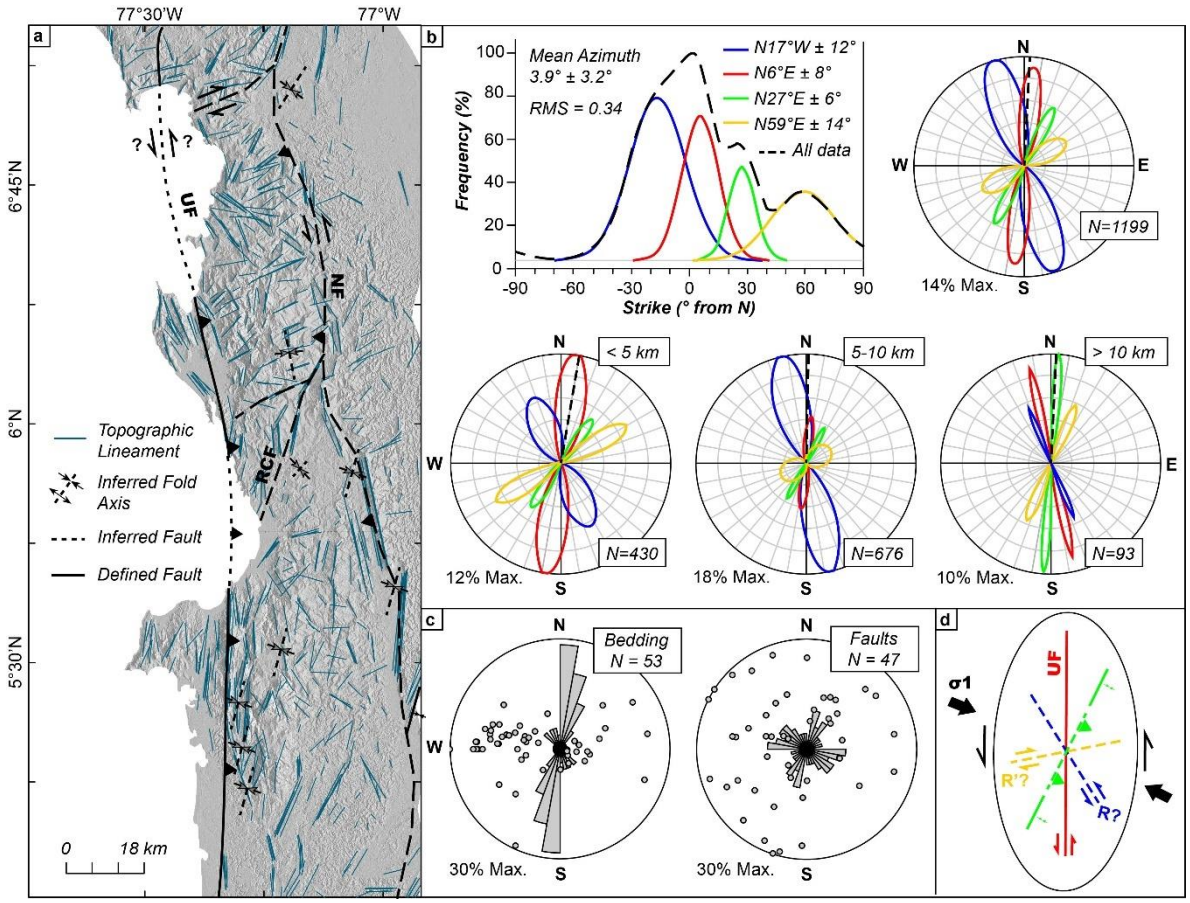

Figure 5.7. Structural analysis from topographic lineament data, combined with new and available field observations from Zapata (2000). a) Map showing the spatial distribution of identified topographic lineaments in the northern coastal forearc and main fault and fold structures. b) Results of the Gaussian fit and azimuthal distribution of full-length, ≤ 5 km, 5-10 km, and ≥ 10 km-long lineaments. c) Rose diagrams for measured bedding planes for the middle-upper Miocene Chorí Unit, showing a well-defined eastward tilting, and identified fault planes within the study area. d) Schematic strain ellipsoid showing the inferred structural arrangement of the northern Colombian forearc; thick black arrows indicate the interpreted direction of maximum compression.

5.4.4. Forearc crustal stress

The compiled focal mechanism parameters for the NCF show a complex spatial distribution, mainly represented by oblique reverse seismogenic fault structures and minor oblique transpressional kinematics on the upper-plate (Fig. 5.8). Strike-slip focal mechanisms, characterized by T and P axes with sub-horizontal plunge angles (Kasaras et al., 2014), are clustered both along the Sandra Ridge and the left-lateral transform boundary between the Caribbean and Nazca plates in southeastern Panama. Nevertheless, focal solutions of earthquakes along the northern coastal forearc are preferentially oblique reverse in nature, with dominant E-W-oriented P-axis trends and sub-horizontal (~26°) plunge angles, suggesting a present-day compressional/transpressional stress regime, with a nearly trench-perpendicular direction of maximum compression (Fig. 5.8). Subordinated SW and NW azimuthal trends of the P-axis are also observed suggesting a complex oblique stress regime of the region (Fig. 5.8).

In contrast, limited focal mechanisms were obtained from the coastal SCF, which may be attributed to scarce shallow seismicity (< 20 km; Fig. 5.8). Earthquakes are located both on the subducting Nazca plate and along the SCF, and they are characterized by P and T-axes with nearly E-W-oriented trends and mean plunge angles of ~60° and 26°, respectively, represented by mostly extensional kinematics (Fig. 5.8). All earthquakes close to the trench along the southern forearc, have extensional focal solutions and are likely related to the flexure and bending of the subducting Nazca plate (Lefeldt and Grevemeyer, 2008), whereas those located on the continental shelf and the forearc region also show compressional features (Fig. 5.8).

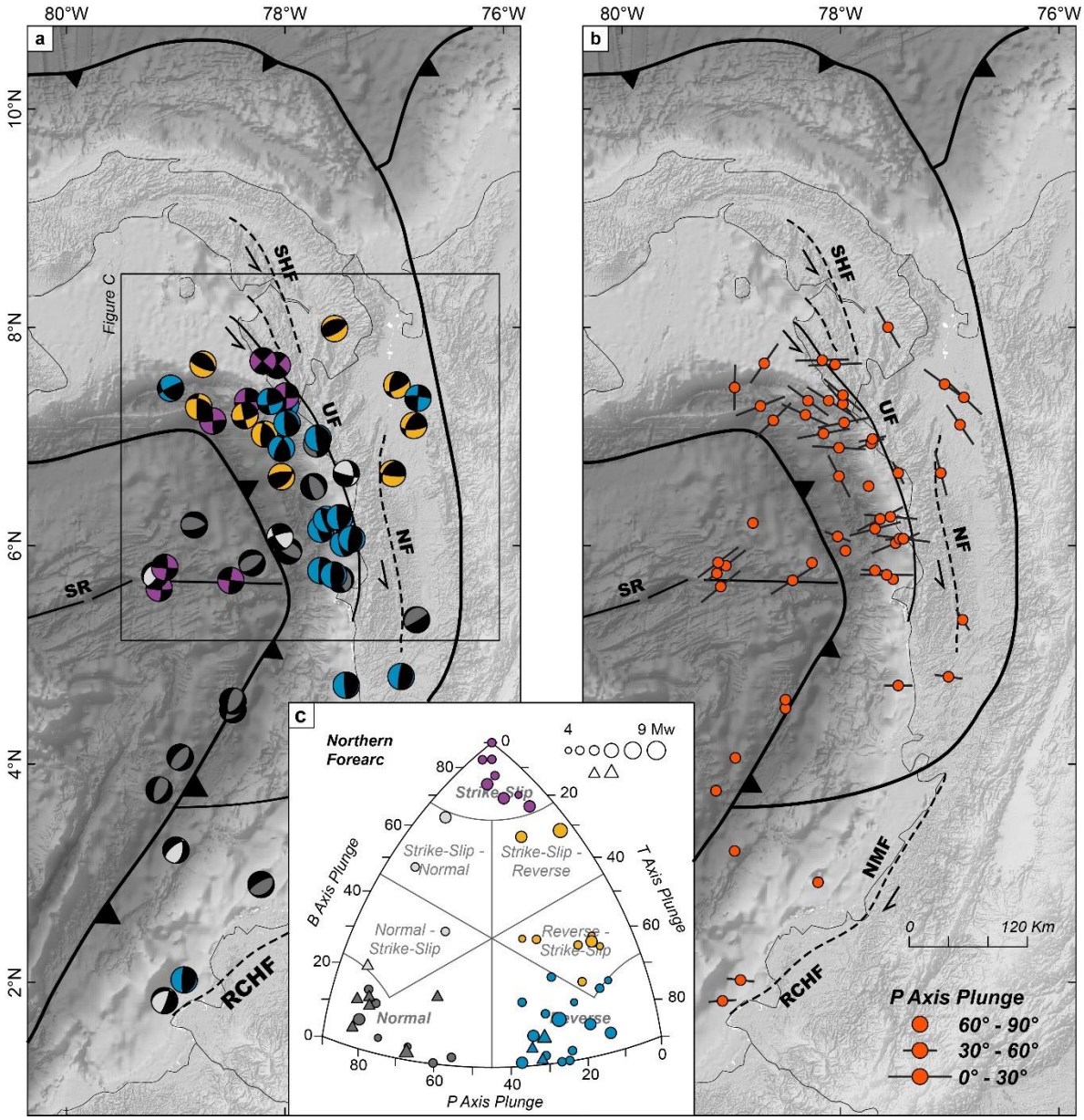

Figure 5.8. Results of the focal mechanisms analysis. a) Map showing the spatial distribution of the obtained earthquake focal mechanisms for shallow events (≤ 20 km). b) Map showing the azimuthal distribution and plunge values of P axis trends. c) Earthquake focal mechanisms classification after Álvarez-Gómez (2019) and Frohlich (1992) for events within the rectangle (northern forearc). Circles and triangles are for earthquake within the NCF and SCF, respectively. NF=Nauca Fault, NMF=Naya-Micay Fault, RCHF=Remolino-El Charco Fault, SHF=Sansón Hills Fault, SR=Sandra Ridge, UF=Utría Fault.

5.4.5. Isostasy

Our results show the presence of multiple non-compensated regions along the Colombian Andes, independent of the selected crustal thickness and density values (Fig. 5.9). For instance, prevalent residual positive short wavelength anomalies are observed along the northern coastal forearc (i.e. Baudó Range), the southern Western Cordillera, and the segment of the Central Cordillera where the active volcanic arc is located (south of ~5°N). Such areas that are close to or exceed the expected isostatic topography are separated by areas with negative residuals represented by the inter-Andean valleys. There is a high sensitivity of the calculated residual topography to the crustal density model, as a 10% decrease in the average crustal density may result in a 25% difference in the resulting values (Fig. 5.9). Conversely, our calculations by adding and subtracting a 5% of the estimated crustal thickness values from (Poveda et al., 2015) are slightly sensitive and show minor variation in the resulting residual topography (Fig. 5.9).

5.4.6. Shear force estimations along the frictional segment of the plate interface

Our estimations of the total shear force (Fs) along the seismogenic zone of the megathrust yielded mean values of 6.1 $\pm$ 1.6 TNm^{-1} and 2.6 $\pm$ 0.7 TNm^{-1}, for the NCF and the SCF, respectively (Fig. 5.10). As expected, increasing the effective friction coefficient results in relatively higher megathrust shear force when Dd is kept constant, which is more evident in low-angle subduction zones. From our analyses, we noted that Fs shifts from 0.6 to 3.7 TNm^{-1} (mean value of 2.1 TNm^{-1}), from 0.9 to 5.6 TNm^{-1} (mean value of 3.2 TNm^{-1}), and from 1.2 to 7.6 TNm^{-1} (mean value of 4.4 TNm^{-1}), for slab dip angles of 30°, 20°, and 15°, respectively (Fig. 5.10). Similarly, when a constant depth for the downdip limit of the seismogenic zone is assumed, which imply widening of SZW as θ decreases, reducing the slab dip angle (θ) to 10° could result in more than double the magnitude of Fs for a subduction zone dipping 20°, whereas it could reduce to almost half if the slab steepens to 30° (Fig. 5.10).

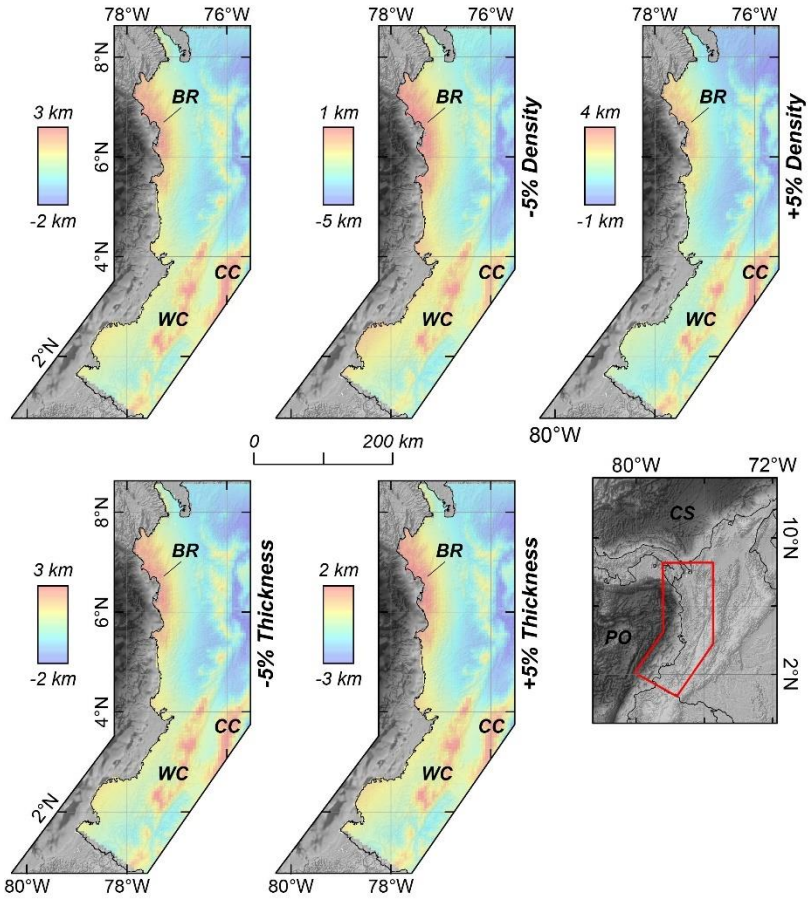

Figure 5.9. Residual topographic maps for westernmost Colombia, calculated as the difference between the expected Airy's isostatic elevation and observed topography, by using variable crustal thickness and density values after Laske et al. (2013), Poveda et al. (2018, 2015) and Yarce et al. (2014). BR=Baudó Range, CC=Central Cordillera, CS=Caribbean Sea, PO=Pacific Ocean, WC=Western Cordillera.

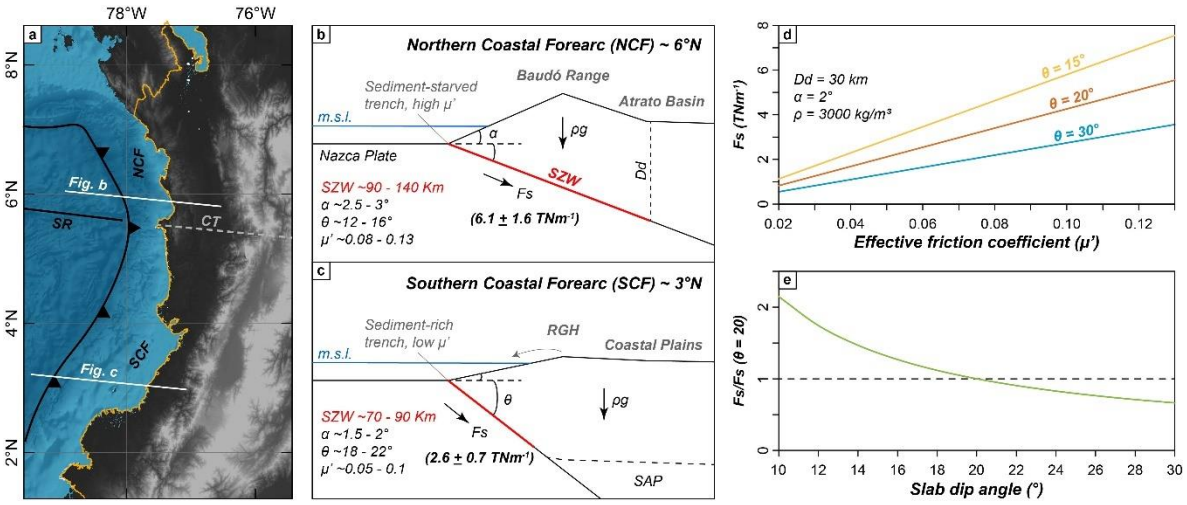

Figure 5.10. Schematic illustration showing the forces acting in the forearc region and results of the shear force (Fs) calculation. a) Map showing the location of the cross sections in (b) and (c), and some tectonic elements of the Colombian Pacific coast discussed in text. CT = Caldas Tear, SR = Sandra Ridge. b) and c) Schematic diagrams showing the proposed tectonic configuration of the NCF and SCF, the shear and gravitational forces acting on the wedge with average density ρ, and the parameters used for calculations of the shear force Fs, after Dielforder et al. (2020), Hayes et al. (2018), Lamb (2006), and Wang and He (1999); μ' is the effective friction coefficient, and ρg represents the gravitational force; m.s.l. = mean sea level, RGH = Remolinogrande-Gorgona high, SAP = South-American plate, SZW = Seismogenic zone width, Dd = Depth of the downdip limit of the seismogenic zone. Reported uncertainties for estimated forces are 1σ. d) Plot showing the linear correlation between μ' and Fs for three different slab dip angles. e) Plot showing the decrease of Fs as a consequence of increasing the slab dip angle. Note that Fs is given relative to its value for a dip angle of 20°.

5.5. Discussion

5.5.1. Late Miocene to present-day deformation/uplift of the NCF

There are at least two major Neogene deformational episodes registered by the Oligocene-middle Miocene Uva Formation and the middle-upper Miocene Chorí Unit. A first event suggested by the Uva/Chorí angular unconformity, deformed the Uva Formation prior to the middle Miocene and could be related to the onset of uplift in the northwesternmost Colombian Andes. This event was coeval with regional shoaling of accumulation settings from bathyal to shallow-marine depths on both the Atrato (Duque-Caro, 1990b), and the correlatable Chucunaque basins, and could be a consequence of the collision of the Panama Arc against the continental South-American margin during the early-middle Miocene (Coates et al., 2004; Duque-Caro, 1990c; León et al., 2018). The presence of clastic dykes and disordered strata within the middle-upper Miocene Chorí Unit (Fig. 5.3), suggest syn-sedimentary intra-basinal tectonic instability in an actively deforming shallow-marine shelf, which may be attributed to either the ongoing arc-continent collision or the compressional tectonics triggered by the onset of Nazca subduction underneath South America at ca. 14-12 Ma (Wagner et al., 2017). Further stratigraphic and provenance analyses on the middle-late Miocene and younger strata could allow determining to what extent this event contributed to the construction of the present-day landscape.

A second, post-late Miocene deformational episode is suggested by the high-angle eastward tilting of the Chorí Unit, as well as the highly deformed zones involving both the middle-upper Miocene rocks and the older Uva Formation (Fig. 5.3), together with the development of fold structures on Oligocene to upper-Miocene strata (Zapata, 2000). This deformational event likely triggered a major uplift (inversion) of the NCF (i.e. onset of Baudó Range uplift) and the cessation of sediment accumulation along the coastal region, whereas in the Atrato Basin, this period was characterized by ongoing deposition and the switching from upper-bathyal to neritic, and then high-energy fluvial settings (Duque-Caro, 1990c; Zapata, 2000). Coeval widespread tectonic activity across the northern Colombian Andes, and eastward migration and widening of the volcanic arc are interpreted to be triggered by the flattening of the Nazca slab between ca. 10-5 Ma (Jaramillo et al., 2019; Monsalve et al., 2019; Siravo et al., 2019). Such flat subduction regime, and the subsequent modification of

the plate interface geometry, could have increased the width of the seismogenic zone and plate coupling (Gutscher, 2002; Pacheco et al., 1993; Wang and He, 1999), and therefore the megathrust shear force, playing a major role on the most recent deformation and uplift along the NCF.

Evidence for ongoing deformation of the coastal NCF includes the presence of Holocene tectonically uplifted beach terraces (González et al., 2014), abundant cliffed headlands, steep slopes and high topographic ruggedness along the Baudó Range, fault-controlled morphological depressions and widespread lineament structures (Figs. 5.2, 5.6 and 5.7). The preservation of the observed long planar and near vertical surfaces such as fault- and fold-related escarpments in the extremely humid tropical forest of the region, is unlikely due to the strong weathering that favors effective surface smoothing or denudation (Phillips, 2005). Thus, it is reasonable to interpret a very recent origin for such structures, which are actively shaping the landscape.

The combined observations from our lineament analysis and the structural constraints, suggest that active deformation is mostly represented by NNW-SSE-oriented fault structures, as well as NE-striking and east-dipping en-echelon fold axis (Fig. 5.7). The nearly N-S-oriented lineaments may be correlated with high-angle oblique reverse faults such as the Utría and Nauca faults, whereas the west-verging folding of middle-upper Miocene strata and associated axis may be represented by subordinated lineament trends with NE-SW strike (Fig. 5.7). Widely distributed fault structures were observed during the fieldwork, which are represented by centimetric to few meters-width, sub-horizontal to vertical steep shear zones (dip angle between 16° and 90° towards the east; Fig. 5.7). Unfortunately, we did not observe kinematic indicators within the deformation zones, which hindered discerning the sense of relative movement. Nevertheless, the consistency between the NW-SE and NE-SW trend of subordinated lineaments and similarly-oriented fault structures (Fig. 5.7), would represent both synthetic and antithetic faults related to a maximum compression in the direction WNW-ESE and regional oblique reverse sinistral kinematics (McClay, 1987). In this context, NNE-SSW oriented lineaments would represent the morphological expression of thrust faults, such as the Utría and Nauca faults, which seemingly represent the tectonic boundaries of the Baudó Range, and are likely inverted, formerly normal fault structures, formed during earlier phases of extensional tectonics, as suggested by their high-dip angle.

Earthquake focal mechanisms suggest a dominant nearly trench-perpendicular (WNW-ESE) compressional regime (Fig. 5.8), which is consistent with previous interpretations from seismic and GPS (Global Positioning System) data (Cortés and Angelier, 2005; Trenkamp et al., 2002), as well as with our lineaments and structural analysis. The dominantly E-W-oriented compressional stress and the heterogeneities within the P-axis trends, together with the existence of strike-slip active seismogenic sources, are consistent with a deformational regime characterized by NW- and -NE-trending strike-slip and oblique reverse fold and fault structures.

5.5.2. Increased shear force along the plate interface and uplift of the NCF

The NCF has been characterized by protracted uplift probably since the middle-late Miocene and it is still active, which has limited the amount of sediments being delivered to the trench, enhancing the erosive or non-accretionary nature of the margin. The uplift of the NCF is in odds with the long-term subsidence expected for an erosive convergent margin, which should be characterized by basal removal of forearc lower crust, and subsequent crustal thinning and basin deepening (Clift and MacLeod, 1999). An alternative mode of subduction erosion that involves basal underplating of tectonically eroded forearc material has been proposed to explain the episodic and spatially localized uplift of some forearc regions such as the outermost Central Andean margin (e.g. Chile and Peru; Genge et al., 2020). This mechanism, however, would imply for the Baudó Range to have a thick crust beneath it. In contrast, available seismic data (Poveda et al., 2015) indicate that the crust is thinner (5-10 km less) than in surrounding regions.

In spite of the large differences in the amount of estimated residual topography, mostly due to the crustal density models used for calculations, the coastal NCF has a short wavelength (< 50 km) non-compensated topography (i.e. Baudó Range; Fig. 5.9). Relatively low crustal thickness estimated for the northern Pacific coast of Colombia (~20 km; Poveda et al., 2018, 2015), also indicates that the elevated topography of this mountain range may be rootless. An additional support is therefore needed, which could be provided by two alternative mechanisms, either upward forcing by mantle dynamics or increased megathrust shear stress and deviatoric compression causing tectonic shortening and local surface uplift (Becker et al., 2014; Dielforder et al., 2020; Lamb, 2006). Upward forcing by mantle

upwelling or increased buoyancy requires a low viscosity and highly hydrated lithospheric mantle wedge (Becker et al., 2014; Faccenna et al., 2011). However, the absence of active arc magmatism north of ~5°N, together with the relatively high S-wave velocities (above ~3.6 km/s) up to 35 km-depth in the northern forearc region (Poveda et al., 2018), where the estimated crustal thickness is around 20-25 km, argues against the presence of a low-velocity and buoyant serpentinized mantle wedge beneath the NCF (Bostock et al., 2002).

In contrast, there are several pieces of evidence suggesting a strong plate interface and associated tectonically-driven uplift. The positive Bouguer anomaly (~75 to 120 mGal; Case et al., 1971; National Hydrocarbons Agency of Colombia, 2010), and the high shear-wave velocities characterizing the coastal region of the NCF (Poveda et al., 2018), suggest the presence of a high-density lithosphere lacking a serpentinized mantle wedge or a highly hydrated lower crust, which may act as lubricants lowering shear stresses (Bostock et al., 2002; Lamb, 2006). Additionally, the limited upper-plate crustal thickness indicates that the subducting Nazca plate could largely contribute to such inferred lithospheric strength and the observed gravity anomaly. This could be accompanied by enhanced mechanical coupling and increased shear stress along the subduction interface beneath the NCF.

Our estimations of Fs along the frictional segment of the megathrust allowed us to show that a shallow and poorly lubricated interface, as we interpret the NCF, result in increased shear force when compared with steeper and sediment-rich subduction zones alike the SCF (Fig. 5.10). Despite our shear force calculations mostly rely on presumed μ' and SZW values, we are still confident on their representativeness of the along-strike tectonic segmentation of the Colombian forearc for the reasons we provide below.

The sharp morphological transition at ca. 5°N latitude, from elevated and rough relief in the NCF to a smooth topography and lowlands in the SCF (Figs. 5.4, 5.5 and 5.6), is linked to a physiographic segmentation of the forearc, represented by the presence of large river systems (e.g. Mira, Patía, San Juan) south of 5°N, which are absent along the northern Pacific coast (Fig. 5.2). These sediment routing systems of the SCF have likely operated since the late Neogene, delivering sediments from the western flank of the Western and Central Cordilleras to the forearc and trench basins (Pardo-Trujillo et al., 2020b). Therefore, the prevalence of a thick trench infill (i.e. water-rich sediments) likely resulted in a more

lubricated (i.e. lower μ') and shear stress-deficient plate interface in the SCF when compared with the sediment-starved trench along the NCF that is probably linked to a stronger megathrust (Lamb, 2006; Lamb and Davis, 2003).

The effects of increasing μ', which can be caused by external forces reducing the amount of sediment delivered into the trench and do not depend on the geometry of the plate interface (e.g. mid- to long-term climate changes; Lamb and Davis, 2003), seems to be more evident for shallow subduction regimes, as long as the depth of the downdip limit of the seismogenic zone (Dd) is kept constant (Fig. 5.10). In such a case, SZW is expected to increase as the slab dip angle flattens, which in turn would result in higher megathrust shear force (Fig. 5.10).

The location of Dd, and therefore the width of the seismogenic zone, is mostly controlled by temperature-related processes regulated by the ability of the cold sinking slab to perturb the thermal regime along the plate interface (Baillard et al., 2015; Heuret et al., 2011). Yet, the prevalence of shallow Dd and wide SZW at shallow subduction zones has been empirically observed (Hayes et al., 2018). Thus, it seems that slab flattening do not considerably change Dd, but rather promotes an increase of SZW, as temperatures required to switch from frictional to viscous mechanical behavior of the megathrust can only be achieved farther inland as a consequence of the retreat of the mantle wedge and the widespread cooling of the subduction interface (Gutscher, 2002).

From the above, it seems reasonable to assume that the NCF must be represented by a wider seismogenic zone when compared with the SCF. This, when combined with the effects of a poorly lubricated plate interface (i.e. high μ') attributed to a sediment-starved trench, must be associated to a relatively higher megathrust shear force that in turn increases deviatoric compression and tectonically-driven uplift. The latter triggers mountain building and the formation of barriers limiting sediment flow into the trench, producing positive feedback that provides an alternative mechanism for the topographic growth of forearc regions at erosive or non-accretionary margins.

5.6. Conclusions

The coastal forearc of the northwesternmost Colombian Andes (NCF; ~5°N-7°N) comprises a Cretaceous oceanic plateau-like basement, on which Neogene deep to shallow-

marine deposits, sourced by inland Cretaceous and older continental-affinity domains, were deposited. Those lithostratigraphic units record multiple deformational events and have been uplifted at least since the middle-late Miocene, driving a switch of sedimentary environments from bathyal depths to fluvial settings. A post-late Miocene event is coeval with widespread upper-plate deformation, and eastward migration and vanishing of arc-related magmatism in the northern Colombian Andes, which is interpreted as consequences of the onset of the Nazca flat-slab subduction regime. Such tectonic scenario would have resulted in a wide frictional segment of the megathrust (i.e. seismogenic zone) associated to increased shear force and subsequent tectonically-driven topographic uplift. The irregular coastal morphology, and the spatial patterns of well-preserved topographic lineaments in the extremely humid and warm conditions of the coastal Baudó Range, suggest an active oblique reverse deformational regime attributed to a nearly trench-perpendicular compression that is also supported by earthquake focal mechanisms. The ongoing uplift and deformation along the coastal NCF resulted in non-compensated short wavelength residual topography. We propose that increased shear force, linked to the shallow Nazca subduction and the prevalence of a non-accretionary margin with a sediment-starved trench, enhanced deviatoric compression of the upper-plate, driving forearc uplift and providing support for the growing topography. Such scenario represents an alternative mechanism for topographic build up along coastal forearcs in erosive margins.

CHAPTER 6

6. Synthesis and General Conclusions

The complex interactions between the Caribbean, Farallon/Nazca and South-American plates since the Late Cretaceous has shaped the topographic growth of the northern Colombian Andes and the circum-Caribbean region. Such interactions involved several geodynamic processes related to both collisional and subduction tectonics, whose magmatic and tectonostratigraphic record is well preserved in the northwesternmost Andean forearc. The results of this research project, when integrated with available geological information, allowed a comprehensive characterization of the petrological and structural imprints of the multiple tectonic processes responsible for the evolution northern Colombian forearc basin, since the formation of its plateau- and arc-like Cretaceous basement to the establishment of its most recent physiographic and structural configuration.

Petrochronological analyses of detrital zircons from modern sediments of the northern Pacific coast (Cupica Gulf) suggest the presence of Upper Cretaceous (~100-80 Ma) mafic-intermediate magmatic rocks akin to a subduction tectonic setting, which are likely exposed somewhere upstream in the central-northern Baudó Range. These rocks are interpreted as representing some of the most primitive magmatic products of the Central American arc (CAA), which, according to recent paleogeographic and tectono-magmatic reconstructions of the circum-Caribbean, could have formed by plume-driven north-northwestward subduction of the Farallon plate beneath the southwestern margin of the Caribbean oceanic plateau (trailing edge of the Caribbean plate). This was coeval with ongoing eastward subduction of Farallon lithosphere beneath the active margin of northwestern South America, which is consistent with a divergent double subduction scenario.

Continuous convergence between northwestern South America and the Farallon plate, led to the closure of the remnant basin associated with the divergent double subduction setting that resulted in the Late Cretaceous (~75-70 Ma) collision of the so-called Ecuadorian-

Colombian-Leeward Antilles arc (ECLA) and its plateau-like basement, which nowadays represents the basement of the north-Andean Western Cordillera. New paleoaltimetry estimations, based on the trace element composition of pre- to post-collisional Cretaceous-Paleocene arc-related magmatic rocks emplaced onto the pre-Cretaceous continental basement of the Colombian Andes, allowed documenting the occurrence of a major event of surface uplift (up to ~2 km) triggered by the above-mentioned collisional episode, representing the early topographic growth of the Colombian Andes. This was contemporaneous with a south-to-north thickening of the continental crust and the continentalization of the sub-Andean foreland basins of Colombia and Ecuador, which supports the northeastward propagation of the arc-continent collision as a consequence of the ongoing drift of the Caribbean plate in the same direction.

The advance of the convergence between the Caribbean and South-American plates resulted in a second collisional episode during the early-middle Miocene, in which the intra-oceanic CAA was docked against the continental paleomargin, represented by the already collided ECLA and deep-marine siliciclastic and hemipelagic-pelagic Cretaceous-Paleocene strata forming the northern segment of the Colombian Western Cordillera. The record of this collisional event and the subsequent deformational subduction-related episodes is preserved in the Neogene tectonostratigraphy of the Atrato Basin (AB).

A detailed analysis of the stratigraphy, sedimentary provenance, and structural features of the Neogene infill of the AB allowed unveiling the main episodes of topographic growth and reorganization of source-to-sink systems triggered by interspersed collisional and subduction tectonics. The newly gathered data, together with published biostratigraphic information, allowed suggesting that the early collision of the CAA during the early-middle Miocene did not involve widespread deformation or topographic uplift around the suture zone. This time period was rather characterized by very slow subsidence and deposition at deep-marine conditions probably as a consequence of ongoing thermal contraction of the vanishing CAA and hemipelagic settling and minor siliciclastic contribution. The advancing collision was subsequently associated with a short-lived inversion of sedimentary basins, together with the shallowing of accumulation depths to upper bathyal-outer neritic conditions and an increase in the siliciclastic input from both the partially emerged CAA and the Western Cordillera (continental paleomargin).

During the transition from collision to subduction, at ~15-13 Ma, there was a major episode of topographic uplift of the Atrato Basin, which was accompanied by the initial growth of a post-collisional magmatic arc and the moderate-rapid exhumation of the Western Cordillera. This time period seemingly represents the onset of mountain building across the northern Colombian forearc, as suggested by a major reorganization of the source-to-sink systems, which caused the isolation of the main forearc depocenters from the northern segment of the Western Cordillera, probably related to the emergence of topographic barriers such as the Dabeiba Arch in the vicinity of the suture zone.

The late Miocene re-establishment of the eastward subduction of the Nazca plate beneath northwestern South America resulted in the constitution of the AB as continental forearc basin. Tectonic erosion and increased megathrust shear force beneath the forearc wedge due to slab flattening drove the most recent topographic uplift of the northwesternmost Andes, which was associated with the emergence of the coastal Baudó Range (i.e. outer forearc high) and the fragmentation of the forearc basin. This late Miocene to recent episode of mountain building caused a shift from marine to terrestrial conditions and the final emergence of the Isthmus of Panama, which had major implications on the constitution of the Chocó biodiversity hotspot and the modern extremely humid rainforest.

The results of this work allowed showing the pulsated nature of the topographic growth of forearc basins, which, in the case of the northwesternmost Andes, seemingly migrated oceanward during the transition from collision to subduction, focusing initially on the vicinity of the suture zone. Ensuing flattening of the subducting slab caused widespread deformation across the orogen, and a major inversion of the marginal basins and the uplift of the outer forearc high, which was seemingly controlled by inverted high-angle thrust faults. The analytical approach and the methodological strategy used in this work showed to be highly valuable for tectonostratigraphic analysis of source-to-sink systems of forearc basin, which allow disentangling the diverse tectonic processes involved in their long-term evolution at accretionary orogens such as the northern Andes.

Bibliography

Aizprua, C., Witt, C., Johansen, S.E., Barba, D., 2019. Cenozoic stages of forearc evolution following the accretion of a sliver from the Late Cretaceous-Caribbean Large Igneous Province: SW Ecuador-NW Peru. Tectonics 38, 1441–1465. https://doi.org/10.1029/2018TC005235

Allen, P.A., Allen, J.R., 2013. Basin analysis: Principles and application to petroleum play assessment, 3rd ed. Wiley-Blackwell.

Almeida, J.J., Villamizar, F., 2012. Petrografía y geoquímica del Batolito Antioqueño en un sector del municipio de Santa Rosa de Osos, Antioquia (Bachelor thesis). Universidad Industrial de Santander, Bucaramanga.

Álvarez-Gómez, J.A., 2019. FMC -arthquake focal mechanis Ems data management, cluster and classification. Softw. X 9, 299–307. https://doi.org/10.1016/j.softx.2019.03.008

Arnott, R.W.C., 2010. Deep-marine sediments and sedimentary systems, in: James, N.P., Dalrymple, R.W. (Eds.), Facies Models 4. Geological Association of Canada, pp. 295–322.

Avellaneda-Jiménez, D.S., Cardona, A., Valencia, V., Barbosa, J.S., Jaramillo, J.S., Monsalve, G., Ramírez-Hoyos, L.F., 2020. Erosion and regional exhumation of an Early Cretaceous subduction/accretion complex in the Northern Andes. Int. Geol. Rev. 62, 186–209. https://doi.org/10.1080/00206814.2019.1596042

Baes, M., Sobolev, S., Gerya, T., Brune, S., 2020. Plume-induced subduction initiation: Single-slab or multi-slab subduction? Geochemistry, Geophys. Geosystems 21, e2019GC008663. https://doi.org/10.1029/2019GC008663

Baes, M., Stern, R.J., Whattam, S., Gerya, T. V., Sobolev, S. V., 2021. Plume-induced subduction initiation: Revisiting models and observations. Front. Earth Sci. 9, 1032. https://doi.org/10.3389/feart.2021.766604

Baillard, C., Crawford, W.C., Ballu, V., Regnier, M., Pelletier, B., Garaebiti, E., 2015.

Seismicity and shallow slab geometry in the central Vanuatu subduction zone. J. Geophys. Res. Solid Earth 120, 5606–5623. https://doi.org/10.1002/2014JB011853

Baker, P.A., Fritz, S.C., Dick, C.W., Eckert, A.J., Horton, B.K., Manzoni, S., Ribas, C.C., Garzione, C.N., Battisti, S., 2014. The emerging field of geogenomics: Constraining geological problems with genetic data. Earth-Science Rev. 135, 38–47. https://doi.org/10.1016/j.earscirev.2014.04.001

Barbosa-Espitia, A.A., Kamenov, G.D., Foster, D.A., Restrepo-Moreno, S.A., Pardo-Trujillo, A., 2019. Contemporaneous Paleogene arc-magmatism within continental and accreted oceanic arc complexes in the northwestern Andes and Panama. Lithos 348–349, 105185. https://doi.org/10.1016/j.lithos.2019.105185

Bayona, G., 2018. El inicio de la emergencia de los Andes del norte: una perspectiva a partir del registro tectónico-sedimentológico del Coniaciano al Paleoceno. Rev. la Acad. Colomb. Ciencias Exactas, Físicas y Nat. 42, 1–15. https://doi.org/10.18257/raccefyn.632

Bayona, G., Baquero, M., Ramírez, C., Tabares, M., Salazar, A.M., Nova, G., Duarte, E., Pardo, A., Plata, A., Jaramillo, C., Rodríguez, G., Caballero, V., Cardona, A., Montes, C., Gómez-Marulanda, S., Cárdenas-Rozo, A.L., 2020. Unraveling the widening of the earliest Andean northern orogen: Maastrichtian to early Eocene intra-basinal deformation in the northern Eastern Cordillera of Colombia. Basin Res. https://doi.org/10.1111/bre.12496

Bayona, G., Cardona, A., Jaramillo, C., Mora, A., Montes, C., Valencia, V., Ayala, C., Montenegro, O., Ibañez-Mejia, M., 2012. Early Paleogene magmatism in the northern Andes: Insights on the effects of Oceanic Plateau–continent convergence. Earth Planet. Sci. Lett. 331–332, 97–111. https://doi.org/10.1016/j.epsl.2012.03.015

Bayona, G., Cortés, M., Jaramillo, C., Ojeda, G., Aristizabal, J.J., Reyes-Harker, A., 2008. An integrated analysis of an orogen-sedimentary basin pair: Latest Cretaceous-Cenozoic evolution of the linked Eastern Cordillera orogen and the Llanos foreland basin of Colombia. Geol. Soc. Am. Bull. 120, 1171–1197. https://doi.org/10.1130/B26187.1

Becker, T.W., Faccenna, C., Humphreys, E.D., Lowry, A.R., Miller, M.S., 2014. Static and dynamic support of western United States topography. Earth Planet. Sci. Lett. 402, 234–246. https://doi.org/10.1016/j.epsl.2013.10.012

Belousova, E., Griffin, W., O'Reilly, S.Y., Fisher, N., 2002. Igneous zircon: trace element composition as an indicator of source rock type. Contrib. to Mineral. Petrol. 143, 602–622. https://doi.org/10.1007/s00410-002-0364-7

Blanco, J.F., Vargas, C.A., Monsalve, G., 2017. Lithospheric thickness estimation beneath Northwestern South America from an S-wave receiver function analysis. Geochemistry, Geophys. Geosystems 18, 1376–1387. https://doi.org/10.1002/2016GC006785

Blisniuk, P.M., Stern, L.A., Chamberlain, P., Zeitler, P.K., Ramos, V.A., Sobel, E.R., Haschke, M., Strecker, M. R., Warkus, F., 2006. Links between mountain uplift, climate, and surface processes in the Southern Patagonian Andes, in: Oncken, O., Chong, G., Franz, G., Giese, P., Götze, H.-. J., Ramos, V.A., Strecker, Manfred R., Wigger, P. (Eds.), The Andes, Active Subduction Orogeny. Frontiers in Earth Sciences. Springer, Berlin, Heidelberg, pp. 429–440. https://doi.org/10.1007/978-3-540-48684-8_20

Blow, W.A., 1969. Late middle Eocene to Recent planktonic foraminiferal biostratigraphy, in: Bronnimann, P., Renz, H.H. (Eds.), First International Conference on Planktonic Microfossils. Geneva, pp. 199–421.

Borrero, C., Pardo, A., Jaramillo, C.M., Osorio, J.A., Cardona, A., Flores, A., Echeverri, S., Rosero, S., García, J., Castillo, H., 2012. Tectonostratigraphy of the Cenozoic Tumaco forearc basin (Colombian Pacific) and its relationship with the northern Andes orogenic build up. J. South Am. Earth Sci. 39, 75–92. https://doi.org/10.1016/j.jsames.2012.04.004

Boschman, L.M., van der Wiel, E., Flores, K.E., Langereis, C.G., van Hinsbergen, D.J.J., 2019. The Caribbean and Farallon plates connected: Constraints from stratigraphy and paleomagnestism of the Nicoya Peninsula, Costa Rica. J. Geophys. Res. Solid Earth 124, 6243–6266. https://doi.org/10.1029/2018JB016369

Bostock, M.G., Hyndman, R.D., Rondenay, S., Peacock, S.M., 2002. An inverted continental

Moho and serpentinization of the forearc mantle. Nature 417, 536–538. https://doi.org/10.1038/417536a

Boutelier, D., Chemenda, A., Burg, J.P., 2003. Subduction versus accretion of intra-oceanic volcanic arcs: insight from thermo-mechanical analogue experiments. Earth Planet. Sci. Lett. 212, 31–45. https://doi.org/10.1016/S0012-821X(03)00239-5

Brown, D., Alvarez-Marrón, J., Pérez-Estaún, A., Puchkov, V., Gorozhanina, Y., Ayarza, P., 2001. Structure and evolution of the Magnitogorsk forearc basin: Identifying upper crustal processes during arc-continent collision in the southern Urals. Tectonics 20, 364–375. https://doi.org/10.1029/2001TC900002

Buchs, D.M., Arculus, R.J., Baumgartner, P.O., Baumgartner-Mora, C., Ulianov, A., 2010. Late Cretaceous arc development on the SW margin of the Caribbean Plate: Insights from the Golfito, Costa Rica, and Azuero, Panama, complexes. Geochemistry, Geophys. Geosystems 11, 1–35. https://doi.org/10.1029/2009GC002901

Buchs, D.M., Coombs, H., Irving, D., Wang, J., Koppers, A., Miranda, R., Coronado, M., Tapia, A., Pitchford, S., 2019a. Volcanic shutdown of the Panama Canal area following breakup of the Farallon plate. Lithos 334–335, 190–204. https://doi.org/10.1016/j.lithos.2019.02.016

Buchs, D.M., Irving, D., Coombs, H., Miranda, R., Wang, J., Coronado, M., Arrocha, R., Lacerda, M., Goff, C., Almengor, E., Portugal, E., Franceschi, P., Chichaco, E., Redwood, S.D., 2019b. Volcanic contribution to the emergence of Central Panama in the Early Miocene. Sci. Rep. 9, 1417. https://doi.org/10.1038/s41598-018-37790-2

Buchs, D.M., Kerr, A.C., Brims, J.C., Zapata-Villada, J.P., Correa-Restrepo, T., Rodríguez, G., 2018. Evidence for subaerial development of the Caribbean oceanic plateau in the Late Cretaceous and palaeo-environmental implications. Earth Planet. Sci. Lett. 499, 62–73. https://doi.org/10.1016/j.epsl.2018.07.020

Bustamante, C., Cardona, A., Archanjo, C.J., Bayona, G., Lara, M., Valencia, V., 2017. Geochemistry and isotopic signatures of Paleogene plutonic and detrital rocks of the Northern Andes of Colombia: A record of post-collisional arc magmatism. Lithos 277, 199–209. https://doi.org/10.1016/j.lithos.2016.11.025

Calvo, C., 2003. Provenance of plutonic detritus in cover sandstones of Nicoya Complex, Costa Rica: Cretaceous unroofing history of a Mesozoic ophiolite sequence. Geol. Soc. Am. Bull. 115, 832–844. https://doi.org/10.1130/0016-7606(2003)115<0832:POPDIC>2.0.CO;2

Cardona, A., León, S., Jaramillo, J.S., Montes, C., Valencia, V., Vanegas, J., Bustamante, C., Echeverri, S., 2018. The Paleogene arcs of the northern Andes of Colombia and Panama: Insights on plate kinematic implications from new and existing geochemical, geochronological and isotopic data. Tectonophysics 749, 88–103. https://doi.org/10.1016/j.tecto.2018.10.032

Cardona, A., León, S., Jaramillo, J.S., Valencia, V., Zapata, S., Pardo-Trujillo, A., Schmitt, A.K., Mejía, D., Arenas, J.C., 2020. Cretaceous record from a Mariana to an Andean-type margin in the Central Cordillera of the Colombian Andes, in: Gómez, J., Pinilla-Pachón, A.O. (Eds.), The Geology of Colombia, Volume 2 Mesozoic. Servicio Geológico Colombiano, Publicaciones Geológicas Especiales, 36, Bogotá, p. 39. https://doi.org/10.32685/pub.esp.36.2019.10

Cardona, A., Valencia, V., Bayona, G., Duque, J., Ducea, M.N., Gehrels, G.E., Jaramillo, C., Montes, C., Ojeda, G., Ruiz, J., 2011. Early-subduction-related orogen in the northern Andes: Turonian to Eocene magmatic and provenance record in the Santa Marta Massif and Rancheria Basin, northern Colombia. Terra Nov. 23, 26–34. https://doi.org/10.1111/j.1365-3121.2010.00979.x

Cardona, A., Weber, M., Valencia, V., Bustamante, C., Montes, C., Cordani, U.G., Muñoz, C.M., 2014. Geochronology and geochemistry of the Parashi granitoid, NE Colombia: Tectonic implication of short-lived Early Eocene plutonism along the SE Caribbean margin. J. South Am. Earth Sci. 50, 75–92. https://doi.org/10.1016/j.jsames.2013.12.006

Case, J.E., Duran, L.G., López, A., Moore, W.R., 1971. Tectonic investigations in western Colombia and eastern Panama. Geol. Soc. Am. Bull. 82, 2685–2712.

Cassel, E.J., Smith, M.E., Jicha, B.R., 2018. The impact of slab rollback on Earth's surface: Uplift and extension in the hinterland of the North American Cordillera. Geophys. Res. Lett. 45, 10996–11004. https://doi.org/10.1029/2018GL079887

Cawood, P.A., Kröner, Alfred, Collins, W.J., Kusky, T.M., Mooney, W.D., Windley, B.F., 2009. Accretionary orogens through Earth history, in: Cawood, P.A., Kröner, A. (Eds.), Earth Accretionary Systems in Space and Time. Geological Society, London, Special Publications, 318, 1-36.

Cediel, F., Restrepo, I., Marín-Cerón, M.I., Duque-Caro, H., Cuartas, C., Mora, C., Montenegro, G., García, E., Tovar, D., Muñoz, G., 2009. Geology and Hydrocarbon Potential, Atrato and San Juan Basins, Chocó (Panamá) Arc. Tumaco Basin (Pacific Realm), Colombia. Fondo Editorial EAFIT, Medellín.

Celestino, M.A.L., Miranda, T.S., Mariano, G., Lima, M.A., Carvalho, B.R.B.M., Falcão, T.C., Topan, J.G., Barbosa, J.A., Gomes, I.F., 2020. Fault damage zones width: Implications for the tectonic evolution of the northern border of the Araripe basin, Brazil, NE, Brazil. J. Struct. Geol. 104116. https://doi.org/10.1016/j.jsg.2020.104116

Champagnac, J.-. D., Molnar, P., Sue, C., Herman, F., 2012. Tectonics, climate, and mountain topography. J. Geophys. Res. Solid Earth 117, B02403. https://doi.org/10.1029/2011JB008348

Chang, Z., Vervoort, J.D., McClelland, W.C., Knaack, C., 2006. U-Pb dating of zircon by LA-ICP-MS. Geochemistry, Geophys. Geosystems 7, 1–14. https://doi.org/10.1029/2005GC001100

Chapman, J.B., Ducea, M.N., DeCelles, P.G., Profeta, L., 2015. Tracking changes in crustal thickness during orogenic evolution with Sr/Y: An example from the North American Cordillera. Geology 43, 919–922. https://doi.org/10.1130/G36996.1

Chen, Z., Schellart, W.P., Duarte, J.C., Strak, V., 2017. Topography of the overriding plate during progressive subduction: A dynamic model to explain forearc subsidence. Geophys. Res. Lett. 44, 9632–9643.

Chiarabba, C., De Gori, P., Faccenna, C., Speranza, F., Seccia, D., Dionicio, V., Prieto, G.A., 2016. Subduction system and flat slab beneath the Eastern Cordillera of Colombia. Geochemistry, Geophys. Geosystems 17, 16–27. https://doi.org/10.1002/2015GC006048

Clift, P.D., Hartley, A.J., 2007. Slow rates of subduction erosion and coastal underplating

along the Andean margin of Chile and Peru. Geology 35, 503–506. https://doi.org/10.1130/G23584A.1

Clift, P.D., MacLeod, C.J., 1999. Slow rates of subbduction erosion estimated from subsidence and tilting of the Tonga forearc. Geology 27, 411–414. https://doi.org/10.1130/0091-7613(1999)027<0411:SROSEE>2.3.CO;2

Clift, P.D., Pecher, I., Kukowski, N., Hampel, A., 2003. Tectonic erosion of the Peruvian forearc, Lima Basin, by subduction and Nazca Ridge collision. Tectonics 22, 1023. https://doi.org/10.1029/2002TC001386

Clift, P.D., Vannucchi, P., 2004. Controls on tectonic accretion versus erosion in subduction zones: Implications for the origin and recycling of the continental crust. Rev. Geophys. 42, RG2001. https://doi.org/10.1029/2003RG000127

Cloos, M., 1993. Lithospheric buoyancy and collisional orogenesis: Subduction of oceanic plateaus, continental margins, island arcs, spreading ridges, and seamounts. Geol. Soc. Am. Bull. 105, 715–737. https://doi.org/10.1130/0016-7606(1993)105<0715

Coates, A.G., Collins, L.S., Aubry, M.-P., Berggren, W.A., 2004. The Geology of the Darien, Panama, and the late Miocene-Pliocene collision of the Panama arc with northwestern South America. Geol. Soc. Am. Bull. 116, 1327. https://doi.org/10.1130/B25275.1

Collot, J.-Y., Ratzov, G., Silva, P., Proust, J.-N., Migeon, S., Hernández, M.J., Michaud, F., Pazmino, A., Barba Castillo, D., Alvarado, A., Khurama, S., 2019. The Esmeraldas Canyon: A helpful marker of the Pliocene-Pleistocene tectonic deformation of the North Ecuador-Southwest Colombia convergent margin. Tectonics 38, 3140–3166. https://doi.org/10.1029/2019TC005501

Copete, J.C., Sánchez, M., Cámara-Leret, R., Balslev, H., 2019. Diversidad de comunidades de palmas en el Chocó biogeográfico y su relación con la precipitación. Caldasia 41, 358–369. https://doi.org/10.15446/caldasia.v41n2.66576

Correa, I., Morton, R., 2010. Pacific coast of Colombia, in: Bird, E.C.F. (Ed.), Encyclopedia of the World's Coastal Landforms. Springer, Dordrecht, pp. 193–197. https://doi.org/10.1007/978-1-4020-8639-7

Cortés, M., Angelier, J., 2005. Current state of stress inthe northern Andes as indicated by

focal mechanisms of earthquakes. Tectonophysics 403, 29–58. https://doi.org/10.1016/j.tecto.2005.03.020

Crameri, F., Magni, V., Domeier, M., Shepard, G.E., Chotalia, K., Cooper, G., Eakin, C.M., Grima, A.G., Gürer, D., Király, A., Mulyukova, E., Peters, K., Robert, B., Thielmann, M., 2020. A transdisciplinary and community-driven database to unravel subduction zone initiation. Nat. Commun. 11, 3750. https://doi.org/10.1038/s41467-020-17522-9

Dalrymple, R.W., 2010. Tidal depositional systems, in: James, N.P., Dalrymple, R.W. (Eds.), Facies Models 4. Geological Association of Canada, pp. 201–232.

Davies, J.H., von Blanckenburg, F., 1995. Slab breakoff: A model of lithosphere detachment and its test in the magmatism and deformation of collisional orogens. Earth Planet. Sci. Lett. 129, 85–102. https://doi.org/10.1016/0012-821X(94)00237-S

Delph, J.R., Thomas, A.M., Levander, A., 2021. Subcretionary tectonics: Linking variability in the expression of subduction along the Cascadia forearc. Earth Planet. Sci. Lett. 556, 116724. https://doi.org/10.1016/j.epsl.2020.116724

DePaolo, D.J., Harrison, T.M., Wielicki, M., Zhao, Z., Zhu, D.-C., Zhang, H., Mo, X., 2019. Geochemical evidence for thin syn-collision crust and major crustal thickening between 45 ans 32 Ma at the southern margin of Tibet. Gondwana Res. 73, 123–135. https://doi.org/10.1016/j.gr.2019.03.011

Dickinson, W.R., 1995. Forearc basins, in: Busby, C.J., Ingersoll, R. V. (Eds.), Tectonics of Sedimentary Basins. Blackwell Science, Oxford, UK, pp. 221–261.

Dickinson, W.R., 1985. Interpreting provenance relations from detrital modes of Sandstones, in: Zuffa, G.G. (Ed.), Provenance of Arenites. pp. 333–361.

Dickinson, W.R., 1973. Widths of modern arc-trench gaps proportional to past duration of igneous activity in associated magmatic arcs. J. Geophys. Res. 78, 3376–3389. https://doi.org/10.1029/JB078i017p03376

Dielforder, A., Hetzel, R., Oncken, O., 2020. Megathrust shear force controls mountain heigth at convergent plate margins. Nature 582, 225–229. https://doi.org/10.1038/s41586-020-2340-7

Duarte, E., Cardona, A., Lopera, S., Valencia, V., Estupiñan, H., 2018. Provenance and diagenesis from two stratigraphic sections of the Lower Cretaceous Caballos Formation in the Upper Magdalena Valley: Geological and reservoir quality implications. Ciencia, Tecnol. y Futur. 8, 5–29. https://doi.org/10.29047/01225383.88

Duque-Caro, H., 1990a. The Choco Block in the northwestern corner of South America : Structural, tectonostratigraphic, and paleogeographic implications. J. South Am. Earth Sci. 3, 71–84. https://doi.org/10.1016/0895-9811(90)90019-W

Duque-Caro, H., 1990b. Neogene stratigraphy, paleoceanography and paleobiogeography in northwest South America and evolution of the Panama Seaway. Palaeogeogr. Palaeoclimatol. Palaeoecol. 77, 203–234. https://doi.org/10.1016/0031-0182(90)90178-A

Duque-Caro, H., 1990c. Estratigrafía, paleoceanografía y paleobiogeografía de la Cuenca del Atrato y la evolución del Istmo de Panamá. Boletín Geológico 31, 4–45.

Duque-Trujillo, J., Bustamante, C., Solari, L., Gómez-Mafla, A., Toro-Villegas, G., Hoyos, S., 2019. Reviewing the Antioquia batholith and satellite bodies: a record of Late Cretaceous to Eocene syn- to post-collisional arc magmatism in the Central Cordillera of Colombia. Andean Geol. 46, 82–101. https://doi.org/10.5027/andgeoV46n1-3120

Dürkefälden, A., Hoernle, K., Hauff, F., Wartho, J.-. A., van den Bogaard, P., Werner, R., 2019. Age and geochemistry of the Beata Ridge: Primary formation during the main phase (~89 Ma) of the Caribbean Large Igneous Province. Lithos 328–329, 69–87. https://doi.org/10.1016/j.lithos.2018.12.021

Dziewonski, A.M., Chou, T.-A., Woodhouse, J.H., 1981. Determination of earthquake source parameters from waveform data for studies of global and regional seismicity. J. Geophys. Res. Solid Earth 86, 2825–2852. https://doi.org/10.1029/JB086iB04p02825

Echeverri, S., Cardona, A., Pardo-Trujillo, A., Borrero, C., Rosero, S., López, S., 2015a. Correlación y geocronología Ar-Ar del basamento Cretácico y el relleno sedimentario Eoceno Superior - Mioceno (Aquitaniano inferior) de la cuenca de ante-arco de Tumaco, SW de Colombia. Rev. Mex. Ciencias Geológicas 32, 179–189.

Echeverri, S., Cardona, A., Pardo-Trujillo, A., Monsalve, G., Valencia, V.A., Borrero, C.,

Rosero, S., López, S., 2015b. Regional provenance from southwestern Colombia fore-arc and intra-arc basins: implications for Middle to Late Miocene orogeny in the northern Andes. Terra Nov. 27, 356–363. https://doi.org/10.1111/ter.12167

Echeverri, S., Pardo-Trujillo, A., Borrero, C., Cardona, A., Rosero, S., Celis, S.A., López, S.A., 2016. Estratigrafía del Neógeno Superior al sur de la Cuenca Tumaco (Pacífico Colombiano): La Formación Cascajal, propuesta de redefinición litoestratigráfica. Boletín Geol. 38, 43–60. https://doi.org/10.18273/revbol.v38n4-2016003

Ekström, G., Nettles, M., Dziewonski, A.M., 2012. The global CMT project 2004-2010: Centroid-moment tensors for 13,017 earthquakes. Phys. Earth Planet. Inter. 200–201, 1–9. https://doi.org/10.1016/j.pepi.2012.04.002

Encinas, A., Sagripanti, L., Rodríguez, M.P., Orts, D., Anavalón, A., Giroux, P., Otero, J., Echaurren, A., Zambrano, P., Valencia, V., 2021. Tectonosedimentary evolution of the Coastal Cordillera and Central Depression of south-Central Chila (36°30'-42°S). Earth-Science Rev. 213, 103465. https://doi.org/10.1016/j.earscirev.2020.103465

England, P., Molnar, P., 1990. Surface uplift, uplift of rocks, and exhumation of rocks. Geology 18, 1173–1177. https://doi.org/10.1130/0091-7613(1990)018<1173:SUUORA>2.3.CO;2

Espurt, N., Funiciello, F., Martinod, J., Guillaume, B., Regard, V., Faccenna, C., Brusset, S., 2008. Flat subduction dynamics and deformation of the South American plate: Insights from analog modeling. Tectonics 27, TC3011. https://doi.org/10.1029/2007TC002175

Faccenna, C., Molin, P., Orecchio, B., Olivetti, V., Bellier, O., Funiciello, F., Minelli, L., Piromallo, C.-, Billi, A., 2011. Topography of the Calabria subduction zone (southern Italy): Clues for the origin of Mt. Etna. Tectonics 30, TC1003. https://doi.org/10.1029/2010TC002694

Faccenna, C., Oncken, O., Holt, A.F., Becker, T.W., 2017. Initiation of the Andean orogeny by lower mantle subduction. Earth Planet. Sci. Lett. 463, 189–201.

Fick, S.E., Hijmans, R.J., 2017. WorldClim 2: new 1-km spatial resolution climate surfaces for global land areas. Int. J. Climatol. 37, 4302–4315. https://doi.org/10.1002/joc.5086

Finzel, E.S., Enkelmann, E., 2017. Miocene-Recent sediment flux in the south-central

Alaskan forearc basin governed by flat-slab subduction. Geochemistry, Geophys. Geosystems 18, 1739–1760. https://doi.org/10.1002/2016GC006783

Finzel, E.S., Enkelmann, E., Falkowski, S., Hedeen, T., 2016. Long-term fore-arc basin evolution in response to changing subduction styles in southern Alaska. Tectonics 35, 1735–1759. https://doi.org/10.1002/2016TC004171

Finzel, E.S., Trop, J.M., Ridgway, K.D., Enkelmann, E., 2011. Upper plate proxies for flat-slab subduction processes in southern Alaska. Earth Planet. Sci. Lett. 303, 348–360. https://doi.org/10.1016/j.epsl.2011.01.014

Folk, R.L., 1980. Petrology of Sedimentary Rocks. Hemphill Publishing Company, Austin, Texas.

Frohlich, C., 1992. Triangle diagrams: ternary graphs to display similarity and diversity of earthquake focal mechanisms. Phys. Earth Planet. Inter. 75, 193–198. https://doi.org/10.1016/0031-9201(92)90130-N

Galvis, J., 1980. Un arco de islas terciarion en el occidente Colombiano. Geol. Colomb. 11, 7–43.

Gao, X., Wang, K., 2014. Strength of stick-slip and creeping subduction megathrusts from heat flow observations. Science (80-.). 345, 1038–1041. https://doi.org/10.1126/science.1255487

Garzione, C.N., Hoke, G.D., Libarkin, J.C., Withers, S., MacFadden, B., Eiler, J., Ghosh, P., Mulch, A., 2008. Rise of the Andes. Science (80-.). 320, 1304–1307. https://doi.org/10.1126/science.1148615

Geldmacher, J., Hanan, B.B., Blichert-Toft, J., Harpp, K., Hoernle, K., Hauff, F., Werner, R., Kerr, A.C., 2003. Hafnium isotopic variations in volcanic rocks from the Caribbean Large Igneous Province and Galápagos hot spot tracks. Geochemistry, Geophys. Geosystems 4, 1062. https://doi.org/10.1029/2002GC000477

Genge, M.C., Witt, C., Chanier, F., Reynaud, J.-. Y., Calderon, Y., 2020. Outer forearc high control in an erosional subduction regime: The case of the central Peruvian forearc (6-10°S). Tectonophysics 228546.

Gentry, A., 1986. Species richness and floristic composition of Chocó region plant communities. Caldasia 15, 71–91.

George, S.W.M., Horton, B.K., Vallejo, C., Jackson, L.J., Gutiérrez, E.G., 2021. Did accretion of the Caribbean oceanic plateau drive rapid crustal thickening in the northern Andes? Geology.

Gianni, G.M., Navarrete, C., Echaurren, A., Díaz, M., Butler, K.L., Horton, B.K., Encinas, A., Folguera, A., 2020. Northward propagation of Andean genesis: Insights from Early Cretaceous synorogenic deposits in the Aysén-Río Mayo basin. Gondwana Res. 77, 238–259. https://doi.org/10.1016/j.gr.2019.07.014

Gómez-Tapias, J., Montes-Ramírez, N.E., Almanza-Meléndez, M.F., Alcárcel-Gutiérrez, F.A., Madrid-Montoya, C.A., Diederix, H., 2017. Geological map of Colombia. Episodes 40, 201–212. https://doi.org/10.18814/epiiugs/2017/v40i3/017023

Gómez-Tapias, J., Nivia, A., Montes, N.E., Almanza, M.F., Alcárcel, F.A., Madrid, C.A., 2015. Notas explicativas: Mapa Geológico de Colombia, in: Gómez-Tapias, J., Almanza, M.F. (Eds.), Compilando La Geología de Colombia: Una Visión a 2015. Servicio Geológico Colombiano, Publicaciones Geológicas Especiales, 33, Bogotá, pp. 9–33.

Gómez, E., Jordan, T.E., Allmendinger, R.W., Cardozo, N., 2005. Development of the Colombian foreland-basin system as consequence of diachronous exhumation of the northern Andes. Geol. Soc. Am. Bull. 117, 1272–1292. https://doi.org/10.1130/B25456.1

Gómez, E., Jordan, T.E., Allmendinger, R.W., Hegarty, K., Kelley, S., Heizler, M., 2003. Controls on architecture of the Late Cretaceous to Cenozoic southern Middle Magdalena Valley Basin, Colombia. Geol. Soc. Am. Bull. 115, 131–147. https://doi.org/10.1130/0016-7606(2003)115<0131:COAOTL>2.0.CO;2

González, J.L., Shen, Z., Mauz, B., 2014. New constraints on Holocene uplift rates for the Baudo Mountain Range, northwestern Colombia. J. South Am. Earth Sci. 52, 194–202.

Grimes, C.B., John, B.E., Kelemen, P.B., Mazdab, F.K., Wooden, J.L., Cheadle, M.J., Hangøj, K., Schwarts, J.J., 2007. Trace element chemistry of zircons from oceanic crust:

A method for distinguishing detrital zircon provenance. Geology 35, 643–646. https://doi.org/10.1130/G23603A.1

Grimes, C.B., Wooden, J.L., Cheadle, M.J., John, B.E., 2015. "Fingerprinting" tectono-magmatic provenance using trace elements in igneous zircon. Contrib. to Mineral. Petrol. 170, 46. https://doi.org/10.1007/s00410-015-1199-3

Groome, W.G., Thorkelson, D.J., 2009. The three-dimensional thermo-mechanical signature of ridge subduction and slab window migration. Tectonophysics 464, 70–83. https://doi.org/10.1016/j.tecto.2008.07.003

Gutscher, M.-A., 2002. Andean subduction styles and their effect on thermal structure and interplate coupling. J. South Am. Earth Sci. 15, 3–10. https://doi.org/10.1016/S0895-9811(02)00002-0

Gutscher, M.-A., Malavieille, J., Lallemand, S., Collot, J.-Y., 1999. Tectonic segmentation of the North Andean margin: impact of the Carnegie Ridge collision. Earth Planet. Sci. Lett. 168, 255–270. https://doi.org/10.1016/S0012-821X(99)00060-6

Gvirtzman, Z., Faccenna, C., Becker, T.W., 2016. Isostasy, flexure, and dynamic topography. Tectonophysics 683, 255–271. https://doi.org/10.1016/j.tecto.2016.05.041

Haffer, J., 1967. On the geology of the Urabá and northern Chocó regions, northwestern Colombia.

Hastie, A.R., Kerr, A.C., 2010. Mantle plume or slab window?: Physical and geochemical constraints on the origin of the Caribbean oceanic plateau. Earth-Science Rev. 98, 283–293. https://doi.org/10.1016/j.earscirev.2009.11.001

Hawkins Jr., J.W., 1995. The geology of the Lau Basin, in: Taylor, B. (Ed.), Backarc Basins. Springer, Boston, pp. 63–138. https://doi.org/10.1007/978-1-4615-1843-3_3

Hayes, G.P., Moore, G.L., Portner, D.E., Hearne, M., Flamme, H., Furtney, M., Smoczyk, G.M., 2018. Slab2, a comprehensive subduction zone geometry model. Science (80-.). 362, 58–61. https://doi.org/10.1126/science.aat4723

Hayward, B.W., Carter, R., Grenfell, H.R., Hayward, J., 2001. Depth distribution of Recent deep-sea benthic foraminifera east of New Zealand, and their potential for improving

paleobathymetric assessments of Neogene microfaunas. New Zeal. J. Geol. Geophys. 44, 555–587. https://doi.org/10.1080/00288306.2001.9514955

Hernández, M.J., Michaud, F., Collot, J.-Y., Proust, J.-N., d'Acremont, E., 2020. Evolution of the Ecuador offshore nonaccretionary-type forearc basin and margin segmentation. Tectonophysics 781, 228374. https://doi.org/10.1016/j.tecto.2020.228374

Heuret, A., Lallemand, S., 2005. Plate motions, slab dynamics and back-arc deformation. Phys. Earth Planet. Inter. 149, 31–51. https://doi.org/10.1016/j.pepi.2004.08.022

Heuret, A., Lallemand, S., Funiciello, F., Piromallo, C., Faccenna, C., 2011. Physical characteristics of subduction interface type seismogenic zones revisited. Geochemistry, Geophys. Geosystems 12, Q01004. https://doi.org/10.1029/2010GC003230

Hijmans, R., 2017. raster: Geographic data analysis and modeling. R package version 2.6-7 [WWW Document]. URL http://cran.r-project.org/package=raster

Hincapié-Gómez, S., Cardona, A., Jiménez, G., Monsalve, G., Hoyos-Ramírez, L., Bayona, G., 2018. Paleomagnetic and gravimetrical reconnaissance of Cretaceous volcanic rocks from the Western Colombian Andes: Paleogeographic connections with the Caribbean Plate. Stud. Geophys. Geod. 62, 485–511. https://doi.org/10.1007/s11200-016-0678-y

Holbourn, A., Henderson, A.S., MacLeod, N., 2013. Atlas of benthic foraminifera. John Wiley & Sons, Ltd.

Horton, B.K., 2018a. Sedimentary record of Andean mountain building. Earth-Science Rev. 178, 279–309. https://doi.org/10.1016/j.earscirev.2017.11.025

Horton, B.K., 2018b. Tectonic regimes of the central and southern Andes: Responses to variations in plate coupling during subduction. Tectonics 37, 402–429. https://doi.org/10.1002/2017TC004624

Hoskin, P.W.O., Schaltegger, U., 2003. The composition of zircon and igneous and metamorphic petrogenesis. Rev. Mineral. Geochemistry 53, 27–62. https://doi.org/10.2113/0530027

Hu, F., Wu, F., Chapman, J.B., Ducea, M.N., Ji, W., Liu, S., 2020. Quantitatively tracking the elevation of the Tibetan Plateau since the Cretaceous: Insights from whole-rock Sr/Y

and La/Yb ratios. Geophys. Res. Lett. 47, e2020GL089202. https://doi.org/10.1029/2020GL089202

Hurtado, C., Roddaz, M., Santos, R. V., Baby, P., Antoine, P.-O., Dantas, E.L., 2018. Cretaceous early-Paleocene drainage shift of Amazonian rivers driven by Equatorial Atlantic Ocean opening and Andean uplift as deduced from the provenance of northern Peruvian sedimentary rocks (Huallaga basin). Gondwana Res. 63, 152–168. https://doi.org/10.1016/j.gr.2018.05.012

Jaramillo, C., 2018. Evolution of the Isthmus of Panama: Biological, paleoceanographic and paleoclimatological implications, in: Hoorn, C., Perrigo, A., Antonelli, A. (Eds.), Mountains, Climate and Biodiversity. John Wiley & Sons, Ltd, pp. 323–338.

Jaramillo, J.S., Cardona, A., León, S., Valencia, V., Vinasco, C., 2017. Geochemistry and geochronology from Cretaceous magmatic and sedimentary rocks at 6°35'N, western flank of the Central cordillera (Colombian Andes): Magmatic record of arc-growth and collision. J. South Am. Earth Sci. 76, 460–481. https://doi.org/10.1016/j.jsames.2017.04.012

Jaramillo, J.S., Cardona, A., Monsalve, G., Valencia, V., León, S., 2019. Petrogenesis of the late Miocene Combia volcanic complex, northwestern Colombian Andes: Tectonic implication of short term and compositionally heterogeneous arc magmatism. Lithos 330–331, 194–210. https://doi.org/10.1016/j.lithos.2019.02.017

Jicha, B.R., Kay, S.M., 2018. Quantifying arc migration and the role of forearc subduction erosion in the central Aleutians. J. Volcanol. Geotherm. Res. 360, 84–99. https://doi.org/10.1016/j.jvolgeores.2018.06.016

Johnson, H.D., Baldwin, C.T., 1996. Shallow clastic seas, in: Reading, H.G. (Ed.), Sedimentary Environments: Processes, Facies and Stratigraphy. Blackwell Publishing Ltd, pp. 232–280.

Jones, R.W., 1994. The challenger foraminifera. Oxford University Press.

Kasaras, I., Kapetanidis, V., Karakonstantis, A., Kaviris, G., Papadimitriou, P., Voulgaris, N., Makropoulos, K. Popandopoulos, G., Moshou, A., 2014. The April-June 2007 Trichonis Lake earthquake swarm (W. Greece); New implications toward causative

fault zone. J. Geodyn. 73, 60–80. https://doi.org/10.1016/j.jog.2013.09.004

Kerr, A.C., Marriner, G.F., Tarney, J., Nivia, A., Saunders, A.D., Thirlwall, M.F., Sinton, C.W., 1997. Cretaceous Basaltic Terranes in Western Colombia : Elemental, Chronological and Sr – Nd Isotopic Constraints on Petrogenesis. J. Petrol. 38, 677–702. https://doi.org/10.1093/petrology/38.6.677

Kerr, A.C., Pearson, D.G., Nowell, G.M., 2009. Magma source evolution beneath the Caribbean oceanic plateau: New insights from elemental and Sr-Nd-Pb-Hf isotopic studies of ODP Leg 165 Site 1001 basalts, in: James, K.H., Lorente, M.A., Pindell, J.L. (Eds.), The Origin and Evolution of the Caribbean Plate. Geological Society, London, Special Publications, 328., pp. 809–827. https://doi.org/10.1144/SP328.31

Kerr, A.C., White, R. V., Thompson, P.M.E., Tarney, J., Saunders, A.D., 2003. No oceanic plateau - No Caribbean plate? The seminal role of an oceanic plateau in Caribbean plate evolution, in: Bartolini, C., Buffler, R.T., Blickwede, J.F. (Eds.), The Circum-Gulf of Mexico and the Caribbean: Hydrocarbon Habitats, Basin Formation, and Plate Tectonics: AAPG Memoir 79. pp. 126–168. https://doi.org/10.1306/M79877C6

Lamb, S., 2006. Shear stresses on megathrust: Implications for mountain building behind subduction zones. J. Geophys. Res. Solid Earth 111, B07401. https://doi.org/10.1029/2005JB003916

Lamb, S., Davis, P., 2003. Cenozoic climate change as a possible cause for the rise of the Andes. Nature 425, 792–797. https://doi.org/10.1038/nature02049

Lara, M., Salazar-Franco, A.M., Silva-Tamayo, J.C., 2018. Provenance of the Cenozoic siliciclastic intramontane Amagá Formation: Implications for the early Miocene collision between Central and South America. Sediment. Geol. 373, 147–162. https://doi.org/10.1016/j.sedgeo.2018.06.003

Laske, G., Masters, G., Ma, Z., Pasyanos, M., 2013. Update on CRUST1.0 - A 1-degree global model of Earth's crust, Geophys. Res. Abstracts, 15, Abstract EGU2013-2658.

Leal-Mejía, H., Shaw, R.P., Melgarejo, J.C., 2019. Spatial-temporal migration of granitoid magmatism and the Phanerozoic tectono-magmatic evolution of the Colombian Andes, in: Cediel, F., Shaw, R.P. (Eds.), Geology and Tectonics of Northwestern South

America. Frontiers in Earth Sciences. Springer, Cham, pp. 253–410. https://doi.org/10.1007/978-3-319-76132-9_5

Lee, C.-T.A., Thurner, S., Patterson, S., Cao, W., 2015. The rise and fall of continental arcs: Interplays between magmatism, uplift, weathering, and climate. Earth Planet. Sci. Lett. 425, 105–119. https://doi.org/10.1016/j.epsl.2015.05.045

Lefeldt, M., Grevemeyer, I., 2008. Centroid depth and mechanism of trench-outer rise earthquakes. Geophys. J. Int. 172, 240–251. https://doi.org/10.1111/j.1365-246X.2007.03616.x

León, S., Avellaneda-Jiménez, D.S., Monsalve, G., Bustamante, C., Valencia, V., 2022. Evidence for magmatic activity of the Central American arc at ~100-84 Ma supports its spontaneous origin by plume-lithosphere interaction. Geol. Soc. Am. Bull.

León, S., Cardona, A., Mejía, D., Botello, G.E., Villa, V., Collo, G., Valencia, V., Zapata, S., Avellaneda-Jiménez, D.S., 2019. Source area evolution and thermal record of an Early Cretaceous back-arc basin along the northwesternmost Colombian Andes. J. South Am. Earth Sci. 94, 102229. https://doi.org/10.1016/j.jsames.2019.102229

León, S., Cardona, A., Parra, M., Sobel, E.R., Jaramillo, J.S., Glodny, J., Valencia, V., Chew, D., Montes, C., Posada, G., Monsalve, G., Pardo-Trujillo, A., 2018. Transition from collisional to subduction-related regimes: an example from Neogene Panama-Nazca-South-America interactions. Tectonics 37, 119–139. https://doi.org/10.1002/2017TC004785

León, S., Monsalve, G., Bustamante, C., 2021a. How Much Did the Colombian Andes Rise by the Collision of the Caribbean Oceanic Plateau? Geophys. Res. Lett. 48, e2021GL093362. https://doi.org/10.1029/2021GL093362

León, S., Monsalve, G., Jaramillo, C., Posada, G., Miranda, T.S., Echeverri, S., Valencia, V., 2021b. Increased megathrust shear force drives topographic uplift in the Colombian coastal forearc. Tectonophysics 820, 229132. https://doi.org/10.1016/j.tecto.2021.229132

Leterrier, J., Maury, R.C., Thonon, P., Girard, D., Marchal, M., 1982. Clinopyroxene composition as a method of identification of the magmatic affinites of paleo-volcanic

series. Earth Planet. Sci. Lett. 59, 139–154. https://doi.org/10.1016/0012-821X(82)90122-4

Loader, M.A., Wilkinson, J.J., Armstrong, R.N., 2017. The effect of titanite crystallisation on Eu and Ce anomalies in zircon and its implications for the assessment of porphyry Cu deposit fertility. Earth Planet. Sci. Lett. 472, 107–119. https://doi.org/10.1016/j.epsl.2017.05.010

Lonsdale, P., 2005. Creation of the Cocos and Nazca plates by fission of the Farallon plate. Tectonophysics 404, 237–264. https://doi.org/10.1016/j.tecto.2005.05.011

Macía, C., 1985. Características petrográficas y geoquímicas de rocas basálticas de la península de Cabo Corrientes (Serranía de Baudó), Colombia. Geol. Colomb. 14, 25–37.

Malkowski, M.A., Sharman, G.R., Johnstone, S.A., Grove, M.J., Kimbrough, D.L., Graham, S.A., 2019. Dilution and propagation of provenance trends in sand and mud: Geochemistry and detrital zircon geochronology of modern sediment from central California (U.S.A.). Am. J. Sci. 319, 846–902. https://doi.org/10.2475/10.2019.02

Mamani, M., Wörner, G., Sempere, T., 2010. Geochemical variations in igneous rocks of the Central Andean orocline (13°S to 18°S): tracing crustal thickening and magma generation through time and space. Geol. Soc. Am. Bull. 122, 162–182. https://doi.org/10.1130/B26538.1

Mann, H.B., Whitney, D.R., 1947. On a test of whether one of two random variables is stochastically larger than the other. Ann. Math. Stat. 18, 50–60.

Marcaillou, B., Collot, J.-Y., 2008. Chronostratigraphy and tectonic deformation of the North Ecuadorian-South Colombian offshore Manglares forearc basin. Mar. Geol. 255, 30–44. https://doi.org/10.1016/j.margeo.2008.07.003

Martinez, F., Parra, M., Gonzalez, R., López, C., Patiño, A., Muñoz, B., Robledo, F., Sobel, E.R., Glodny, J., 2022. Deciphering the Late Paleozoic-Cenozoic tectonic history of the inner Central Andes forearc: An update from the Salar de Punta Negra Basin of northern Chile. Front. Earth Sci. 9, 790526. https://doi.org/10.3389/feart.2021.790526

Martinez, F., Peña, M., Parra, M., López, C., 2021. Contraction and exhumation of the

western Central Andes induced by basin inversion: New evidence from “Pampean” subduction segment. Basin Res. 33, 2706–2724. https://doi.org/10.1111/bre.12580

Martinod, J., Regard, V., Letourmy, Y., Henry, H., Hassani, R., Baratchart, S., Carretier, S., 2016. How do subduction processes contribute to forearc Andean uplift? J. Geodyn. 96, 6–18. https://doi.org/10.1016/j.jog.2015.04.001

Mason, C.C., Romans, B.W., Stockli, D.F., Mapes, R.W., Fildani, A., 2019. Detrital zircon reveal sea-level and hydroclimate controls on Amazon River to deep-sea fan sediment transfer. Geology 47, 563–567. https://doi.org/10.1130/G45852.1

McClay, K.R., 1987. The mapping of geological structures. Geological Society of London handbook. Open University Press.

McDonough, W.F., Sun, S. -s., 1995. The composition of the Earth. Chem. Geol. 120, 223–253. https://doi.org/10.1016/0009-2541(94)00140-4

McGirr, R., Seton, M., Williams, S., 2020. Kinematic and geodynamic evolution of the Isthmus of Panama region: Implications for Central American Seaway closure. Geol. Soc. Am. Bull. 133, 867–884. https://doi.org/10.1130/B35595.1

McKay, M.P., Jackson Jr., W.T., Hessler, A.M., 2018. Tectonic stress regime recorded by zircon Th/U. Gondwana Res. 57, 1–9. https://doi.org/10.1016/j.gr.2018.01.004

Mibe, K., Kawamoto, T., Matsukage, K.N., Fei, Y., Ono, S., 2011. Slab melting versus slab dehydration in subduction-zone magmatism. Proc. Natl. Acad. Sci. U. S. A. 108, 8177–8182. https://doi.org/10.1073/pnas.1010968108

Molnar, P., England, P., Martinod, J., 1993. Mantle dynamics, uplift of the Tibetan Plateau, and the Indian Monsoon. Rev. Geophys. 31, 357–396. https://doi.org/10.1029/93RG02030

Monsalve, G., Jaramillo, J.S., Cardona, A., Schulte-Pelkum, V., Posada, G., Valencia, V., Poveda, E., 2019. Deep crustal faults, shear zones, and magmatism in the Eastern Cordillera of Colombia: Growth of a plateau from teleseismic receiver function and geochemical Mio-Pliocene volcanism constraints. J. Geophys. Res. Solid Earth 124. https://doi.org/10.1029/2019JB017835

Montes, C., Cardona, A., Jaramillo, C., Pardo, A., Silva, J.C., Valencia, V., Ayala, C., Pérez-Angel, L.C., Rodríguez-Parra, L.A., Ramírez, V., Niño, H., 2015. Middle Miocene closure of the Central American Seaway. Science (80-.). 348, 226–229. https://doi.org/10.1126/science.aaa2815

Montes, C., Cardona, A., McFadden, R., Moron, S.E., Silva, C.A., Restrepo-Moreno, S.A., Ramirez, D.A., Hoyos, N., Wilson, J., Farris, D.W., Bayona, G., Jaramillo, C., Valencia, V., Bryan, J., Flores, J.A., 2012. Evidence for middle Eocene and younger land emergence in central Panama: Implications for Isthmus closure. Geol. Soc. Am. Bull. 124, 780–799. https://doi.org/10.1130/B30528.1

Montes, C., Guzman, G., Bayona, G., Cardona, A., Valencia, V.A., Jaramillo, C., 2010. Clockwise rotation of the Santa Marta massif and simultaneous Paleogene to Neogene deformation of the Plato-San Jorge and Cesar-Rancheria basins. J. South Am. Earth Sci. 29, 832–848. https://doi.org/10.1016/j.jsames.2009.07.010

Montes, C., Rodríguez-Corcho, A.F., Bayona, G., Hoyos, N., Zapata, S., Cardona, A., 2019. Continental margin response to the multiple arc-continent collisions: The northern Andes-Caribbean margin. Earth-Science Rev. 198, 102903. https://doi.org/10.1016/j.earscirev.2019.102903

Mora-Bohórquez, J.A., Ibañez-Mejia, M., Oncken, O., de Freitas, M., Vélez, V., Mesa, A., Serna, L., 2017. Structure and age of the Lower Magdalena Valley Basin basement, northern Colombia: New reflection-seismic and U-Pb-Hf insights into the termination of the central andes against the Caribbean basin. J. South Am. Earth Sci. 74, 1–26. https://doi.org/10.1016/j.jsames.2017.01.001

Mora-Páez, H., Kellogg, J.N., Freymueller, J.T., Mencin, D., Fernandes, R.M.S., Diederix, H., LaFemina, P., Cardona-Piedrahita, L., Lizarazo, S., Peláez-Gaviria, J.R., Díaz-Mila, F., Bohórquez-Orosco, O., Giraldo-Londoño, L., Corchuelo-Cuervo, Y., 2019. Crustal deformation in the northern Andes - A new GPS velocity field. J. South Am. Earth Sci. 89, 76–91. https://doi.org/10.1016/j.jsames.2018.11.002

Mora-Páez, H., Mencin, D.J., Molnar, P., Diederix, H., Cardona-Piedrahita, L., Peláez-Gaviria, J.R., Corchuelo-Cuervo, Y., 2016. GPS velocities and the construction of the Eastern Cordillera of the Colombian Andes. Geophys. Res. Lett. 43, 8407–8416.

https://doi.org/10.1002/2016GL069795

Mora, A., Villagómez, D., Parra, M., Caballero, V.M., Spikings, R., Horton, B.K., Mora-Bohórquez, J.A., Ketcham, R.A., Arias-Martínez, J.P., 2020. Late Cretaceous to Cenozoic uplift of the Northern Andes: Paleogeographic implications, in: Gómez, J., Mateus-Zabala, D. (Eds.), The Geology of Colombia, Volume 3 Paleogene - Neogene. Servicio Geológico Colombiano, Publicaciones Geológicas Especiales, 37, Bogotá, pp. 89–121. https://doi.org/10.32685/pub.esp.37.2019.04

Mora, J.A., Oncken, O., Le Breton, E., Mora, A., Veloza, G., Vélez, V., de Freitas, M., 2018. Controls on forearc basin formation and evolution: Insights from Oligocene to Recent tectono-stratigraphy of the Lower Magdalena Valley basin of northwest Colombia. Mar. Pet. Geol. 97, 288–310. https://doi.org/10.1016/j.marpetgeo.2018.06.032

Mountney, N.P., Westbrook, G.K., 1997. Quantitative analysis of Miocene to recent forearc basin evolution along the Colombian convergent margin. Basin Res. 9, 177–196. https://doi.org/10.1046/j.1365-2117.1997.00040.x

Moxon, I.W., Graham, S.A., 1987. History and controls of subsidence in the Late Cretaceous-Tertiary Great Vally forearc basin, California. Geology 15, 626–629. https://doi.org/10.1130/0091-7613(1987)15<626:HACOSI>2.0.CO;2

Mukasa, S.B., 1986. Zircon U-Pb ages of super-units in the Coastal batholith, Peru: Implications for magmatic and tectonic processes. Geol. Soc. Am. Bull. 97, 241–254. https://doi.org/10.1130/0016-7606(1986)97<241:ZUAOSI>2.0.CO;2

Müller, R.D., Sdrolias, M., Gaina, C., Roest, W.R., 2008. Age, spreading rates, and spreading asymmetry of the world's ocean crust. Geochemistry, Geophys. Geosystems 9, Q04006. https://doi.org/0.1029/2007GC001743

Myers, N., Mitteimer, R.A., Mitteimer, C.G., da Fonseca, G.A.B., Kent, J., 2000. Biodiversity hotspots for conservation priorities. Nature 403, 853–858.

Nakakuki, T., Mura, E., 2013. Dynamics of slab rollback and induced back-arc basin formation. Earth Planet. Sci. Lett. 361, 287–297. https://doi.org/10.1016/j.epsl.2012.10.031

National Hydrocarbons Agency of Colombia, 2010. Total Bouguer Anomalies Map of

Colombia. 1:2.500.000.

Noda, A., 2016. Forearc basins: Types, geometries, and relationships to subduction zone dynamics. Geol. Soc. Am. Bull. 128, 879–895. https://doi.org/10.1130/B31345.1

O' Dea, A., Lessios, H.A., Coates, A.G., Eytan, R.I., Restrepo-Moreno, S.A., Cione, A.L., Collins, L.S., de Queiroz, A., Farris, D.W., Norris, R.D., Stallard, R.F., Woodburne, M.O., Aguilera, O., Aubry, M.-P., Berggren, W.A., Budd, A.F., Cozzuol, M.A., Coppard, S.E., Duque-Caro, H., Finnegan, S., Gasparini, G.M., Grossman, E.L., Johnson, K.G., Keigwin, L.D., Knowlton, N., Leigh, E.G., Leonard-Pingel, J.S., Marko, P.B., Pyenson, N.D., Rachello-Dolmen, P.G., Soibelzon, E., Soibelzon, L., Todd, J.A., Vermeij, G.J., Jackson, J.B.C., 2016. Formation of the Isthmus of Panama. Sci. Adv. 2, e1600883. https://doi.org/10.1126/sciadv.1600883

Odin, G.S., Matter, A., 1981. De glauconiarum origine. Sedimentology 28, 611–641. https://doi.org/10.1111/j.1365-3091.1981.tb01925.x

Oguchi, T., Aoki, T., Matsuta, N., 2003. Identificacion of an active fault on the Japanese Alps from DEM-based hill shading. Comput. Geosci. 29, 885–891. https://doi.org/10.1016/S0098-3004(03)00083-9

Ojeda, A., Havskov, J., 2001. Crustal structure and local seismicity in Colombia. J. Seismol. 5, 575–593. https://doi.org/10.1023/A:1012053206408

Oncken, O., Chong, G., Franz, G., Giese, P., Gotze, H.-J., Ramos, V.A., Strecker, M.R., Wigger, P., 2006. The Andes: Active Subduction Orogeny, Frontiers in Earth Sciences. Springer-Verlag Berlin Heidelberg.

Ordoñez, O., Pimentel, M.M., Armstrong, R.A., Goia, S.M.C.L., Junges, S., 2001. U-Pb SHRIMP and Rb-Sr ages of the Sonsón Batholith, in: III South American Symposium on Isotope Geology. Pucon, Chile.

Osorio-Granada, E., Restrepo-Moreno, S.A., Muñoz-Valencia, J.A., Trejos-Tamayo, R.A., Pardo-Trujillo, A., Barbosa-Espitia, A.A., 2017. Detrital zircon typology and U/Pb geochronology for the Miocene Ladrilleros-Juanchaco sedimentary sequence, Equatorial Pacific (Colombia): New constraints on provenance and paleogeography in northwestern South America. Geol. Acta 15, 201–215.

https://doi.org/10.1344/GeologicaActa2017.15.3.4

Pacheco, J.F., Sykes, L.R., Scholz, C.H., 1993. Nature of seismic coupling along simple plate boundaries of the subduction type. J. Geophys. Res. Solid Earth 98, 14133–14159. https://doi.org/10.1029/93JB00349

Pardo-Trujillo, A., Cardona, A., Giraldo, A.S., León, S., Vallejo, D.F., Trejos-Tamayo, R., Plata, A., Ceballos, J.A., Echeverri, J.S., Barbosa-Espitia, A.A., Slattery, J., Salazar, A.F., Botello, G.E., Celis, S., Osorio-Granada, E., Giraldo-Villegas, C.A., 2020a. Sedimentary record of the Cretaceous-Paleogene arc-continent collision in the northwestern Colombian Andes: Insights from stratigraphic and provenance constraints. Sediment. Geol. 401, 105627. https://doi.org/10.1016/j.sedgeo.2020.105627

Pardo-Trujillo, A., Echeverri, S., Borrero, C., Arenas, A., Vallejo, F., Trejos, R., Plata, A., Flores, J.A., Cardona, A., Restrepo, S., Barbosa, A., Murcia, H., Giraldo, C., Celis, S., Osorio, J.A., López, S.A., 2020b. Cenozoic geologic evolution of the southern Tumaco forearc basin (SW Colombian Pacific), in: Gómez, J., Mateus-Zabala, D. (Eds.), The Geology of Colombia, Volume 3 Paleogene-Neogene. Servicio Geológico Colombiano, Publicaciones Geológicas Especiales, 37, Bogotá, pp. 215–247. https://doi.org/10.32685/pub.esp.37.2019.08

Pardo-Trujillo, A., Moreno-Sánchez, M., Gomez-Cruz, A.D.J., 2002. Estratigrafía de algunos depósitos del Cretáceo Superior en las Cordilleras Central y Occidental de Colombia: Implicaciones Regionales. Geo. Eco. Trop. 26, 113.

Paris, G., Machette, M.N., Dart, R.L., Haller, K.M., 2000. Map and databse of Quaternary faults and folds in Colombia and its offshore regions. U. S. Geological Survey Open-File Report 00-0284.

Parra, M., Mora, A., Jaramillo, C., Torres, V., Zeilinger, G., Strecker, M.R., 2010. Tectonic controls on Cenozoic foreland basin development in the north-eastern Andes, Colombia. Basin Res. 22, 874–903.

Parra, M., Mora, A., López, C., Rojas, L.E., Horton, B.K., 2012. Detecting earliest shortening and deformation advance in thrust-belt hinterlands: Example from the Colombian Andes. Geology 40, 175–178. https://doi.org/10.1130/G32519.1

Parra, M., Mora, A., Sobel, E.R., Strecker, M.R., González, R., 2009. Episodic orogenic front migration in the northern Andes: Constraints from low-temperature thermochronology in the Eastern Cordillera, Colombia. Tectonics 28, TC4004. https://doi.org/10.1029/2008TC002423

Pearce, J.A., Harris, N.B.W., Tindle, A.G., 1984. Trace element discrimination diagrams for the tectonic interpretation of granitic rocks. J. Petrol. 25, 956–983. https://doi.org/10.1093/petrology/25.4.956

Pearce, J.A., Peate, D.W., 1995. Tectonic implications of the composition of volcanic arc magmas. Annu. Rev. Earth Planet. Sci. 23, 251–285. https://doi.org/10.1146/annurev.ea.23.050195.001343

Pennington, W.D., 1981. Subduction of the Eastern Panama Basin and seismotectonics of northwestern South America. J. Geophys. Res. Solid Earth 86, 10753–10770. https://doi.org/10.1029/JB086iB11p10753

Pérez-Escobar, O.A., Lucas, E., Jaramillo, C., Monro, A., Morris, S.K., Bogarín, D., Greer, D., Dodsworth, S., Aguilar-Cano, J., Sanchez-Meseguer, A., Antonelli, A., 2019. The origin and diversification of the hyperdiverse flora in the Chocó biogeographic region. Front. Plant Sci. 10, 1328. https://doi.org/10.3389/fpls.2019.01328

Perez, N.D., Levine, K.G., 2020. Diagnosing an ancient shallow-angle subduction event from Cenozoic depositional and deformational records in the central Andes of southern Peru. Earth Planet. Sci. Lett. 541, 116263. https://doi.org/10.1016/j.epsl.2020.116263

Phillips, J.D., 2005. Weathering instability and landscape evolution. Geomorphology 67, 255–272. https://doi.org/10.1016/j.geomorph.2004.06.012

Pindell, J., Maresch, W. V., Martens, U., Stanek, K., 2012. The Greater Antillan Arc: Early Cretaceous origin and proposed relationship to Central American subduction mélanges: implications for models of Caribbean evolution. Int. Geol. Rev. 54, 131–143. https://doi.org/10.1080/00206814.2010.510008

Pindell, J.L., Kennan, L., 2009. Tectonic evolution of the Gulf of Mexico, Caribbean and northern South America in the mantle reference frame : an update. Geol. Soc. London, Spec. Publ. 328, 1–55. https://doi.org/10.1144/SP328.1

Plint, A.G., 2010. Wave- and storm-dominated shoreline and shallow-marine systems, in: James, N.P., Dalrymple, R.W. (Eds.), Facies Models 4. Geological Association of Canada, pp. 167–200.

Poveda, E., Julià, J., Schimmel, M., Perez-Garcia, N., 2018. Upper and middle crustal velocity structure of the Colombian Andes from ambient noise tomography: Investigating subduction-related magmatism in the overriding plate. J. Geophys. Res. Solid Earth 123, 1459–1485. https://doi.org/10.1002/2017JB014688

Poveda, E., Monsalve, G., Vargas, C.A., 2015. Receiver functions and crustal structure of the northwestern Andean region, Colombia. J. Geophys. Res. Solid Earth 120, 2408–2425. https://doi.org/10.1002/2014JB011304

Poveda, G., Mesa, O.J., 2000. On the existence of Lloró (the rainiest locality on Earth): Enhanced ocean-land atmosphere interaction by a low-level jet. Geophys. Res. Lett. 27, 1675–1678. https://doi.org/10.1029/1999GL006091

Profeta, L., Ducea, M.N., Chapman, J.B., Paterson, S.R., Henriquez-Gonzales, S.M., Kirsch, M., Petrescu, L., DeCelles, P.G., 2015. Quantifying crustal thickness over time in magmatic arcs. Sci. Rep. 5, 17786. https://doi.org/10.1038/srep17786

R Development Core Team, 2017. R: A language and environment for statistical computing.

Rahbek, C., Borregaard, M.K., Antonelli, A., Colwell, R.K., Holt, B.G., Nogues-Bravo, D., Rasmussen, C.M.O., Richardson, K., Rosing, M.T., Whittaker, R.J., Fjeldså, J., 2019. Building mountain biodiversity: Geological and evolutionary processes. Science (80-.). 365, 1114–1119. https://doi.org/10.1126/science.aax0151

Ramírez, D.A., Foster, D.A., Min, K., Montes, C., Cardona, A., Sadove, G., 2016. Exhumation of the Panama basement complex and basins: Implications for the closure of the Central American seaway. Geochemistry, Geophys. Geosystems 17, 1758–1777. https://doi.org/10.1002/2016GC006289

Ramos, V.A., 2009. Anatomy and global context of the Andes: Main geologic features and the Andean orogenic cycle, in: Backbone of the Americas: Shallow Subduction, Plateau Uplift and Ridge and Terrane Collision. Geological Society of America Memoir 204. pp. 31–65. https://doi.org/10.1130/2009.1204(02)

Ranero, C.R., von Huene, R., 2000. Subduction erosion along the Middle America convergent margin. Nature 404, 748–752. https://doi.org/10.1038/35008046

Reiners, P.W., Brandon, M.T., 2006. Using Thermochronology To Understand Orogenic Erosion. Annu. Rev. Earth Planet. Sci. 34, 419–466. https://doi.org/10.1146/annurev.earth.34.031405.125202

Reyes-Harker, A., Ruiz-Valdivieso, C.F., Mora, A., Ramirez-Arias, J.C., Rodriguez, G., de la Parra, F., Caballero, V., Parra, M., Moreno, N., Horton, B.K., Saylor, J.E., Silva, A., Valencia, V., Stockli, D., Blanco, V., 2015. Cenozoic paleogeography of the Andean foreland and retroarc hinterland of Colombia. Am. Assoc. Pet. Geol. Bull. 99, 1407–1453. https://doi.org/10.1306/06181411110

Ridgway, K.D., Trop, J.M., Finzel, E.S., 2011. Modification of continental forearc basins by flat-slab subduction processes: a case study from southern Alaska, in: Busby, C., Azor, A. (Eds.), Tectonics of Sedimentary Basins: Recent Advances. Blackwell Publishing Ltd, pp. 327–346. https://doi.org/10.1002/9781444347166.ch16

Riley, S.J., DeGloria, S.D., Elliot, R., 1999. A Terrain Ruggedness Index that quantifies topographic heterogeneity. Intermt. J. Sci. 5, 23–27.

Rodríguez-Olarte, D., Mojica-Corzo, J.I., Taphonr-Baechle, D.C., 2011. Northern South America - Magdalena and Maracaibo Basins, in: Albert, J.S., Reis, R.E. (Eds.), Historical Biogeography of Neotropical Freshwaters Fishes. University of California Press, pp. 243–257. https://doi.org/10.1525/california/9780520268685.003.0015

Rodríguez, G., Arango, M.I., Zapata, G., Bermúdez-Cordero, J.G., 2016. Estratigrafía, petrografía y análisis multi-método de procedencia de la Formación Guineales, norte de la Cordillera Occidental de Colombia. Boletín Geol. 38, 101–124.

Rodríguez, G., Sierra, M.I., 2010. Las Sedimentitas de Tripogadí y las Brechas de Triganá : Un registro de Eoceno en el noroccidente de Sur América. Geol. Colomb. 35, 74–86.

Rodríguez, G., Zapata, G., 2012. Características del plutonismo Mioceno Superior en el segmento norte de la Cordillera Occidental e implicaciones tectónicas en el modelo geológico del noroccidente Colombiano. Bol. Ciencias la Tierra 31, 5–22.

Rodríguez, G., Zapata, G., Gómez, J.F., 2013. Geología de la plancha 114 - Dabeiba. Escala

1:100.000.

Rooney, T.O., Franceschi, P., Hall, C.M., 2011. Water-saturated magmas in the Panama Canal region: a precursor to adakite-like magma generation? Contrib. to Mineral. Petrol. 161, 373–388. https://doi.org/10.1007/s00410-010-0537-8

Rosenbaum, G., Mo, W., 2011. Tectonic and magmatic responses to the subduction of high bathymetric relief. Gondwana Res. 19, 571–582. https://doi.org/10.1016/j.gr.2010.10.007

Rutledge, S., Mahatsente, R., 2017. Fore-arc structure, plate coupling and isostasy in the Central Andes: Insight from gravity data modelling. J. Geodyn. 104, 27–35. https://doi.org/10.1016/j.jog.2016.12.003

Salvini, F., Billi, A., Wise, D.U., 1999. Strike-slip fault-propagation cleavage in carbonate rocks: the Mattinata Fault Zone, Southern Apennines, Italy. J. Struct. Geol. 21, 1731–1749. https://doi.org/10.1016/S0191-8141(99)00120-0

Sarmiento-Rojas, L.F., 2019. Cretaceous stratigraphy and paleo-facies maps of northwestern South America, in: Cediel, F., Shaw, R.P. (Eds.), Geology and Tectonics of Northwestern South America. Frontiers in Earth Sciences. Springer, Cham, pp. 673–747. https://doi.org/10.1007/978-3-319-76132-9_10

Saylor, J.E., Horton, B.K., 2014. Nonuniform surface uplift of the Andean plateau revealed by deuterium isotopes in Miocene volcanic glass from southern Peru. Earth Planet. Sci. Lett. 387, 120–131. https://doi.org/10.1016/j.epsl.2013.11.015

Scheiber, T., Fredin, O., Viola, G., Jarna, A., Gasser, D., Łapińska-Viola, R., 2015. Manual extraction of bedrock lineaments from high-resolution LiDAR data: methodological bias and human perception. GFF 137, 362–372. https://doi.org/10.1080/11035897.2015.1085434

Sdrolias, M., Müller, R.D., 2006. Controls on back-arc basin formation. Geochemistry, Geophys. Geosystems 7, Q04016. https://doi.org/10.1029/2005GC001090

Serrano, L., Ferrari, L., López-Martínez, M., Petrone, C.M., Jaramillo, C., 2011. An integrative geologic, geochronologic and geochemical study of Gorgona Island, Colombia: Implications for the formation of the Caribbean Large Igneous Province.

Earth Planet. Sci. Lett. 309, 324–336. https://doi.org/10.1016/j.epsl.2011.07.011

Siravo, G., Faccenna, C., Gérault, M., Becker, T.W., Fellin, M.G., Herman, F., Molin, P., 2019. Slab flattening and the rise of the Eastern Cordillera, Colombia. Earth Planet. Sci. Lett. 512, 100–110. https://doi.org/10.1016/j.epsl.2019.02.002

Soesoo, A., Bons, P.D., Gray, D.R., Foster, D.A., 1997. Divergent double subduction : Tectonic and petrologic consequences. Geology 25, 755–758. https://doi.org/10.1130/0091-7613(1997)025<0755

Spikings, R.A., Simpson, G., 2014. Rock uplift and exhumation of continental margins by the collision, accretion, and subduction of buoyant and topographically prominent oceanic crust. Tectonics 33, 1–21. https://doi.org/10.1002/2013TC003425

Stern, C.R., 2011. Subduction erosion: Rates, mechanisms and its role in arc magmatism and the evolution of the continental crust and mantle. Gondwana Res. 20, 284–308. https://doi.org/10.1016/j.gr.2011.03.006

Stern, R.J., 2002. Subduction zones. Rev. Geophys. 40, 3-1-3–38. https://doi.org/10.1029/2001RG000108

Stern, R.J., Gerya, T., 2018. Subduction initiation in nature and models: A review. Tectonophysics 746, 173–198. https://doi.org/10.1016/j.tecto.2017.10.014

Stow, D., Smillie, Z., 2020. Distinguishing between deep-water sediment facies: Turbidites, contourites and hemipelagites. Geosciences 10, 68. https://doi.org/10.3390/geosciences10020068

Stow, D.A. V., Reading, H.G., Collinson, J.D., 1996. Deep seas, in: Reading, H.G. (Ed.), Sedimentary Environments: Processes, Facies and Stratigraphy. Blackwell Publishing Ltd, pp. 395–453.

Syracuse, E.M., Maceira, M., Prieto, G.A., Zhang, H., Ammon, C.J., 2016. Multiple plates subducting beneath Colombia, as illuminated by seismicity and velocity from the joint inversion of seismic and gravity data. Earth Planet. Sci. Lett. 444, 139–149. https://doi.org/10.1016/j.epsl.2016.03.050

Tassara, A., 2010. Control of forearc density structure on megathrust shear strength along

the Chilean subduction zone. Tectonophysics 495, 34–47. https://doi.org/10.1016/j.tecto.2010.06.004

Tetreault, J.L., Buiter, S.J.H., 2012. Geodynamic models of terrane accretion: Testing the fate of island arcs, oceanic plateaus, and continental fragments in subduction zones. J. Geophys. Res. Solid Earth 117, B08403. https://doi.org/10.1029/2012JB009316

Thompson, P.M.E., Kempton, P.D., White, R. V., Saunders, A.D., Kerr, A.C., Tarney, J., Pringle, M.S., 2004. Elemental, Hf-Nd isotopic and geochronological constraints on an island arc sequence associated with the Cretaceous Caribbean plateau: Bonaire, Dutch Antilles. Lithos 74, 91–116. https://doi.org/10.1016/j.lithos.2004.01.004

Timm, C., Davy, B., Haase, K., Hoernle, K., Graham, I.J., de Ronde, C.E.J., Woodhead, J., Basset, D., Hauff, F., Mortimer, N., Seebeck, H.C., Wysoczanski, R.J., Caratori-Tontini, F., Gamble, J.A., 2014. Subduction of the oceanic Hikurangi Plateau and its impact on the Kermadec arc. Nat. Commun. 5, 4923. https://doi.org/10.1038/ncomms5923

Tistl, M., Burgath, K.P., Höhndorf, A., Kreuzer, H., Muñoz, R., Salinas, R., 1994. Origin and emplacement of Tertiary ultramafic complexes in northwest Colombia: Evidence from geochemistry and K-Ar, Sm-Nd and Rb-Sr isotopes. Earth Planet. Sci. Lett. 126, 41–59. https://doi.org/10.1016/0012-821X(94)90241-0

Tozer, B., Sandwell, D.T., Smith, W.H.F., Olson, C., Beale, J.R., Wessel, P., 2019. Global bathymetry and topography at 15 arc sec: SRTM15+. Earth Sp. Sci. 6, 1847–1864. https://doi.org/10.1029/2019EA000658

Trail, D., Watson, E.B., Tailby, N.D., 2012. Ce and Eu anomalies in zircon as proxies for the oxidation state of magmas. Geochim. Cosmochim. Acta 97, 70–87. https://doi.org/10.1016/j.gca.2012.08.032

Trenkamp, R., Kellogg, J.N., Freymueller, J.T., Mora, H., 2002. Wide plate margin deformation, southern Central America and northwestern South America, CASA GPS observations. J. South Am. Earth Sci. 15, 157–171.

Tschanz, C.M., Marvin, R.F., Cruz, J., Mehnert, H.H., Cebula, G.T., 1974. Geologic Evolution of the Sierra Nevada de Santa Marta, Northeastern Colombia. Geol. Soc. Am. Bull. 85, 273–284. https://doi.org/10.1130/0016-7606(1974)85<273

Tukey, J.W., 1977. Exploratory Data Analysis. Addison-Wesley Publishing Company.

Uyeda, S., Kanamori, H., 1979. Back-arc opening and the mode of subduction. J. Geophys. Res. 84, 1049–1060.

Vallejo, C., Spikings, R.A., Horton, B.K., Luzieux, L., Romero, C., Winkler, W., Thomsen, T.B., 2019. Late Cretaceous to Miocene stratigraphy and provenance of the coastal forearc and Western Cordillera of Ecuador: Evidence for accretion of a single oceanic plateau fragment, in: Horton, B.K., Folguera, A. (Eds.), Andean Tectonics. Elsevier, pp. 209–236. https://doi.org/10.1016/B978-0-12-816009-1.00010-1

Vallejo, C., Spikings, R.A., Luzieux, L., Winkler, W., Chew, D.M., Page, L., 2006. The early interaction between the Caribbean Plateau and the NW South American Plate. Terra Nov. 18, 264–269. https://doi.org/10.1111/j.1365-3121.2006.00688.x

Vargas, C.A., Gutiérrez, G.A., Sarmiento, G.A., 2020. Subduction of an extinct rift and its role in the formation of submarine landslides in NW South America, in: Georgiopoulou, A., Amy, L.A., Benetti, S., Chaytor, J.D., Clare, M.A., Gamboa, D., Haughton, P.D.W., Moernaut, J., Mountjoy, J.J. (Eds.), Subaqueous Mass Movements in the Context of Observations of Contemporary Failure, Geological Society, London, Special Publications, 500. pp. 311–322. https://doi.org/10.1144/SP500-2019-189

Vargas, C.A., Mann, P., 2013. Tearing and breaking off of subducted slabs as the result of collision of the Panama Arc-indenter with Northwestern South America. Bull. Seismol. Soc. Am. 103, 2025–2046. https://doi.org/10.1785/0120120328

Vermeesch, P., 2021. Maximum depositional age estimation revisited. Geosci. Front. 12, 843–850. https://doi.org/10.1016/j.gsf.2020.08.008

Vermeesch, P., 2018. IsoplotR: A free and open toolbox for geochronology. Geosci. Front. 9, 1479–1493. https://doi.org/10.1016/j.gsf.2018.04.001

Villagómez, D., Spikings, R.A., 2013. Thermochronology and tectonics of the Central and Western Cordilleras of Colombia: Early Cretaceous–Tertiary evolution of the Northern Andes. Lithos 160–161, 228–249. https://doi.org/10.1016/j.lithos.2012.12.008

Villagómez, D., Spikings, R.A., Magna, T., Kammer, A., Winkler, W., Beltrán, A., 2011. Geochronology, geochemistry and tectonic evolution of the Western and Central

cordilleras of Colombia. Lithos 125, 875–896. https://doi.org/10.1016/j.lithos.2011.05.003

Viveen, W., Schlunegger, F., 2018. Prolonged extension and subsidence of the Peruvian forearc during the Cenozoic. Tectonophysics 730, 48–62. https://doi.org/10.1016/j.tecto.2018.02.018

Vogt, K., Gerya, T. V., 2014. From oceanic plateaus to allochthonous terranes: Numerical modelling. Gondwana Res. 25, 494–508. https://doi.org/10.1016/j.gr.2012.11.002

von Eynatten, H., Dunkl, I., 2012. Assessing the sediment factory: The role of single grain analysis. Earth-Science Rev. 115, 97–120. https://doi.org/10.1016/j.earscirev.2012.08.001

von Huene, R., Ranero, C.R., Vannucchi, P., 2004. Generic model of subduction erosion. Geology 32, 913–916. https://doi.org/10.1130/G20563.1

von Huene, R., Scholl, D.W., 1991. Observations at convergent margins concerning sediment subduction, subduction erosion, and the growth of continental crust. Rev. Geophys. 29, 279–316. https://doi.org/10.1029/91RG00969

Wagner, L.S., Jaramillo, J.S., Ramírez-Hoyos, L.F., Monsalve, G., Cardona, A., Becker, T.W., 2017. Transient slab flattening beneath Colombia. Geophys. Res. Lett. 44. https://doi.org/10.1002/2017GL073981

Wagreich, M., 1995. Subduction erosion and Late Cretaceous subsidence along the northern Austroalpine margin (Eastern Alps, Austria). Tectonophysics 242, 63–78. https://doi.org/10.1016/0040-1951(94)00151-X

Wang, J.-G., Hu, X., Garzanti, E., BouDagher-Fadel, M.K., Liu, Z.-C., Li, J., Wu, F.-Y., 2020. From extension to tectonic inversion: Mid-Cretaceous onset of Andean-type orogeny in the Lhasa block and early topographic growth of Tibet. Geol. Soc. Am. Bull. 132, 2432–2454. https://doi.org/10.1130/B35314.1

Wang, K., He, J., 1999. Mechanics of low-stress forearcs: Nankai and Cascadia. J. Geophys. Res. Solid Earth 104, 15191–15205. https://doi.org/10.1029/1999JB900103

Weber, M., Cardona, A., Paniagua, F., Cordani, U., Sepúlveda, L., Wilson, R., 2009. The

Cabo de la Vela Mafic-Ultramafic Complex, Northwestern Colombian Caribbean region: a record of multistage evolution of a Late Cretaceous intra-oceanic arc, in: James, K.H., Lorente, M.A., Pindell, J.L. (Eds.), The Origin and Evolution of the Caribbean Plate, Geological Society, London, Special Publications, 328. pp. 549–568. https://doi.org/10.1144/SP328.22

Weber, M., Gómez-Tapias, J., Cardona, A., Duarte, E., Pardo-Trujillo, A., Valencia, V., 2015. Geochemistry of the Santa Fé Batholith and Buriticá Tonalite in NW Colombia - Evidence of subduction initiation beneath the Colombian Caribbean Plateau. J. South Am. Earth Sci. 62, 257–274. https://doi.org/10.1016/j.jsames.2015.04.002

Wegner, W., Wörner, G., Harmon, R.S., Jicha, B.R., 2011. Magmatic history and evolution of the Central American Land Bridge in Panama since Cretaceous times. Geol. Soc. Am. Bull. 123, 703–724. https://doi.org/10.1130/B30109.1

Whattam, S.A., Montes, C., Mcfadden, R.R., Cardona, A., Ramirez, D., Valencia, V., 2012. Age and origin of earliest adakitic-like magmatism in Panama: Implications for the tectonic evolution of the Panamanian magmatic arc system. Lithos 142–143, 226–244. https://doi.org/10.1016/j.lithos.2012.02.017

Whattam, S.A., Montes, C., Stern, R.J., 2020. Early central American forearc follows the subduction initiation rule. Gondwana Res. 79, 283–300. https://doi.org/10.1016/j.gr.2019.10.002

Whattam, S.A., Stern, R.J., 2015. Late Cretaceous plume-induced subduction initiation along the southern margin of the Caribbean and NW South America: The first documented example with implications for the onset of plate tectonics. Gondwana Res. 27, 38–63. https://doi.org/10.1016/j.gr.2014.07.011

Wise, D.U., Funicello, R., Parotto, M., Salvini, F., 1985. Topographic lineament swarms: Clues to their origin from domain analysis of Italy. Geol. Soc. Am. Bull. 96, 952–967. https://doi.org/10.1130/0016-7606(1985)96<952:TLSCTT>2.0.CO;2

Wright, J.E., Wyld, S.J., 2011. Late Cretaceous subduction initiation on the eastern margin of the Caribbean-Colombian Oceanic Plateau: One Great Arc of the Caribbean (?). Geosphere 7, 468–493. https://doi.org/10.1130/GES00577.1

Xie, X., Heller, P.L., 2009. Plate tectonics and basin subsidence history. Bull. Geol. Soc. Am. 121, 55–64. https://doi.org/10.1130/B26398.1

Yarce, J., Monsalve, G., Becker, T.W., Cardona, A., Poveda, E., Alvira, D., Ordoñez-Carmona, O., 2014. Seismological observations in Northwestern South America: Evidence for two subduction segments, contrasting crustal thicknesses and upper mantle flow. Tectonophysics 637, 57–67. https://doi.org/10.1016/j.tecto.2014.09.006

Zagorevski, A., Lissenberg, C.J., van Staal, C.R., 2009. Dynamics of accretion of arc and backarc crust to continental margins: Inferences from the Annieopsquotch accretionary tract, Newfoundland Appalachians. Tectonophysics 479, 150–164. https://doi.org/10.1016/j.tecto.2008.12.002

Zagorevski, A., van Staal, C.R., 2011. The record of Ordovician arc-arc and arc-continent collisions in the Canadian Appalachians during the closure of Iapetus, in: Brown, D., Ryan, P.D. (Eds.), Arc-Continent Collision. Springer-Verlag Berlin Heidelberg, pp. 341–371. https://doi.org/10.1007/978-3-540-88558-0_12

Zapata-Villada, J.P., Cardona, A., Serna, S., Rodríguez, G., 2021. Late Cretaceous to Paleocene magmatic record of the transition between collision and subduction in the Western and Central Cordillera of northern Colombia. J. South Am. Earth Sci. 112, 103557. https://doi.org/10.1016/j.jsames.2021.103557

Zapata, G., 2000. Geología de las planchas 163 Nuquí, 164 Quibdó, 183 Coquí y 184 Lloró, Departamento del Chocó. Escala 1:100.000. Memoria Explicativa.

Zapata, S., Cardona, A., Jaramillo, J.S., Patiño, A., Valencia, V., León, S., Mejía, D., Pardo-Trujillo, A., Castañeda, J.P., 2019. Cretaceous extensional and compressional tectonics in the Northwestern Andes, prior to the collision with the Caribbean oceanic plateau. Gondwana Res. 66, 207–226. https://doi.org/10.1016/j.gr.2018.10.008

Zapata, S., Patiño, A., Cardona, A., Parra, M., Valencia, V., Reiners, P., Oboh-Ikuenobe, F., Genezini, F., 2020. Bedrock and detrital zircon thermochronology to unravel exhumation histories of accreted tectonic blocks: An example from the Western Colombian Andes. J. South Am. Earth Sci. 103, 102715. https://doi.org/10.1016/j.jsames.2020.102715

Zhu, D.-C., Wang, Q., Cawood, P.A., Zhao, Z.-D., Mo, X.-X., 2017. Raising the Gangdese Mountains in southern Tibet. J. Geophys. Res. Solid Earth 122, 214–223. https://doi.org/10.1002/2016JB013508

Zindler, A., Hart, S., 1986. Chemical geodynamics. Annu. Rev. Earth Planet. Sci. 14, 493–571. https://doi.org/10.1146/annurev.ea.14.050186.002425